New Ways to Create and to Detect
Nonlocal Cooper Pairs in Solid-State Nanodevices

Von der Fakultät für Elektrotechnik, Informationstechnik, Physik
der Technischen Universität Carolo-Wilhelmina zu Braunschweig

zur Erlangung des Grades eines Doktors

der Naturwissenschaften (Dr. rer. nat.)

genehmigte Dissertation

von Alexander Schroer

aus Münster (Westf.)

eingereicht am: 26.07.2016

Disputation am: 16.11.2016

1. Referent: Prof. Dr. Patrik Recher
2. Referent: Prof. Dr. Alfredo Levy Yeyati

Druckjahr: 2016

Dissertation an der Technischen Universität Braunschweig,
Fakultät für Elektrotechnik, Informationstechnik, Physik

Abstract

New strategies to generate and to detect spin-entangled pairs of electrons in mesoscopic solid-state heterostructures are proposed.

A bilayer-graphene device is designed in which Cooper pairs from an s-wave superconductor are injected into an electrostatically-defined topological channel. Due to a particular band structure, two electrons of a Cooper pair propagate in opposite directions and are hence spatially separated if atomic-scale defects are sparse. Neither energy filtering nor Coulomb repulsion are required. The device can be interpreted as a normal/superconducting/normal junction, in which emission of nonlocal singlets is equivalent to local Andreev reflection, in contrast to the widespread identification of Cooper pair splitting with crossed Andreev reflection.

To detect entanglement, the Josephson current through two parallel single-level quantum dots is investigated at all occupations. Combining exact diagonalization and perturbation theory, signatures of nonlocal Cooper pair transport are identified in the critical current, a macroscopic quantity. The model reproduces recent experimental observations and predicts a nonlocal triplet ground state on the quantum dots due to a tunable superconductor-mediated exchange coupling, which, too, is visible in the critical current exactly if nonlocal Cooper pairs are transported.

Entanglement detection is pursued, too, by converting spin-entangled Cooper pairs into polarization-entangled photons, which are subsequently probed by a Bell-type measurement. A closed emission cycle is constructed, such that no correlations between the photons and the electrons remain, which are detrimental for entanglement transfer. Inevitable side channels and imperfections are identified and accounted for by a particular measurement protocol.

Furthermore, it is discussed how spin–charge separation can be used to extract signatures of nonlocal spin singlets from the average current through an electronic beam splitter. This complements a known mechanism based on exchange statistics by which only the more difficult-to-access noise is sensitive for entanglement. The device can be realized

by two crossed nanowires or by quantum-Hall edge states in Corbino geometry.

The thesis also contains a review on entanglement and on recent theoretical and experimental progress in solid-state systems towards entanglement detection and generation, focusing on Cooper pair splitting.

Zusammenfassung

Neue Strategien um spinverschränkte Elektronenpaare in mesoskopischen Festkörperheterostrukturen zu erzeugen und nachzuweisen werden vorgeschlagen.

Eine Bilagengraphenstruktur wird entworfen, in der Cooperpaare von einem s-Wellensupraleiter in einen elektrisch definierten topologischen Kanal injiziert werden. Durch die spezielle Bandstruktur bewegen sich zwei Cooperpaarelektronen in entgegengesetzte Richtungen und werden räumlich getrennt, wenn die atomare Störstellendichte gering ist. Weder Energiefilter noch Coulombabstoßung werden benötigt. Die Struktur kann als normal/supraleitend/normal-Übergang interpretiert werden, in dem nichtlokale Singulettemission äquivalent zu lokaler Andreevreflexion ist, im Gegensatz zur üblichen Identifikation mit gekreuzter Andreevreflexion.

Zur Verschränkungsdetektion wird der Josephsonstrom durch zwei parallele Einzustandquantenpunkte bei allen Besetzungen untersucht. Durch exakte Diagonalisierung und Störungstheorie werden Signaturen nichtlokalen Cooperpaartransports im kritischen Strom, einer makroskopischen Größe, identifiziert. Das Modell reproduziert aktuelle experimentelle Beobachtungen und sagt einen nichtlokalen Quantenpunkttriplettgrundzustand durch eine supraleitervermittelte Austauschkopplung vorher, der im kritischen Strom sichtbar ist, genau wenn nichtlokale Cooperpaare transportiert werden.

Verschränkungsdetektion wird auch verfolgt, indem spinverschränkte Cooperpaare in polarisationsverschränkte Photonen konvertiert werden, die mit einer Bell-artigen Messung untersucht werden. Ein geschlossener Emissionszyklus wird konstruiert, sodass keine Korrelationen zwischen Photonen und Elektronen verbleiben, die die Verschränkungsübertragung behindern. Unabdingbare Nebeneffekte werden identifiziert und durch ein spezielles Messprotokoll behoben.

Desweiteren wird diskutiert, wie Spin–Ladungstrennung verwendet werden kann, um Signaturen nichtlokaler Spinsinguletts aus dem mittleren Strom durch einen elektronischen Strahlteiler zu extrahieren.

Dies ergänzt einen bekannten Mechanismus, bei dem, mithilfe der Austauschstatistik, nur das schwerer zugängliche Rauschen sensitiv für Verschränkung ist. Die Struktur ist durch gekreuzte Nanodrähte oder Quantenhallrandkanäle in Corbinogeometrie realisierbar.

Die Dissertation enthält auch eine Zusammenfassung über Verschränkung und aktuelle theoretische und experimentelle Fortschritte in Festkörpersystemen bezüglich Verschränkungsdetektion und -erzeugung, insb. Cooperpaarspaltung.

List of publications

1. *Detection of Spin Entanglement via Spin–Charge Separation in Crossed Tomonaga–Luttinger Liquids*, A. Schroer, B. Braunecker, A. Levy Yeyati, and P. Recher, Phys. Rev. Lett. **113**, 266401 (2014)

2. *Detection of nonlocal spin entanglement by light emission from a superconducting p–n junction*, A. Schroer and P. Recher, Phys. Rev. B. **92**, 054514 (2015)

3. *Valley-based Cooper pair splitting via topologically confined channels in bilayer graphene*, A. Schroer, P. G. Silvestrov, and P. Recher, Phys. Rev. B. **92**, 241404(R) (2015)

4. *Signatures of nonlocal Cooper-pair transport and of a singlet–triplet transition in the critical current of a double-quantum-dot Josephson junction*, B. Probst, F. Domínguez, A. Schroer, A. Levy Yeyati, and P. Recher, Phys. Rev. B. **94**, 155445 (2016)

Acknowledgments

My supervisor Prof. Patrik Recher did not only give me the opportunity to work on and to contribute to an exciting topic but also to learn how science works and to travel across Europe. I will miss the inspiring discussions which would often last for hours and explore every last detail. Thank you.

My sincere thanks also go to Bernd, Alfredo, Peter, Benedikt, and Fernando, who where directly involved, too, in one or more of the projects this thesis comprises. Working with you is fruitful and fun.

To all my colleagues and friends at the TU: you made my time in Braunschweig a fantastic one and broadened my horizon, not only with respect to physics. I hope I could do a little of the same for you.

Finally, I'm very happy that Prof. Alfredo Levy Yeyati agreed to co-referee this thesis and Prof. Andreas Hangleiter to chair the defense exam.

It goes without saying that I am greatly indebted to Anna and to my family.

Contents

1 Introduction

When random people ask me what I do, I like to say, "We develop models of electronic structures which are so small that quantum effects become important." I found out — by trial and error — that this statement is just as fuzzy as it needs to be in order not to scare away anyone immediately. Probably this is because electronic devices becoming smaller and smaller is an everyday experience for all of us and because everyone has already heard something about this 'mysterious' quantum theory. But while the statement is certainly correct, it is somewhat misleading. Indeed, it sounds as if quantum mechanics were an uninvited guest, who sneaks in, more or less inevitably, when engineering small circuits and is to be dealt with. The truth is, quantum effects are extremely elusive and fragile, although we are working hard to invent devices specifically to expose them and to make use of them. Temperature higher than liquid helium can destroy them. Distances larger than microns can destroy them. Stray fields can destroy them. Inelastic scatterers on the atomic scale can destroy them. The sheer amount of particles present in a solid can destroy them. And the list goes on. Yet, quantum mechanics is so different from the classical world that it is worth exploring already for its own sake entirely. The field of mesoscopic physics is an exciting combination of testing fundamental features of nature, of inventing ways to combine them into something new, and of the technical challenge to overcome all of the obstacles like temperature, scale, and disorder which separate us from the microscopic world. The first commercial devices based on quantum effects, e.g., SQUIDS, superconducting interference devices, which measure magnetic fields with enormous precision utilizing the Josephson effect, are already available. Strictly speaking, classical electronics

is entirely based on quantum theory, too, because it relies on energy bands, on the exclusion principle, and on distribution functions. But this is not the explicit quantum behavior I am going to concentrate on. What I *will* concentrate on is quantum entanglement. More precisely, I will discuss how to produce pairs of entangled electrons, which show beyond-classical correlations, in the solid-state environment using superconductors and I will discuss how to detect them. This is of fundamental interest because while theory predicts that these pairs exist, so far the experiments were able to prove only pairs of isolated photons to be entangled but not pairs of electrons moving through a solid. Furthermore, quantum entanglement is a central ingredient for quantum computation and quantum simulation which, if realized, can dramatically impact the way we solve hard problems using computers. The idea to create and detect entangled pairs in the solid state is by no means a new one but the strategies I present are. Therefore this thesis is called *New Ways to Create and to Detect Nonlocal Cooper Pairs in Solid-State Nanodevices*.

In this introductory chapter, I will define and explain the basic concepts of entanglement, of its generation, and of its detection. I will discuss why entanglement is worth investigating and summarize what has already been achieved in theory and in experiment — and what has not. This will necessarily be selective and a little vague in some places but it will serve to put the subsequent chapters into context. For a summary of the original results presented in the main part of the thesis please have a look at Chap. 1.4.

1.1 Quantum information and entanglement

When Heisenberg, Schrödinger, Dirac, and their contemporaries set out to overcome the deficits of classical physics in the early twentieth century, their newly conceived quantum theory [1–3] almost immediately found eminent opposition. Despite its impressive predictive power, one of quantum mechanics' best-known opponents was Einstein. He himself contributed the quantum interpretation of the photoeffect [4] and he did not necessarily consider the new theory to be incorrect but he

thought it to be incomplete. Indeed, he showed that it has implications which outright contradict common sense [5].

The two new principles which challenged his intuition and still challenge ours, namely superposition and entanglement, are both consequences of the assumption that the states of a system which can be attributed definite measurement values are orthonormal vectors in Hilbert space: first, the superposition principle is the implication that, when we take the structure of the vector space seriously, the state of the system may also be a linear combination of two states with different measurement values for the same quantity, which obviously has no immediate interpretation. It appears, however, to be the essential ingredient to explain, e.g., the famous double slit experiment [6]. The Copenhagen interpretation, which postulates that the state "collapses" probabilistically onto exactly one of the superimposed states which corresponds to the observed measurement outcome [7], works well but it feels awkward because it treats the observer on an entirely different footing than the observed system. An appealing way to overcome this hierarchical problem is decoherence [8]: during the measurement the observed system necessarily interacts with the macroscopic measurement apparatus. In the unitary time evolution of the joint observer–observand system, which, too, is governed by the Schrödinger equation, the enormous amount of degrees of freedom causes the state to evolve into a superposition of states in each of which the system has a well-defined state in agreement with the value displayed by the measurement device. When averaging over the possible states of the environment (i.e., tracing out or integrating out the observing system) the corresponding probabilities as predicted by standard quantum mechanics should be obtained. So the standard projective measurement interpretation is a for-all-practical-purposes description of a process which does not distinguish between the observer and the observed system. On a philosophical level, the question remains why the universe decides on one of the superimposed macroscopic states, or, basically, why there are discernible events. But maybe this is just one of the basic laws of nature and almost certainly it is beyond quantum theory itself to explain. What is for sure is that superpositions are ubiquitous already in single particle systems any energy eigenstate of which is a superposition of various states with different real space positions. So superposition is

well-understood, well-controlled, and — from the perspective of this thesis — the less interesting of the two oddities of quantum mechanics.

Entanglement, the other one, is arguably much more puzzling. Like superposition, it is an immediate consequence of the algebraic structure of quantum mechanics. If two or more subsystems are described in their respective vector spaces, the canonical way linear algebra provides to build a state space of all systems together is the tensor product. The structure of the tensor product ensures that the composite system has the right number of degrees of freedom, i.e., the product of each subsystem's degrees of freedom. The tensor product, however, also has the notable property that there are elements of the joint space, which cannot be expressed as the tensor product of vectors from the individual spaces. Put in physical terms, the joint system can be in a state, in which it is impossible to attribute a well-defined state to the individual subsystems even if we allow the subsystems to be in quantum superpositions. Rather, the joint system itself is in a superposition in which the state of one subsystem is linked to, or entangled with, the state of another. This is, in fact, just what happens to the measurement devices and the observed system I discussed before. The most famous example in the case of two microscopic systems is the spin singlet. Two spin-1/2 systems, A and B, the state of each of which can be expressed by two basis vectors $|\uparrow\rangle_{A,B}$ and $|\downarrow\rangle_{A,B}$ are described in the joint state space spanned by $\{|\uparrow\rangle_A \otimes |\uparrow\rangle_B, |\uparrow\rangle_A \otimes |\downarrow\rangle_B, |\downarrow\rangle_A \otimes |\uparrow\rangle_B, |\downarrow\rangle_A \otimes |\downarrow\rangle_B\} \equiv \{|\uparrow\uparrow\rangle, |\uparrow\downarrow\rangle, |\downarrow\uparrow\rangle, |\downarrow\downarrow\rangle\}$, where I employ the Dirac notation as I will always do in the following. But the choice of the basis should be arbitrary, so we are free to use

$$\left|\Phi^+\right\rangle = \frac{1}{\sqrt{2}}\Big(|\uparrow\uparrow\rangle + |\downarrow\downarrow\rangle\Big), \tag{1.1.1}$$

$$\left|\Phi^-\right\rangle = \frac{1}{\sqrt{2}}\Big(|\uparrow\uparrow\rangle - |\downarrow\downarrow\rangle\Big), \tag{1.1.2}$$

$$\left|\Psi^+\right\rangle = \frac{1}{\sqrt{2}}\Big(|\uparrow\downarrow\rangle + |\downarrow\uparrow\rangle\Big), \tag{1.1.3}$$

$$\left|\Psi^-\right\rangle = \frac{1}{\sqrt{2}}\Big(|\uparrow\downarrow\rangle - |\downarrow\uparrow\rangle\Big), \tag{1.1.4}$$

instead. The states (1.1.1) to (1.1.4) are often called *Bell states* and

they are entangled. The state $|\Psi^-\rangle$ happens to be the spin singlet and plays the central part in this thesis, although by local operations on only one of the spins at the same time all Bell states can easily be transformed into one another up to a phase. So concerning entanglement they are somewhat equivalent. Clearly, the two subsystems are tightly linked in the state $|\Psi^-\rangle$: if spin A is up, spin B is down and vice versa. Importantly, which situation is realized is decided only when the state is measured. This is fundamentally different from classical anticorrelation. We might not know which state the system is in but only that both subsystems will have opposite spin. A classically anticorrelated state is completely determined upon preparation like we know that when we take a left glove out of the wardrobe a right glove will still be inside. A quantum superposition is not lack of knowledge but an unambiguous state. Only once one of the spins is actually measured both collapse onto a state in which they are opposite. To the best of our knowledge, this is true for any distance between the spins and happens instantaneously without interaction. In the case of the spin singlet, which is rotationally invariant, the strange behavior is manifest in the observation that both spins are always opposite, no matter which measurement axis is chosen and whether the axis is chosen before or after the state is prepared. This is not possible for the classically anticorrelated state described by the density matrix $\rho = (|{\uparrow\downarrow}\rangle\langle{\uparrow\downarrow}| + |{\downarrow\uparrow}\rangle\langle{\downarrow\uparrow}|)/2$.

Whereas classical anticorrelations are determined when preparing the two subsystems, possible isolated from each other, entanglement is necessarily established by interactions. This is because if the joint system evolves with a noninteracting Hamiltonian, the subsystems evolve independently such that superpositions can arise only within each of them. E.g., the spin singlet is the ground state of the spin–spin Hamiltonian $H = J\mathbf{S}_1\cdot\mathbf{S}_2$ if $J > 0$. This example demonstrates that entanglement is by no means exotic but appears rather naturally in two-particle systems like, e.g., the Helium atom and double quantum dots, where precisely this type of spin coupling is mediated by virtual exchange processes. In superconductors, which will be the source of entanglement in this thesis, Cooper pairs are spin singlets formed by attractive interactions usually mediated by phonons [9]. Seemingly one exception is electron–hole entanglement which can be established already at a biased tunnel barrier [10]. When an electron tunnels through the barrier, a hole with

opposite spin is left behind. If this happens spin independently, the electron and the hole become entangled and can even violate a Bell inequality [11]. But the hole is not an individual particle. It represents the absence of the electron and it makes perfect sense that there are coherent correlations between the electron not having tunneled and having tunneled. If the hole is viewed as a property of the Fermi sea, interactions, in this case the fermionic exchange interactions, sneak back into the picture. Entanglement can also be created by postselection, i.e., by measurements [12, 13] but, again, measurements can be understood as interactions with a macroscopic system. In Chap. 5, I will demonstrate that, like correlation measurements, interactions can also be used to *detect* entanglement.

Once the entangled state is created, however, interactions can be switched off, e.g., by large spatial separation. Still, as we see from Eqs. (1.1.1) to (1.1.4), measuring one subsystem affects the other. Mutual influence between two systems even without interaction is precisely what Einstein, together with Podolsky and Rosen, rejected. In the seminal "EPR" paper [5] they assume that for two entangled subsystems which do not interact the state of, say, system 2 cannot be influenced by measurements on system 1. Therefore, they argue, all wave functions for system 2 which can result from measurements on system 1 must describe exactly the same state. But this is not the case, e.g., in the case of the singlet the spin polarization axis in system 2 after measurement depends on the measurement axis in system 1. States with different spin axes can be told apart by repeated measurements to estimate the quantum expectation values. This contradicts the initial assumption. The authors reasoned that there has to be additional information about the state determined upon preparation, even if some of it might be hidden from our view, maybe by a law of nature. This led to their considering quantum mechanics to be incomplete. Bell realized that the innocuous assumption that there is no mutual influence because there is no interaction between the entangled systems should, in fact, be put to the test [14]. He constructed observables specifically to confirm entanglement experimentally. He proposed to measure certain correlations which should be bounded in classical systems. This is expressed by Bell inequalities and will be discussed in more detail in Chap. 1.3.1. The important point is that, using Bell's

ideas, entanglement was confirmed in 1972 by Freedman and Clauser [15]. In 1982, Aspect et al. conducted a similar experiment [16] in which the decisions what measurements to perform on each subsystem were spacelikely separated and again found quantum theory to be correct. More confirmations followed [17–19] and by now Bell tests have become somewhat of a routine task in quantum optics labs.

When it comes to the interpretation of this result, like in the times of Schrödinger, Dirac, and Heisenberg against Einstein, Podolsky, and Rosen, the community is divided even today, although the borders have somewhat shifted: there are (the large majority of) physicists who yielded to the immense success of quantum mechanics — it has, indeed, suffered not a single unanimously acknowledged failure — accepted it as the way nature works, and use it as a framework to build more specific theories and to explain their experiments. And there are those still arguing over the interpretation and over possible alternatives to quantum mechanics. This discussion, while important and interesting in its own right, has had little impact on our understanding of the world or on technology. I belong to the first faction. This thesis does not deal with whether quantum mechanics is right, at least not more than any theory does which can be verified experimentally. If entanglement cannot be generated or detected by the methods presented, this does not imply that there is no entanglement in nature. Rather it means that there are essential effects in a particular experimental realization which are not included in the specific theory built on top of quantum mechanics but which destroy the entanglement which we know must have been there at some point. Identifying and clearing away these effects is a major task on the route towards solid-state quantum-information devices.

This is a major paradigm shift. Originally, the questions were whether quantum theory is correct and whether entanglement exists. The Bell inequalities were designed as a test of quantum theory itself. In this context, it is important to rule out all possible loopholes which allow for alternative explanations of the measurement result, mostly for the violation of a Bell-type inequality. Even if the separation between two measurements is spacelike (*Communication loophole*) each measurement is not actually performed on the same state, because the state is irrevocably changed in the process. So it is vital that all the states are prepared the same way and that all are equally likely to be

detected (*Detection loophole*). Closing all remaining loopholes is still an active area of research [20–22]. As far as quantum information is concerned, Bell inequalities are regarded as indicators of entanglement, as are a number of other quantities, and therefore called entanglement witnesses [23]. The special behavior of the Josephson current through a double quantum dot system may serve as such an indicator as detailed in Chap. 3.

Quantum information aims at exploiting superposition and entanglement, both of which are beyond-classical effects, to build beyond-classical machines [24]. Any two-level system such as a spin-1/2 particle can take two values $|0\rangle$ and $|1\rangle$ similar to the bits classical computers use to represent numbers in binary. When the two-level system is viewed as a quantum bit, or qubit, it can, however, also be in a superposition of $|0\rangle$ and $|1\rangle$. Then several qubits can be in the superposition, say, $(|011\rangle + |100\rangle)\sqrt{2}$, which is readily interpreted as the superposition of the numbers 3 and 4. If a function f can be represented as a linear quantum mechanical operator, e.g., because it is the time-evolution operator of a carefully designed system, the state will be transformed into the superposition $f(3) + f(4)$. Obviously we could evaluate f not only with two numbers but with many more just by using a superposition of more states as the input. Crucially, the time and the amount of memory it takes to evaluate f does not change because, after all, we are still evaluating f with respect to exactly one quantum state. This is called quantum parallelism and makes a hypothetical quantum computer intrinsically more powerful than a classical computer, which has to evaluate f for all possible inputs one by one. Importantly, while the *operator* which encodes f is linear in Hilbert space like any quantum mechanical operator, the *function* f is arbitrary. Unfortunately, quantum parallelism is not immediately useful since once the output $f(3) + f(4) + \ldots$ is measured, the state collapses on only one value, say $f(4)$. Entanglement is the second important ingredient for quantum information. A preshared entangled pair is like an additional (single-use) communication channel for quantum data. Using an entangled pair and a classical channel it is possible to transfer a qubit state from one party to another [25] (quantum teleportation), an entangled pair and a classical bit can convey 2 bits of information [26] (quantum dense coding), and several entangled pairs can be used for guaranteed

secure communication [27] (quantum key exchange). These protocols have been verified experimentally with entangled photons [28–31]. The real surge for quantum-enhanced machines, however, was started by Shor. He was the first who came up with an algorithm which utilized quantum parallelism and then let different outputs interfere in a sophisticated way to solve a real world problem: prime factorization [32]. This is remarkable because the best known classical algorithm which does prime factorization requires resources, i.e., time and memory, that grow exponentially with the size of the number to be factored, whereas Shor's algorithm exhibits only a polynomial growth. This is exciting for computer scientists because it is a long standing question (one of the Millennium problems, actually) whether some problems are fundamentally more difficult than others, and it is possibly even more exciting for cryptographers because prime factorization and similar problems being hard is what modern asymmetric cryptography derives its security from. Indeed, if there was a quantum computer capable of running Shor's algorithm, the finance system, governments, the world wide web, in short, everything which uses one or another form of protected electronic communication, would be in deep trouble. Luckily, there is still time to adapt since leading experimental groups are only beginning to combine many interacting qubits and Shor's algorithm will need millions to outperform classical computers. Furthermore, there are the new encryption schemes which employ quantum effects to detect if a secure communication channel has been tampered with [27]. Basically, eavesdropping on a transmission implies some sort of measurement which disturbs its quantum state and will always be detectable. In contrast to quantum computers, early quantum cryptography systems are already commercially available. Of course, the question arises how much effort we should invest into a technology which, for all we know, can be used above all for breaking today's encryption schemes, only to replace them by new ones. But there is one additional application of quantum computers: simulating other quantum systems. Simulating quantum systems suffers from the same exponential growth in resources as prime factorization, simply because the dimensionality of the state space of a many-particle system grows exponentially with the number of particles. Yet it is highly desirable to simulate, e.g., chemical reactions in drug design or strongly correlated metals to find a room temperature superconductor. The idea of quantum simulation goes

back to Feynman [33]. Since quantum mechanical systems do exist in nature, there is little reason to assume that quantum systems could not be used to imitate other quantum systems. Based on Feynman's ideas, Lloyd proved that it is indeed possible to approximate the time evolution of arbitrary systems efficiently, i.e., without exponential resources, if superposition and entanglement are available and well controlled [34]. The first steps of quantum simulation are already being successfully taken in the cold atoms community [35]. It is true that the universal quantum computer might be just too complicated to be built in the near future. It is possible that somebody finds a classical algorithm which factors primes as efficiently as Shor's does. But quantum simulation can already be useful with not quite as many qubits, and so possibly be realized on a shorter time scale [36]. In either case, today's systems need to be scaled up dramatically. It is hard to believe that there is a platform better suited to do so than the solid state, considering the immense technological expertise the semiconductor industry has developed to build classical electronic devices. Unfortunately, while entangled photons have been created already in the seventies [15], entangling massive electrons in a controlled fashion turns out to be a much harder task. The electron spin can have very long coherence times beyond 100 ns [37] in semiconductors and consequentially a large coherence length. This makes the spin an attractive and conceptually simple candidate for a solid state qubit [38, 39] (although there are other exciting possibilities like superconducting qubits [40]). In particular, the spin qubit, being an electron, always comes with an electric charge which can be used to move it around and to perform read-out operations based on spin–charge conversion. The downside is that, in a solid state environment, each electron is usually surrounded by extremely many other electrons it is indistinguishable from and interacting with. This is not a big problem when the spin qubit is stationary, e.g., captured in a closed-shell quantum dot. But it becomes more important in the case of flying qubits propagating through wires. Burkard et al. found that a sizable amount of the entanglement of two electrons injected into a Fermi liquid can still be recovered within the quasiparticle lifetime [41]. In Chap. 5, I will discuss how entanglement is still visible even if the electron is injected not into a Fermi liquid but into a Tomonaga-Luttinger liquid, where it decays into separate charge and spin excitations. In any case, the first question is: how can pairs

of propagating spin-entangled electrons be created in the solid state in a controlled fashion?

1.2 Cooper pair splitting

One source of entanglement which has received a great deal of attention in the last decade are s-wave superconductors. This is because when they are in the ground state, the conduction electrons close to the Fermi level form pairs of opposite spin and opposite momentum, Cooper pairs, which happen to be spin singlets. If it is possible to separate one of the pairs without influencing its spin wave function a nonlocal "split" entangled pair will be obtained. The yield will be the better the more electrons are actually paired up, i.e., the closer the superconductor is to its ground state. This is a viable requirement because of the finite excitation gap in the Bardeen–Cooper–Schrieffer spectrum. Cooper pair splitting generally requires very low temperatures and, being a nonequilibrium process, a source drain voltage smaller than the gap energy. Then, one electron can tunnel out of the superconductor and leave it in an excited state of at least the gap energy with an unpaired electron on top of the Bardeen–Cooper–Schrieffer condensate. Since this energy can be provided neither by the voltage bias nor by the temperature, the excitation is virtual. Either the electron has to tunnel back into the superconductor (no transport) or the second electron has to tunnel out of it as well. Cooper pair splitting happens if each electron tunnels into a different lead. The idea of Cooper pair splitting is closely connected (although not equivalent, cf. Chap. 2) to crossed Andreev reflection [42]: if two leads are weakly tunnel coupled to a superconductor such that most incoming quasiparticles are reflected at the interfaces, a hole incident from one lead can be transmitted as an electron in the *other* lead. In both leads the number of electrons is increased by one. Usually, however, crossed Andreev reflection is rather the exception than the rule. This is true in particular if the contacts are separated by more than the coherence length, on which the wave function of an unpaired particle with an energy below the excitation gap decays in the superconductor. More often, local Andreev reflection takes place, which puts two electrons into the same lead. As we have

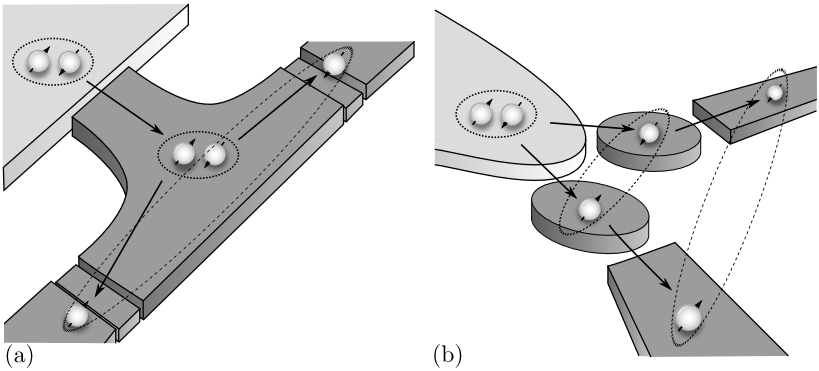

Figure 1.1: Cooper pair splitter as proposed by (a) Lesovik et al., Ref. 43, and (b) Recher et al., Ref. 44. In (a), the splitting mechanism relies on the electrons of a Cooper pair having energies $\varepsilon_1, \varepsilon_2$ which sum to twice the Fermi energy E_F in the superconductor (white), $\varepsilon_1 + \varepsilon_2 = 2E_F$. The Cooper pairs tunnel into the normal region (gray), where two energy filters (lowered regions) with narrow transmittances around ε_1 and ε_2, respectively, are transparent for only one of the electrons each. The superconductor/normal transmission is strong but energy filtering turned out to be fragile and splitting at $\varepsilon_1 = \varepsilon_2$ is impossible by design. In (b), high Coulomb repulsion on two quantum dots (ovals) ensures that two electrons cannot tunnel simultaneously into the same lead and the superconducting gap prohibits sequential transport of both electrons into the same lead. This allows for Cooper pair emission at $\varepsilon_1 = \varepsilon_2$ but it is suppressed if the spatial separation of the quantum dots exceeds the coherence length in the superconductor.

seen in the previous section, talking about entanglement is meaningful only when the system (the singlet) can be divided into two subsystems (one electron in each lead). Putting two electrons into the same lead is, therefore, undesirable.

Simultaneously, Lesovik et al. [43] and Recher et al. [44] came up with two independent ideas how to enhance the nonlocal emission process over local ones. Lesovik et al. exploited the fact that the energy of the two electrons of a Cooper pair adds up to twice the Fermi energy E_F of the superconductor, $\varepsilon_{1,2} = E_F \pm \Delta\varepsilon$. When building a Y

junction of an energy filter with resonance energy ε_1 at the first terminal, an energy filter with resonance energy ε_2 at the second terminal, and a superconductor at the last terminal, each electron of a Cooper pair injected from the superconductor into the Y junction can leave through one lead only [Fig. 1.1(a)]. Under the assumption of perfect filtering, the authors iteratively derive the overall scattering matrix of the Y junction and obtain a non-zero amplitude for crossed Andreev reflection, whereas normal transmission and local Andreev reflection are impossible by construction. Recently, the same reasoning has been applied to a one-dimensional geometry [45]. In this case it is even possible to eliminate all processes other than crossed Andreev reflection. It is, however, dubious, whether this is really a benefit if one aims at entanglement production (Chap. 2). Roughly, when all particles are Andreev reflected, there is not one emitted electron with either spin up or spin down but there is always both one electron with spin up and one electron with spin down. This is a product state. In general, energy filtering has two drawbacks: experimentally, it turned out to be rather fragile and it works only if $\Delta\varepsilon$ exceeds the selectivity of the energy filters. In this case, the entangled electrons have different orbital wave functions, which can be undesirable, e.g., if the entanglement is to be detected by exchange interactions as I will discuss later on.

The latter aspect is what Recher et al. focused on. They proposed to use the Coulomb repulsion between the two electrons to prevent them from entering the same lead. The original proposal [44] put a quantum dot between the superconductor and each lead [Fig. 1.1(b)]. The spatial confinement on the quantum dots implies a large charge density so double occupancy incurs a high energy penalty. Sequential transport, i.e., if one electron is left behind unpaired in the superconductor until the other has left the quantum dot again, is suppressed by the superconducting gap. On the other hand, some room is required to accommodate two quantum dots (usually on the order of 100 nm) and I already mentioned that there is an exponential suppression of the amplitude for crossed Andreev reflection, i.e., of the splitting efficiency, with the separation between the leads. Recher et al. showed that there is a parameter regime in which the nonlocal Cooper pair current is large compared to the local current. Specifically, the bulk superconducting gap Δ and the Coulomb repulsion on the quantum dots need to be large

compared to the bias voltage between the superconductor and the normal leads to enforce the splitting mechanism. At the same time, the level broadening on the quantum dots needs to be smaller than the bias voltage, such that Fermi-sea electrons from the leads cannot participate in the transport process and destroy the entanglement. In a similar fashion, the quantum dots should almost always be empty or otherwise, during pair transport, an entangled electron might be exchanged with an unrelated one. This requires the quantum dots to be coupled more strongly to the leads than to the superconductor. As always when quantum effects are of interest, the temperature needs to be as low as possible. In this case, it should at least be smaller than the bias voltage in order to exclude thermal carriers from the splitting process. If these conditions are met, the resonance condition $\varepsilon_1+\varepsilon_2 = 2E_F$, where the on-site energies $\varepsilon_{1,2}$ of the quantum dots now take the role of Lesovik's energy filters, may be fulfilled by $\varepsilon_1 = \varepsilon_2 = E_F$ and still the ratio between the desired nonlocal current I_{NL} and the parasitic local current I_{L},

$$\frac{I_{\mathrm{NL}}}{I_{\mathrm{L}}} \propto \left[\frac{\sin(k_F r)}{k_F r}\right]^2 e^{-\frac{2r}{\pi\xi}}, \tag{1.2.1}$$

can become large. Here, k_F is the Fermi vector in the superconductor, r is the separation between the quantum dots, and $\xi = \hbar v_F/\Delta$ is the coherence length of the superconductor with v_F its Fermi velocity. The exponential (and algebraic) suppression with r is explicitly visible. If the coherence length is interpreted as the spread of a Cooper pair, the shape of Eq. (1.2.1) appears quite plausible although the details depend on the geometry, in particular, on the dimensionality of the superconductor [46]. Disorder weakens the decay if the quantum dots are separated further than the mean free path but closer than the coherence length [47]. Loosely speaking, disorder scattering keeps the quasiparticle which remains when one electron of a Cooper has already left the superconductor close to the interface. The oscillations, on the other hand, appear to be rather a fundamental feature and will be particularly important in Chap. 4.

The delay time between the two electrons is given by the time the superconductor stays in the virtual excited state with an unpaired electron, i.e., roughly $\hbar/\Delta$. A typical order-of-magnitude estimate is $\Delta \sim 1$ meV, which is about the value of pure niobium. Two electrons per $\hbar/\Delta$ cor-

responds to a current of 0.5 μA. The total output current of a Cooper pair splitter is determined by the transparency of the tunnel barriers (and the voltage). It needs to be significantly smaller than 0.5 μA because otherwise the individual entangled pairs are not well separated and cannot be identified. Identifying pairs does not conflict with all electrons being indistinguishable in general; rather the individual wave packets emitted from the Cooper pair splitter are distinguishable. In the experiments, the gap energy Δ tends to be smaller than 1 meV because the superconducting material is a different one, e.g., aluminum, or because the superconductivity is merely proximity-induced. This gives an even lower bound on the current. In an electron–hole scattering picture, a low emission rate translates to a low amplitude for Andreev processes. As a consequence, the limit of unit Andreev efficiency, which is often pursued in recent literature [45, 48–51], does correspond to strong Cooper pair splitting but is of little use when aiming for entanglement (cf. Chap. 2).

It is also worth noting that there are some important but often not explicitly mentioned assumptions on the quantum dots [44]. For the entangler to work, the electrons already present on the quantum dots may not participate in the transport, i.e., the level spacing needs to be large compared to voltage and temperature. Otherwise there might be unwanted spin flips. When the valence electrons on the "empty" quantum dot further comprise a spin singlet they can effectively be ignored, which is done most of the time. I will follow this convention from now on.

Using Coulomb repulsion to suppress local pairs is not restricted to quantum dots. Certain one-dimensional leads, e.g., carbon nanotubes, exhibit sufficiently strong intrinsic interactions that the quantum dots are not required [46, 52]. This has been analyzed within the Tomonaga–Luttinger liquid model (Chap. 5). Along the same lines, the dynamical Coulomb blockade in highly resistive leads has been predicted to enhance Cooper pair splitting [53].

Similar to the proposal for Cooper pair splitting via energy filtering, which exploits that the electrons come with opposite energies with respect to the chemical potential of the superconductor, alternative

strategies use that they also have opposite spin. The most straightforward approach is probably to use ferromagnetic leads with opposite polarization. Splitting Cooper pairs by spin is particularly robust, too, in the context of helical quantum spin-Hall states [54] realized at the edge of two-dimensional topological insulators. In the absence of time-reversal-symmetry breaking, e.g, in the absence of magnetic disorder, a spin-down electron will always propagate in one direction and a spin-up electron in the other. Unit-efficiency splitting has been predicted [51] and even Majorana fermions have been found to be helpful [55]. Clearly, however, no matter how efficient the splitting process might be, it does not produce entangled pairs because it is known beforehand which spin propagates into which direction. This variation of Cooper pair splitting is fun but currently it does not appear to have any meaningful application. It was proposed to introduce a tunnel coupling between the two edges of a narrow topological insulator strip [50] or to extend the superconductor over both edges [56] to overcome this problem. Then, however, the topological protection is sacrificed and additional resonance conditions have to be fulfilled by gating or by doping to suppress processes competing with Cooper pair splitting. A different approach is to employ the electrons' opposite momentum for splitting and leave the spin untouched. In Chap. 2, I will investigate the special situation in graphene, where opposite momentum means opposite valley, which is a good quantum number as long as the material is free of atomic-scale defects, a reasonable assumption with modern-day fabrication techniques.

In the experimental community, quantum-dot-based Cooper pair splitters are rather popular. The first was realized in 2009 by the Schönenberger group using an aluminum superconductor put across an indium-arsenide nanowire such that one quantum dot formed on its left and one on its right (Fig. 1.2) [58]. When the left quantum dot is brought into resonance with the superconductor, it has a finite conductance G_L due to local subgap transport. The striking observation was an increase of up to $\Delta G_L \approx 0.1 G_L$ that occurred when bringing the *right* dot into resonance and only when the superconductivity was not quenched by a magnetic field. The ratio $\Delta G/(G + \Delta G)$ is commonly defined as the splitting efficiency in the experimental literature. Almost 10% is a surprisingly large result because the distance between the quantum dots in

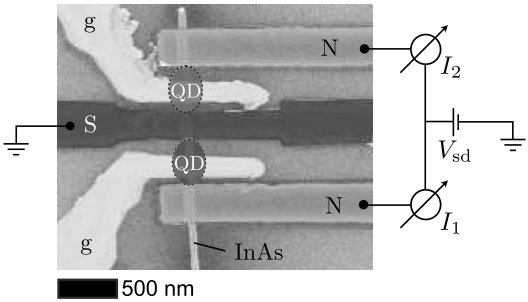

Figure 1.2: Scanning electron microscope image of a functional Cooper pair splitter. A superconducting strip (S) of aluminum and two normal leads (N) are fabricated in contact to a molecular-beam-epitaxy-grown indium-arsenide nanowire (InAs) by electron-beam lithography. Two quantum dots (QD) form in the segments of the nanowire between the superconductor and the normal leads, which can be tuned by top gates (g) and a global backgate. Based on Ref. 57 with kind permission. SEM image © 2011 American Physical Society

this structure was roughly 150 nm while the Fermi wavelength in aluminum is only 3.6 Å. According to the model, Eq. (1.2.1), there should be no significant splitting at all. This is true even when taking into account that the mean free path in the aluminum electrode was about 5 nm. The authors speculate that the aluminum contact induces superconductivity in the nanowire via the proximity effect and so the superconductor which really matters is the central piece of the nanowire. It has a much lower carrier density and so a longer Fermi wavelength. This is a plausible interpretation. In addition, the nanowire is pseudo-one dimensional so the spatial decay is weaker, maybe absent [46], and the induced pairing, which is smaller than the bulk pairing, corresponds to an even longer coherence length. From an applied perspective, a nonlocal-to-local ratio of 1 to 10 is mediocre at best. The authors optimistically point out that the efficiency of parametric down conversion, the state-of-the-art source of entangled photons, is worse by orders of magnitude [59]. On the other hand, a one-to-ten splitting ratio can in principle be obtained by purely random partitioning without any Coulomb repulsion [60]. A reason is probably that the couplings

between the superconductor and the quantum dots and between the quantum dots and the leads are comparable to or even larger than the superconducting gap. This favors sequential transport but appears to be a problem inherent to this type of realization.

In parallel to the Schönenberger group, a Cooper pair splitter was realized by Herrmann et al. with a carbon nanotube instead of a nanowire [61]. They, too, observed a subgap current when applying a bias voltage between the superconducting lead and the normal leads, which became particularly large, when both dots were in resonance. They used a set of rate equations to extract the nonlocal contributions and estimated an efficiency of even 50%. Wei et al. attempted to build a Cooper pair splitter based on the dynamical Coulomb blockade in metallic leads without quantum dots [62]. Positive cross-correlations between the currents into the normal leads indicated the presence of nonlocal Andreev processes in suitable regimes whereas in other configurations, electron cotunneling became dominant and produced negative cross-correlations. An efficiency of 10% has been reported for a graphene-based device [63].

The Schönenberger group later expanded on their work. They applied a finite voltage offset between the normal leads, which implements an energy filtering mechanism, and were able to tune the ratio between cotunneling and crossed Andreev tunneling [57]. Replacing the nanowire by a carbon nanotube they pushed the splitting efficiency to about 90% [64]. This is almost enough to perform significant Bell tests, which I discuss in the next section. The latest idea is to add more gates to have better control over the quantum dot characteristics [65]. This yields rich behavior and can maybe finally overcome the notoriously strong coupling between the superconductor and the quantum dots. The original setup was also revisited by Das et al. who obtained a higher efficiency of about 50% but, more importantly, found positive cross-correlations in the nonlocal current fluctuations [66]. This is further evidence of Cooper pair splitting and particularly valuable since it has turned out that a cross-conductance similar to what was employed as a signature of Cooper pair splitting in the early experiments effect might also be caused by interference of different coherent paths within the splitter, where an electron first visits one quantum dot but then leaves through the other [67].

Superconductors are not the only conceivable source of spin entanglement. Shortly after the Cooper pair splitter was invented, Oliver et al. [68] and Saraga and Loss [69] proposed entanglers built from a Y junction of a quantum dot and two energy filters (which, too, are quantum dots in Saraga and Loss's design). The quantum dot is filled with two uncorrelated electrons taken from a lead. Due to interactions they equilibrate into the singlet ground state. On a larger time scale, they leave through the filters into separate leads. The energy structure of the quantum dot and of the filters is engineered such that the local singlet state on the quantum dot is in resonance with the nonlocal singlet in the leads while both local pair transport and sequential transport are suppressed. Scattering events can produce entangled pairs [12], too, in particular, when scattering two electrons at a magnetic impurity [70]. Moreover, it has been investigated how collective phenomena like the Kondo effect can produce nonlocal entanglement [71].

It is also worth mentioning that noninteracting particles can become entangled by postselection [12, 13, 72]. The reason is that measurements affect the investigated (sub)system in a nonunitary manner. With this additional ingredient helical states *can* be used to build entanglement sources. When a suitable product state is prepared, e.g., in a Corbino geometry [73], a subsequent charge measurement can project it down onto a nonlocal pair state.

1.3 Entanglement detection

Given its broad experimental confirmation it is safe to assume that Cooper pair splitting works. What is not yet clear is whether the electrons remain spin entangled after having been split. Entanglement is the main motivation for Cooper pair splitting so it, too, has to be demonstrated before we can declare Cooper pair splitting a success entirely. Indeed, from what we know, without the spin entanglement Cooper pair splitting is a mere transport curiosity without probable application.

On the theory side this is usually a simple matter: if the model does not know about spin, i.e., if it is SU(2) invariant, the Cooper pairs

will never lose their spin-singlet nature: only the orbital wave function evolves dynamically whereas the spin part is completely decoupled. Spin degeneracy will be a main ingredient of the topological Cooper pair splitter presented in Chap. 2 and sets this proposal apart from similar ones. But, of course, when the spin degree of freedom is completely decoupled in theory, this is a result of the enormous amount of simplification and abstraction required to obtain tractable models of mesoscopic systems in the first place. Various factors like spin-orbit interaction, magnetic impurities, nuclear spins, and inelastic scattering may invalidate this assumption provided they are sufficiently strong.

The information-theory approach to quantify entanglement is the *entanglement entropy* [10]. In the case of a bipartite pure state, it is the entropy of subsystem 1 after tracing out subsystem 2. Obviously, the entanglement entropy of a product state is zero. Otherwise it is larger than zero. Mixed states are more difficult because, in general, the same density matrix can be represented by different mixtures of different pure states. The entanglement entropy is therefore obtained as the average entanglement entropy minimized over all possible bipartite decompositions of the density matrix [10]. In the special case of two qubits, i.e., in the case of two two-level systems, the *concurrence* is an easier-to-obtain but equivalent quantity [74]. Both the entanglement entropy and the concurrence are defined as properties of the density matrix and not in terms of physical observables and I am not aware of a simple way to construct them without knowing the full density matrix, i.e., without performing a full quantum state tomography. Instead, I will resort to other quantities, which are directly related to measurable observables. One is the Bell parameter. It is explicitly related to polarization or spin measurements. If it exceeds a classical threshold, the state under consideration is entangled. The reverse is not true. The Bell test is only based on statistics and requires the minimum amount of trust in the model, as long as the measurement process is described and controlled adequately. The downside is that it is very hard to implement in the solid state. There exist other quantities the measurement of which is potentially more feasible but which rely to some extent on assumptions about the entangler or about the detector. I will refer to them as indirect entanglement tests. The extreme example is the nonlocal conductance measurement performed on the first Cooper pair

splitter by the Schönenberger group. If we believe that the spin wave function is untouched in the splitting process as predicted theoretically (basically by simply neglecting all of the spin dynamics), the nonlocal conductance, which hints at the *charge* splitting process, already proves nonlocal entanglement. Obviously, this 'proof' leaves something to be desired but a compromise between feasibility and credibility appears to be the best we can hope for at the moment. I will discuss both the Bell test and indirect entanglement tests in more detail below. The classification and quantification of multipartite entanglement is still under debate and irrelevant for this thesis.

1.3.1 Direct methods: the Bell test

The Bell test (or its main quantity, the Bell parameter) constitutes a powerful tool for entanglement detection. It was invented when the validity of quantum mechanics was under debate, in particular, whether entanglement was real or not. Bell was the first to come up with inequalities of three correlation functions which are fulfilled by any classical bipartite system completely determined upon preparation but — and this is what is remarkable — not obeyed by certain entangled quantum states, e.g., the spin singlet [14]. A little later, Clauser, Horne, Shimony, and Holt presented another Bell-type inequality, which uses four correlation functions but dropped difficult-to-meet requirements on the observables imposed by Bell [75]. This CHSH inequality is probably what most people think of when it comes to Bell's inequality, and it works as follows [24]: suppose there are two subsystems A and B and we can measure two local observables in each subsystem, A_1 and A_2 in system A, and B_1 and B_2 in system B. Each of these observables shall only take the values $+1$ and -1. Then the Bell parameter

$$\mathcal{B} = \langle A_1 B_1 \rangle + \langle A_1 B_2 \rangle + \langle A_2 B_1 \rangle - \langle A_2 B_2 \rangle \tag{1.3.1}$$

is bounded by $-2 < \mathcal{B} < 2$ if the measurements in the subsystems are independent of one another. The angular brackets $\langle \cdot \rangle$ denote the

expectation value. To see this, rewrite

$$\begin{aligned}\mathcal{B} &= \langle (A_1 + A_2)B_1 + (A_1 - A_2)B_2 \rangle \\ &= \sum_{a_1,a_2,b_1,b_2=\pm 1} \rho(a_1, a_2, b_1, b_2)\Big[(a_1 + a_2)b_1 + (a_1 - a_2)b_2\Big] \\ &\leq \sum_{a_1,a_2,b_1,b_2=\pm 1} 2\rho(a_1, a_2, b_1, b_2) = 2, \end{aligned} \tag{1.3.2}$$

where ρ is the classical probability distribution which describes the state and is fixed at preparation. To establish the inequality note that exclusively either $a_1 + a_2 = 0$ or $a_1 - a_2 = 0$. The same reasoning provides the lower bound -2. A quantum state, on the other hand, cannot be described by ρ alone because the measurement of A_i may influence the result of B_j if there is entanglement. In fact, the singlet, $\langle\cdot\rangle \to \langle\Psi^-|\cdot|\Psi^-\rangle$, with the observables $A_1 = \sigma_x$, $A_2 = \sigma_z$, $B_1 = -(\sigma_x + \sigma_z)/\sqrt{2}$, and $B_2 = -(\sigma_x - \sigma_z)/\sqrt{2}$, gives $\mathcal{B} = 2\sqrt{2} > 2$. Here, σ_i are the Pauli matrices acting on subsystem A and B respectively. The observables can immediately be interpreted as polarization measurements along different axes. There exists a similar set of observables for each of the other three Bell states such that $\mathcal{B} = 2\sqrt{2}$. For bipartite two-level systems this is the maximum possible value [76], and hence the Bell states are called *maximally entangled*. The CHSH inequality can be used as it is to test an entanglement source. The source is required to produce as many identical entangled pairs as is required to estimate the expectation values in Eq. (1.3.1) with sufficient precision. If the Bell parameter is significantly larger than 2 in the statistical sense, entangled states are produced. Otherwise no statement is possible. It follows that the source has to have an efficiency (possibly enhanced by postselection, as done, e.g., in Chap. 4) of more than $2/2\sqrt{2} \approx 71\%$. Otherwise the admixture of nonentangled pairs reduces the Bell parameter below 2 and no statement is possible although some pairs might be entangled.

As for the experiments, it turned out, unfortunately, that implementing a solid-state Bell test is an even harder task than building the Cooper pair splitter (assuming for now, that the latter works as desired in principle). At a first glance this may be surprising. Entangled pairs were captured in the lab of Freedman and Clauser as early as 1972

[15]. They used a two-photon cascade in calcium atoms to produce pairs of polarization-entangled photons and found that the CHSH inequality was violated by more than six standard deviations. In 1982, Aspect et al. conducted an even more famous experiment in which the measurement for each photon was decided on randomly and with spacelike separation in the sense of special relativity [16]. This settled the issue whether quantum mechanics is a "complete theory" in favor of quantum mechanics.

Although the principles developed with the polarization degree of freedom in mind can be adapted directly to the spin of the electron, from a practical point of view, the situation becomes much more involved when photons flying through the vacuum are to be replaced by electrons propagating in a condensed-matter system. For one thing, this is due to the quasiparticle nature of solid-state electrons I have already touched on briefly in Chap. 1.1. But with a Cooper pair splitter of sufficient efficiency and when postselecting pairs successfully retrieved from the Fermi liquid of the leads, this obstacle can probably be overcome. Furthermore, the (spin-)coherence length is on the order of microns (up to 100 μm in dilute two-dimensional electron gases [37]), whereas photons can carry entanglement over more than 100 km [20]. Any measurement device needs to be implemented on correspondingly small scales but, again, this appears to be within reach of modern fabrication technology. The major obstacle is spin detection. The equivalents of rotatable polarization filters, i.e., rotatable spin filters on the nanometer scale, are required. The best candidates are likely based on spin–charge conversion: an obvious choice are ferromagnetic contacts, the conductance of which depends on the carrier spin because the conduction band is Stoner split. But this approach requires controlling the magnetization of a tiny body and taking care of stray fields. Alternatively, a quantum dot which is occupied by a single spin-up electron with respect to an externally applied magnetic field is transparent for a spin-down electron if the doubly-occupied state is resonant with the energy of the spin-down electron. A spin-up electron of the same energy would need to be transported via an intermediate virtual triplet state, in which the two electrons occupy different orbitals and hence the energy of which is higher [77]. This type of spin filter has already been built [78], although at a magnetic field above 10 T, which is clearly in conflict with

superconductivity. But, in principle, it could be possible to integrate one filter in each lead of a Cooper pair splitter such that they can be rotated separately [79]. A more recent proposal is to inject the electron into a helical guided mode such that spin up and spin down propagate in opposite directions but meet again at a beam splitter. Different spin orientations then translate to different amplitudes for reflection and transmission [80, 81]. Yet another idea is to use (zigzag) carbon-nanotube quantum dots as spin filters. Their curvature increases the spin-orbit interaction, which is usually very weak in graphene [82, 83], and the conduction band as well as the valence band become spin split with respect to the symmetry axis of the nanotube. If, in addition, a perpendicular magnetic field on the order of 1 T is applied to break the time-reversal symmetry, the direction of spin polarization depends on the valley. In this way, four pairwise antiparallel spin-directions could be filtered with a single quantum dot and a single fixed external magnetic field [84, 85]. Four directions are enough to implement the CHSH inequality. With any type of spin filter, the joint spin-polarization probability of both electrons is converted into current correlations and can already be obtained from their zero-frequency component [86, 87]. The complete statistical information has been investigated with full counting statistics, too [88]. Nevertheless, apart from the technological challenge, there are at least two problems with CHSH measurements. First, the Bell test was designed with discrete two-valued observables in mind. Current, unlike spin or polarization, is a continuous unbounded observable. It needs to be checked that the spin values S_z extracted from the current measurement are always $+1$ or -1, i.e., that the variance of S_z^2 vanishes. Otherwise a violation of the Bell inequality is possible without entanglement. This check requires fourth-order correlation measurements [89]. Furthermore, the question arises, how to pick two electrons which actually belong to the same Cooper pair for the correlation measurements. Even very low currents on the order of a few picoampere consist of millions of electrons per second. Correlation measurements have to be conducted with a correspondingly high time resolution. The less time there is to average over, the more of a problem background noise due to the Fermi sea becomes. This complicates the correlation measurements considerably, in particular those in fourth order. There is a large number of proposals for measuring the Bell inequality with spin filters [81, 86, 88, 90, 91] but when it

comes to experiments, in short, electronic Bell tests appear to be quite a formidable challenge for the time being.

1.3.2 Indirect methods

The proposals for entanglement detection in this thesis approach the problem from a different angle than from the Bell inequalities, as do a number of other publications in the field. Very broadly speaking, the idea is to construct a device in which a specific observation can only be explained convincingly if it is assumed that the two electrons under investigation form a nonlocal singlet state. This opens up a vast number of new possibilities but it comes with three major caveats.

The first caveat is fundamental: whatever the specific test, it is not meant to prove fundamental properties of nature. In the language of Bell tests, this means that there are gaping loopholes, which allow for an interpretation of the measurement outcome in terms of a local realistic theory. Within the solid state community, few people care because, really, almost everybody believes in quantum mechanics and so if we can prove that we can produce nonlocal singlets, entanglement is merely a consequence. In Chap. 4, I suggest to convert split Cooper pairs to photons and to use a CHSH Bell test on *them*. The Bell test will be able to detect the photons' entanglement just fine without, e.g., the communication loophole. This is actually the main motivation — use the technology which is readily available in the optics community. But the solid-state device which converts Cooper pairs into photons is extremely small and arguably the electrons from which the entanglement is supposed to originate are never really separated.

The second caveat is technical: as opposed to the Bell inequality, it is almost impossible to prove (and to my knowledge it has never been attempted in a single proposal) that there might not be an alternative explanation for whatever the proposed signature. This is because whereas Bell's argument uses only statistics and the axioms of quantum mechanics, other detection schemes rely more or less heavily on a specific model to describe a particular solid-state device. In other words, a certain amount of trust is required. Ultimately, it is a question of personal judgment how convincing the signature is deemed to be. The

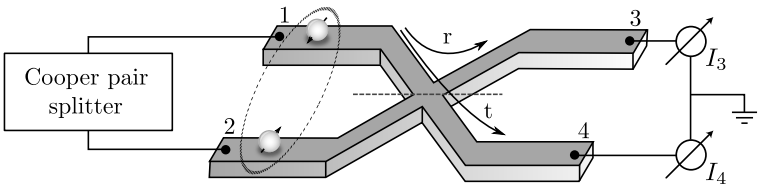

Figure 1.3: Electronic beam splitter. In a four-terminal structure, two electrons are incident from leads 1 and 2. At the crossing they can either be reflected, $1 \to 3$, $2 \to 4$, with amplitude r or transmitted, $1 \to 4$, $2 \to 3$, with amplitude t. Backscattering into lead 1 or 2 is neglected. Distinguishable particles, e.g., opposite-spin electrons, are scattered independently. The orbital wave function of a spin-singlet, however, is symmetric and both electrons have an increased probability to leave in the same lead (bunching). Conversely, the orbital wave function of a spin triplet is antisymmetric and its two electrons cannot enter the same lead (antibunching). While this has no influence on the average current, it affects the current noise. Hence, bunching is an indirect signature of entanglement.

Tomonaga–Luttinger liquid beam splitter presented in Chap. 5 offers the exciting possibility to detect entanglement via collective excitations caused by electron–electron interactions in one-dimensional wires. Obviously, if one doubts that the nanowire device under investigation is adequately described as a Tomonaga–Luttinger liquid, this detection scheme appears deeply flawed.

The third caveat is practical: there is a tendency for the proposed devices to be rather complex hybrid structures. In this way, the problems of noise measurements and spin filters are traded for difficulties in manufacturing the device itself. This is not a bad thing. The more diverse the challenges are, the more likely it is that somebody can at some point solve one of them. In Chap. 3, I deliberately avoid this issue by extracting signatures of nonlocal transport from a robust observable which has already been measured in a device which has already been built: the critical Josephson current through a double quantum dot between superconducting leads [92].

In spite of these restrictions, while a conclusive solid-state Bell test

might provide the only definite answer, it is certainly worth investigating alternative approaches in the meantime. A very common strategy employs the orbital symmetry of the two-particle wave function under particle exchange, which is a unique property of the singlet state. Its spin wave function is odd so the orbital wave function has to be even. All of the three triplet states or all of the other three Bell states have an even spin wave function and so an odd orbital wave function. Hence the two electrons of a singlet can be put in a single place while the electrons of a triplet cannot. Based on this, Burkard et al. designed a scheme in which a singlet can be identified by scattering initially separated electrons at an electronic beam splitter [41]. The essence of their argument is (slightly different from how they present it) the following: the simplest possible beam splitter is a symmetric device with two ingoing and two outgoing leads (Fig. 1.3). With noninteracting (quasi)particles, we can describe the dynamics of this structure to all orders with an s-matrix [93], such that

$$\begin{pmatrix} a_{3\sigma} \\ a_{4\sigma} \end{pmatrix} = \begin{pmatrix} r & -t \\ t & r \end{pmatrix} \begin{pmatrix} a_{1\sigma} \\ a_{2\sigma} \end{pmatrix}, \tag{1.3.3}$$

where $a_{i\sigma}$ annihilates quasiparticles with spin σ in lead i and where $r, t \in \mathbb{R}$ are the amplitudes for reflection and transmission at the beam splitter. To ensure unitarity, $r^2 + t^2 = 1$. A nonlocal singlet S or a nonlocal entangled triplet T_0 incident from channels 1 and 2 is $|S/T_0\rangle = \frac{1}{\sqrt{2}}(a^\dagger_{1\uparrow}a^\dagger_{2\downarrow} \mp a^\dagger_{1\downarrow}a^\dagger_{2\uparrow})\,|\rangle$ with $|\rangle$ the Fermi sea. Using the relation (1.3.3), we can rewrite these states in the basis of outgoing modes as

$$|S\rangle = \Big[-\sqrt{2}rta^\dagger_{3\uparrow}a^\dagger_{3\downarrow} + \sqrt{2}rta^\dagger_{4\uparrow}a^\dagger_{4\downarrow} + \frac{r^2-t^2}{\sqrt{2}}(a^\dagger_{3\uparrow}a^\dagger_{4\downarrow} - a^\dagger_{3\downarrow}a^\dagger_{4\uparrow}) \Big]\,|\rangle \tag{1.3.4}$$

$$|T_0\rangle = \frac{1}{\sqrt{2}}\Big(a^\dagger_{3\uparrow}a^\dagger_{4\downarrow} + a^\dagger_{3\downarrow}a^\dagger_{4\uparrow}\Big)\,|\rangle\,. \tag{1.3.5}$$

With this, we can calculate immediately the expectation value $\langle\cdot\rangle \equiv \langle S/T_0| \cdot |S/T_0\rangle$ of the current in, say, lead 3, which is proportional to the expectation value of the number operator $\langle I_3\rangle \sim \langle n_3\rangle = \langle \sum_\sigma a^\dagger_{3\sigma}a_{3\sigma}\rangle = 1$ for both singlet and triplet (because $r^2 + t^2 = 1$). This is also exactly what one would expect if two uncorrelated particles scatter independently into two leads. So the (average) current cannot be employed

to detect entanglement. This is true quite generally for Fermi-liquid systems as I will demonstrate in Chap. 5. Progress can be made, however, when considering the current noise. Eq. (1.3.5) shows that the electrons of a triplet $|T_0\rangle$ never leave in the same lead — they cannot because their orbital wave function is antisymmetric. Therefore their scattering state is *noiseless* at zero temperature. Burkard et al. referred to this behavior as *antibunching*. For the singlet $|S\rangle$, on the other hand, we see that for $r = t$ the electrons *always* enter the same lead. They *bunch* and the state has more noise than the standard Schottky noise of uncorrelated electrons for which the probability of bunching is $2r^2t^2 \leq 1/2$. By calculating the variance $\langle n_3^2\rangle - \langle n_3\rangle^2$ we can easily verify that for any r, t the noise of the singlet is twice as large as the noise of uncorrelated spin anti-parallel electrons. Burkard et al. derived this result in the slightly more general case of dispersive leads with the Landauer-Bütticker formula [93]. Unsurprisingly, (anti)bunching emerges only if the two electrons are injected at the same energy such that they actually have orbital overlap after having scattered into the same lead. The considerations also generalize nicely to include backscattering, multimode leads and wave-packet injection [94–97] as well as inelastic scattering [98] with essentially the same result: given orbital overlap, the singlet contribution of an incoming state can be obtained from its zero-frequency current noise. The scattering statistics were analyzed beyond second order using full counting statistics [99]. The higher cumulants change, too, when the state is a singlet or a triplet instead of a product state. But in order to distinguish the entangled triplet from nonentangled triplets, spin-dependent measurements are required, e.g., spin-polarized counting statistics. This shows that an analysis based only on bunching and antibunching is fundamentally limited. It is only conclusive if the entanglement comes as a singlet contribution to the state under investigation and so at best a lower bound on the total entanglement can be established.

Bunching and antibunching in two-dimensional electron gases has been speculated about by Maître et al. [90]. In beam splitters made from carbon nanotubes, spin-orbit interaction and external magnetic fields lead to a rich scattering behavior at low energies [85] but further means to characterize the states beyond singlet, triplet, and spin anti-parallel product states have not been found. While a beam splitter and a

Cooper pair splitter have not yet been successfully implemented in a single device, antibunching of spin-parallel electrons has been demonstrated with beam splitters made from highly ballistic edge channels [100, 101]. These experiments are referred to as *electron optics* [102], which is fitting because, of course, the idea of bunching and antibunching is borrowed from optics, were (boson) statistics were observed as bunching in the Hanbury-Brown-Twiss experiment [103] and as a dip in Hong-Ou-Mandel interferometry [104].

Since the invention of the Cooper pair splitter in 2001, the extent to which single spins confined in quantum dots or two spins confined in a double quantum dot can be controlled has grown enormously. This development is driven mostly by the spin qubit community. Scherübl et al. proposed [105] to prepare a known two-spin state in a double quantum dot, then bring the dots into resonance with a nearby superconductor for a certain amount of time, and measure the final occupation. A Cooper pair should not be able to tunnel onto the quantum dots — assuming that it remains in a spin-singlet state — if the double quantum dot was prepared as a triplet, so its charging state stays (1,1) with unit probability. On the other hand, if the quantum dots are prepared in the singlet state, the final charging state will be (2,2) if the time over which the double quantum dot is in resonance with the superconductor is half a Rabi cycle. With the current experimental techniques it appears feasible to interpolate between these situations. This produces a characteristic dependence of the final charging state on the initial configuration, or, put differently, the current out of the Cooper pair splitter is the quantity of interest instead of the noise which is measured in beam-splitter setups. An approach based on filtered currents was also proposed by Braunecker et al. [84]. They consider the quantum dots of the Cooper pair splitter to be made from a carbon nanotube, as, e.g., in Refs. 58 and 66, but, different to existing implementations, the nanotube is assumed to be bent such that the symmetry axis of the nanotube is different in each dot. Then, the spin-orbit interaction together with an external magnetic field lifts all degeneracies such that the quantum dots become spin filters with two mutually different axes as I discussed before. This opens up the way for a CHSH measurement. One of four different spin directions can be chosen on each quantum dot by bringing the respective levels into resonance via gate voltages,

such that there are 16 configurations in which mostly spin-polarized current flows out of the superconductor. It is not possible, however, to isolate the desired nonlocal current due to crossed Andreev reflection from parasitic local pair currents. Nevertheless, in certain parameter regimes the admixture of entangled pairs will be sufficiently large that a violation of the Bell inequality should be observable even without correcting for local currents. As of yet, this regime has not been reached experimentally, though.

Finally, the combination of quantum optics and Cooper pair splitting is a promising approach. The quantum dots are assumed to be coupled to the electromagnetic field in a microcavity or in a nanocavity [106]. Different types of coupling allow for different types of entanglement detection. Generally speaking, two schemes have emerged.

In the first type, the optical properties of the system are used to extract indirect information on the singlet nature of the Cooper pair injected onto the quantum dot, e.g., a specific shift in the resonance frequency of the cavity. This is very similar in spirit to the approach of Scherübl et al., who use control over the spins in the double quantum dot to transfer information about the singlet into the final charging state. In carbon-nanotube quantum dots, the electric field couples to the electron spin via the spin-orbit interaction. This can induce local spin flips and allows for an optically induced singlet–triplet transition [107]. Interestingly, the sign of the matrix element for this process depends on which dot is coupled more strongly to the cavity because the singlet is odd under exchange. Hence it vanishes in a symmetric setup. It has been predicted that the lasing threshold of the cavity is a sensitive indicator of the size of the singlet–triplet transition amplitude [107]. In addition, the resonance frequency of the cavity shifts depending on the average occupation of the quantum dots [108]. Conversely, exciting the transition by microwave irradiation, a characteristic current response in the splitter is obtained [108, 109].

In the second type of scheme, the spin entanglement itself is transferred to a pair of polarization-entangled photons. This sets the stage for a conventional optical Bell test. If the Cooper pair splitter is the only conceivable source of entanglement in the setup, observing that the photons violate a Bell inequality implies that the electrons were

entangled. Again, different coupling mechanisms allow for different conversion strategies. Nigg et al. suggested a driven scheme [110], in which first valence band levels of the quantum dots are brought into resonance with the superconductor and populated with a nonlocal singlet. Afterwards the electrons are optically excited into the conduction band. The linewidth of the cavity is chosen such that the electrons relax into a third band which is not spin degenerate but polarized. So depending on the spin of the injected electron, either a spin flip is required or not, which results in the emission of a linear or a circular polarized photon. If the injected two-electron state is entangled, the photons are emitted in a polarization-entangled state (in an unconventional basis), which can be detected with a standard optical CHSH measurement. Simultaneously, we proposed a different scheme, which I discuss in detail in Chap. 4. It does not require driving but relies on electron–hole recombination in a p–n junction. Here the selection rules ensure that if a spin-up electron and a spin-down hole recombine, a right-circular photon is emitted. If a spin-down electron and a spin-up hole recombine, a left-circular photon results. Again, the resulting photon state is entangled provided that the electrons remain spin entangled when split. Both proposals require the superconductor to couple to the valence band of the quantum dots, i.e., p-type superconductivity. Hybrid devices of superconductors, semiconductors, and optical elements are challenging to fabricate but not out of reach [111–114].

1.4 About this thesis

This thesis aims at contributing to both Cooper pair splitting and to entanglement detection. I will present one new Cooper pair splitter which requires neither energy filtering nor Coulomb blockade to split the electrons (although it still requires interactions to establish entanglement in the superconductor, of course), and three detection schemes, based on the Josephson effect, on the Bell inequality, and on spin–charge separation, respectively. This happens to be chronologically reversed but I feel that it is the most natural order. The chapters are mostly independent, however, and can be read in any order.

Chap. 2 is based on Ref. 115. I investigate a bilayer-graphene sheet which contains a domain wall between two regions of different stacking order or opposite interlayer potential. Along such domain walls, valley-chiral one-dimensional modes emerge. If a superconductor is brought close to the channel, Cooper pairs can tunnel into it, and their two electrons move in opposite directions because time-reversal symmetry dictates that they belong to different valleys. This way of Cooper pair splitting is purely kinematic and requires neither energy filters nor Coulomb repulsion. As long the valley isospin is preserved, i.e., in the absence of atomic-scale disorder, it is robust. I present a material-specific effective normal/superconducting/normal (NSN) model of the one-dimensional channel close to the superconductor and extract the conductance carried by spin-entangled, split electron pairs. Notably, Cooper pair splitting is equivalent to local Andreev reflection in this setup. So far, NSN junctions have only been analyzed with respect to crossed Andreev reflection in this context. In addition, entangled electrons can be obtained only if the amplitude of local Andreev reflection is small, whereas often unit-efficiency Andreev reflection is pursued.

In Chap. 3, following Ref. 116, I present the first of three strategies for entanglement detection. In contrast to the other schemes, which are proposals, this one is based on an experiment performed by the Tarucha group [92]. They studied the critical current through a double-quantum-dot Josephson junction, i.e., through two quantum dots which are embedded in parallel between two superconducting leads and identify signatures of nonlocal transport, where one electron of a Cooper pair tunnels through each quantum dot. I consider a model of the setup which can reproduce this behavior, both in the limit of narrow-band superconductors, which can be investigated exactly, and in the limit of wide-band superconductors, which is accessible by perturbation theory. Interactions on the quantum dots are treated exactly in both cases. In addition, I discuss a new signature of nonlocal transport, which is based on the valence electrons of the quantum dots surprisingly undergoing a tunable phase transition between nonlocal singlet and nonlocal triplet if the superconducting gap is not too large. The results of Chap. 3 were obtained in close collaboration with B. Probst and F. Domínguez. In particular, B. Probst performed the diagrammatic calculations and F. Domínguez contributed the numerical treatment of the multi-level

model.

Chap. 4 actually proposes to use a Bell test but only after the electronic entanglement has been transferred onto photons as presented in Ref. 117. It is crucial that the entanglement is, indeed, transferred and not merely encoded in the photons. If correlations remain between the photons and the electrons, decoherence in the electronic subsystem destroys the entanglement of the photons. This requirement is trivially met if the electronic subsystem returns to its initial state after one emission cycle. This is achieved in a superconducting p–n junction in which the n and the p side are connected through two optical quantum dots, which are embedded in a photonic nanocavity each. A Cooper pair from the n side is split onto the two dots, the electrons relax into the valence band emitting a photon each, and the pair is absorbed coherently into the p-side superconductor. Provided that the electrons remain spin entangled while split across the quantum dots, the photons are polarization entangled. I describe how a CHSH measurement can be used to detect the entanglement over a range of microscopic parameters, even though imperfections and parasitic processes are inevitable in this scheme.

Finally, Chap. 5 deals with maybe the most exotic effect (apart from entanglement itself). I argue that spin–charge separation can be used to detect entanglement. In an electronic beam splitter realized as a tunnel contact between two one-dimensional conductors like nanowires or quantum-Hall edge states, the average current measured after the crossing is different for singlets, triplets, and product states. This is a remarkable non-Fermi-liquid feature since noninteracting beam splitters do not exhibit signatures of entanglement in the current. This one-dimensional system is modeled as a spinful Tomonaga–Luttinger liquid instead, which describes interactions exactly. The current may be easier to access than noise, which is traditionally employed to detect entanglement and which is further suppressed by the interactions. This chapter is based on Ref. 118.

2

Splitting Cooper Pairs in Bilayer Graphene

Until now, all of the experimentally realized Cooper pair splitters rely on Coulomb repulsion. This is somewhat surprising because there are three natural aspects in which the two electrons of a Cooper pair differ: they have opposite spin, opposite energy, and opposite momentum. Neither, however, is readily employed in a splitting mechanism: spin filtering destroys the entanglement, energy filtering does not work at zero bias, and momentum is vulnerable to disorder. While the first two are rather fundamental limitations, disorder can in principle be dealt with. Prada and Sols proposed to embed a potential double barrier in a long interface between a two-dimensional superconductor and a two-dimensional electron gas [119]. Ideally, the interface is then transparent only for electrons with certain quantized perpendicular momenta k_x and at any given energy $E \sim \sqrt{k_x^2 + k_y^2}$, the magnitude of the momentum parallel to the interface, $|k_y|$, is fixed, too. Since translational invariance along the interface is retained, the electrons of a Cooper pair still come at opposite momenta $\pm k_y$ and can be transmitted simultaneously with momenta $(k_x, \pm k_y)$ if the barrier is transparent close to the Fermi energy in the superconductor. They leave the interface in different directions forming a V shape with a well-defined angle and can possibly be collected individually from the electron gas at two spatially separated terminals. Obviously, a large number of V shapes overlap, shifted along the interface, unless the emission happens only within a narrow region along the y direction. This is in conflict with the infinitely long interface required for momentum conservation along the y axis but the

authors estimate that a decent intermediate regime can be found. Another problem is that sufficiently strong disorder in the normal-state electron gas completely breaks the filtering mechanism because electrons are scattered into the wrong terminal or miss it altogether.

At this point, it is worth considering Cooper pair splitting in the context of new materials with properties different from the ordinary electron gas. I already discussed the role of topological insulators in Chap. 1, which host helical edge states: they come with an intrinsic protection against disorder scattering (as long as the time-reversal symmetry is not broken) but, precisely due to helicity, it is difficult to achieve spin-oblivious splitting, which is required for entanglement. In this chapter, I will focus on graphene. Similar to quantum spin-Hall states, the low-energy spectrum of graphene has a linear dispersion relation but, in contrast to quantum spin-Hall states, graphene is two dimensional and spin degenerate. In addition, the two inequivalent valleys K and K', or $K_\pm = \pm(4\pi/3a, 0)$, where $a = 2.46$ Å is the graphene lattice constant, provide another degeneracy in the dispersion relation of graphene [120]. Since the valleys are separated by the entire Brillouin zone, scattering between them requires disorder on the atomic scale. This means that, in sufficiently clean sheets, scattering between the valleys is strongly suppressed away from the sample edges. This holds even in the presence of external electromagnetic fields because, viewed on the atomic scale, they are smooth. Then, the valley index is simply another conserved quantum number. Apart from disorder, superconductivity couples both of the valleys [121, 122]. This is because the two electrons of a Cooper pair have opposite momenta, i.e., they reside at opposite ends of the Brillouin zone, not simply at opposite relative momenta with respect to one Dirac point. In an Andreev-scattering picture, which is much more common in the graphene community, Andreev reflection mixes an electron and a hole with the *same* momentum, energy, and spin. But again, in order to create a hole with a large positive momentum close to valley K, an electron has to be removed which contributes a large *negative* momentum, i.e., an electron from valley K'. The observation that the valleys are connected by superconductivity but conveniently remain isolated otherwise is the central idea of the graphene based Cooper pair splitter. Opposite valleys do not, however, directly imply opposite sense of motion. Since the dispersion

relation is rotationally invariant around each of the Dirac points, within each valley carriers can move in any direction. So we are still facing the same problem as Prada and Sols. The challenge is to establish a splitting mechanism based on the valley quantum number and, as always, to promote it over competing channels. Cayssol proposed [48] a graphene/superconductor/graphene structure, where the Dirac point is higher in energy by V_{RL} in the right graphene region than in the left region. So an electron incident from the left graphene region at energy V_{RL} cannot be transmitted to the right region because there its energy is right at the Dirac point where the density of states vanishes. If, in addition, the Fermi energy is $V_{RL}/2$ above the Dirac point in the left region (i.e., at $V_{RL}/2$ below the Dirac point in the right region), local Andreev reflection is suppressed by the same mechanism: the incident electron at energy V_{RL} is above the Fermi level by $V_{RL}/2$. But the hole with energy $V_{RL}/2$ is an electron missing at the energy $V_{RL}/2$ below the Fermi sea, which is again at the Dirac point and so the process is not possible. This behavior indeed allows for Cooper pair splitting and has a special noise signature [123]. The disadvantage is that this scheme works only in a carefully chosen energetic configuration. Linder et al. were able to relax this restriction [49], only, however, at the expense of introducing ferromagnetic leads, i.e., spin filtering, which defeats the purpose of entanglement generation. Gómez et al. proposed a device, which, too, is based on a graphene/superconductor/graphene junction [124]. The "superconductor", which is actually a region in the sheet of graphene with a proximity-induced pairing amplitude, will be n-type doped because it is close to the real metallic superconductor which causes the proximity effect. So when the normal regions are p-type doped due to suitably applied gate voltages, a p–n–p junction results. Electrons crossing a p–n junction in graphene experience negative refraction [125] so the n region serves as a Veselago lens [126]. But if an incident electron is converted into a hole by an Andreev process, this effect is canceled and ordinary refraction occurs. This leads to transmitted electrons and Andreev-transmitted holes having different focal points and hence being separated in space.

Graphene has attracted attention unlike any other new material in the last years. This is, of course, mainly due to its unconventional band structure, but probably also because it can be modeled quite accu-

rately in a tight-binding approach with well-justified approximations [127] so that the low-energy Dirac Hamiltonian is simple to deal with and yet sufficiently accurate to make quantitative predictions. I will, however, suggest to use bilayer graphene. Bilayer graphene is arguably even more exciting than monolayer graphene: it has the more common quadratic dispersion at low energies but while, like in monolayer graphene, the carrier density can be controlled by applying a uniform gate voltage, the band gap in bilayer graphene can be tuned, too, by applying a voltage *between* the two layers. If both layers are held at the same potential, bilayer graphene is gapless like monolayer graphene. This allows for smooth electrostatic confinement in contrast to monolayer graphene, where it is thwarted by Klein tunneling [122]. Smooth electrostatic confinement potentially induces less scattering than the alternative sharp sample edges, which is highly desirable for coherent transport. Being a more complex system, however, tractable low-energy models of bilayer graphene are less accurate then models of the monolayer. In both cases a nearest-neighbor tight-binding model is constructed from the $2p_z$ orbitals and expanded around the Dirac points K and K'. The bilayer unit cell, however, contains four carbon atoms whereas the monolayer unit cell contains only two. This has two implications: first, there are three additional interlayer hopping matrix elements, $A_1 \leftrightarrow A_2$, $B_1 \leftrightarrow B_2$, and $A_1 \leftrightarrow B_2$, where A_i and B_i label the two inequivalent atoms in layer i. I will only consider Bernal stacking, where B_1 is aligned directly below A_2 and so the interlayer hopping is dominated by the amplitude $t_{B1\leftrightarrow A2} \sim 0.1 t_{Ai\leftrightarrow Bi}$. Neglecting the skew couplings, as is often done, is therefore a valid approximation but will not go completely unnoticed. E.g., the hopping amplitude $t_{A1\leftrightarrow B2}$ introduces trigonal warping [128], which I will discuss when considering the microscopic model of the bilayer graphene Cooper pair splitter. Second, the resulting low-energy model has four bands, two of which are often integrated out [129]. This is a particularly good approximation for the bilayer graphene Cooper pair splitter because it relies on transport only below the superconducting gap. The higher-energy bands are separated from the lower-energy bands by the interlayer coupling $t_{B1\leftrightarrow A2} \sim 300$ meV, which is substantially larger than any conventional superconducting gap energy $\Delta \lesssim 1$ meV. Graphene as well as bilayer graphene have the additional benefit of small spin-orbit interaction and few nuclear spins [130–132]. This allows for long spin-coherent trans-

port.

Martin et al. discovered a particularly powerful way to create electrostatic confinement in bilayer graphene [133]. At a domain wall between two regions of opposite interlayer voltage, one-dimensional zero modes emerge, which are valley chiral, i.e., carriers in opposite valleys move in opposite directions. Specifically, there are four subgap zero modes in each valley, which form spin-degenerate pairs. In contrast, ordinary confinement in an ungapped region with zero interlayer voltage by two gapped regions with equal finite interlayer voltage produces neither zero modes nor chirality. Valley chirality ensures that left and right moving modes are separated as far as possible in the periodic Brillouin zone which provides the best protection possible against backscattering in terms of momentum. It means that only extremely short-ranged scatterers, i.e., atomic-scale defects, can lead to backscattering. This is reminiscent of the zero modes which emerge at the edge of topological insulators or, more generally, at domain walls between topologically trivial and topologically nontrivial regions [134]. E.g., in the quantum spin-Hall effect, zero modes emerge which are protected against backscattering because they are helical, i.e., spin chiral. As long as time-reversal symmetry is not broken, backscattering is not allowed. In the case of the bilayer-graphene channels, the valley isospin symmetry prevents backscattering. A Chern number can be defined separately for each valley which changes by two across the domain wall indicating the presence of two zero modes [133]. Both valleys have opposite Chern numbers, so when the complete Brillouin zone is taken into account, bilayer graphene is always topologically trivial. This lead Li et al. to refer to bilayer graphene as a *marginally topological* material [135]. The topological nature of the channel implies that it emerges irrespective of the precise shape of the interlayer voltage as long as it changes sign. One illustrative difference to ordinary topological materials is that there are no topologically protected edge modes at the sample boundaries, i.e., at the interface between the marginally topological bilayer graphene and the topologically trivial vacuum: the vacuum has no meaningful valley quantum number. Hence, it depends on the exact boundary conditions, e.g., on how the lattice is terminated, whether edge states exist and, if so, how many. Topological modes in the bulk of bilayer graphene have already been observed with mean free

paths over several hundreds of nanometers, which clearly shows their robustness against backscattering. Ju et al. identified smooth tilt-shift boundaries in a bilayer graphene sheet, i.e., domain walls between AB stacking and BA stacking, in near field microscopy [136]. Changing the stacking order in a uniform field has been predicted to be almost identical to changing the direction of the field in a uniformly stacked sample [137, 138]. Having contacted the ends of a stacking boundary, Ju et al. observed electronic subgap transport consistent with the theoretical predictions.

Valley chirality is just what is needed to turn the fact that Cooper pair electrons have opposite momentum and hence belong to different valleys into a splitting mechanism. With valley-chiral guided modes, momentum-based splitting does not rely on ballistic transport anymore. It is even conceivable to build an electron optics-like setup in which the Cooper pair splitter and a beam splitter for entanglement detection are integrated in the same device because electrostatically-defined channels allow for a high degree of control.

The setup I will discuss is shown in Fig. 2.1(a). A large sheet of bilayer graphene hosts a valley-chiral channel at a domain wall defined by electrostatic gating or by a stacking boundary, which is contacted by normal metal leads at both ends. In between, a superconducting contact is brought close to the channel. When a voltage bias smaller than both the superconducting gap and the bilayer graphene bulk band gap is applied between the superconductor and the normal contacts, Cooper pairs tunnel through the isolating bulk of the bilayer graphene sheet into the channel. Since the two electrons of the pair belong to different valleys, they propagate in opposite directions and are split kinematically without energy filtering and without Coulomb repulsion. They remain spin entangled and finally enter opposite contacts.

2.1 Effective scattering description

Without going into the microscopic details, insight can already be gained from an ad-hoc effective one-dimensional model. The guided mode has three regions [Fig. 2.1(a)]: in the left region and in the right

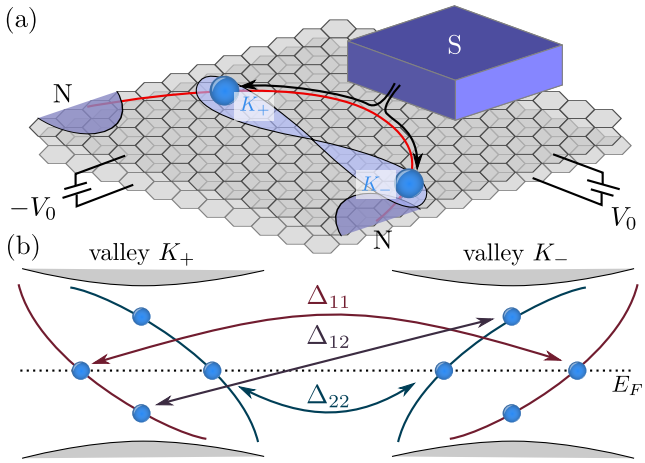

Figure 2.1: (a) At a domain wall (red) in bilayer graphene between different interlayer voltages $\pm V_0$ or different stacking order, a topological valley-chiral channel forms. Cooper pairs tunneling into it from a nearby s-wave superconductor (S) are split because the two electrons belong to opposite valleys $K_\pm$ and thus have opposite velocities. They remain spin entangled and propagate to separate normal leads (N). (b) In each valley, two subgap modes along the domain wall emerge. Energy and momentum conservation along the NS interface fix four points in the spectrum where Cooper pairs are injected. Figure and caption reproduced from the original publication, Ref. 115.

region, it is sufficiently far away from the superconductor to be in the normal state. Close to the Fermi surface it will have a linear dispersion $\epsilon(k) \approx \pm v_F k$ with positive velocity $\partial\varepsilon/\partial k = +v_F$ in valley K and with negative velocity $\partial\varepsilon/\partial k = -v_F$ in valley K' such that we can suppress the momentum quantum number in favor of energy. The corresponding hole spectrum $-\varepsilon(-k)$ is obtained by mirroring the dispersion at the $k = 0$ axis and at the $\varepsilon = 0$ axis, where k denotes the momentum along the channel and ε denotes the energy relative to the chemical potential of the superconductor. As a consequence, electrons and holes within the same valley move in opposite directions. The central region is close to the superconductor so the proximity effect [139] induces a finite pairing amplitude Δ, which mixes electron and hole states such that a gap opens at the Fermi level, $\varepsilon = 0$. The resulting normal/superconducting/normal structure is depicted in Fig. 2.2. In the operation mode as a Cooper pair splitter, the N regions are attached to leads at a chemical potential (for electrons) lower by $\delta\mu$ than the chemical potential in the superconductor. Hence, the incoming modes, which propagate from the reservoirs towards the superconducting region are empty between energies $-\delta\mu < \varepsilon < 0$. Equivalently, in an electron–hole picture, where we consider only positive-energy excitations, the incoming hole states at energies $0 < \varepsilon < \delta\mu$ are filled. It is desirable to work in an electron–hole picture instead of an electron-only picture because the particle number is conserved in both ordinary and superconducting scattering processes. When a hole at energy ε reaches the superconducting region, four different events are possible: first, the hole can be transmitted through the superconducting region with the amplitude $t_{hh}(\varepsilon)$ or, second, reflected with the amplitude $r_{hh}(\varepsilon)$. But since we assume that the valley is preserved and because the guided mode is valley chiral, reflection is not possible, $r_{hh} = 0$. This assumes that the transition from the normal region to the superconducting region is sufficiently smooth, too, such that it does not induce intervalley scattering. Indeed, in the microscopic derivation we will find that the induced superconductivity decays on the scale of several tens of nanometers, which is substantially larger than the lattice constant of a few angstrom. Third, the hole can be transmitted as an electron with amplitude $t_{eh}(\varepsilon)$, or, fourth, reflected as an electron with amplitude $r_{eh}(\varepsilon)$. The latter two processes are crossed Andreev reflection and local Andreev reflection, respectively. But because the valley is

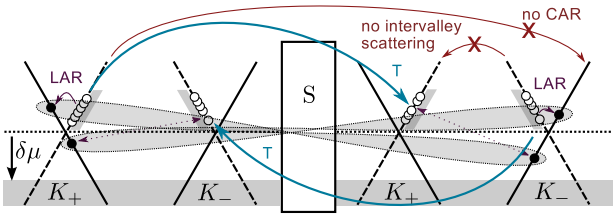

Figure 2.2: Scattering interpretation of Cooper pair splitting. Incoming holes (open circles) filled up to the bias $\delta\mu$ are transmitted (T) or undergo local Andreev reflection (LAR). Reflection and crossed Andreev reflection are zero by valley chirality. Local Andreev reflection creates an outgoing electron (filled circle) on the same side and no outgoing hole on the opposite side, i.e., an electron of opposite spin, momentum, and energy (dashed arrow), which are spin entangled (text). Figure and caption reproduced from the original publication, Ref. 115.

preserved and because electrons and holes in the same valley move in opposite direction, only local Andreev reflection is possible, whereas crossed Andreev reflection vanishes, $t_{eh} = 0$. This appears to be at odds with the aim to build a Cooper pair splitter. The identification of crossed Andreev reflection with Cooper pair splitting is widely acknowledged [43–45, 48–50, 58, 61, 63, 64, 123, 140] and maximizing the amplitude of crossed Andreev reflection is pursued by many authors.

While it is a natural assumption that nonlocal entangled pairs are produced always by nonlocal, i.e., crossed, Andreev reflection, it turns out not to be correct. The process *competing* with Andreev reflection is equally important. In the situation under discussion, there is only one such competing channel: unless the incoming hole is locally Andreev reflected as an electron, it is transmitted through the superconducting region as a hole. The important observation is that if the spin-s hole at energy ε is Andreev reflected as a spin-s electron at energy ε, no hole is transmitted to the other side of the superconducting region. The absence of the spin-s hole at energy ε implies an additional spin-$-s$ electron to be present at energy $-\varepsilon$. These two electrons form the split Cooper pair. The process happens coherently with either spin so, in

fact, the outgoing state is a spin singlet. In this situation, the nonlocality is contributed not by the Andreev process but by the competing process, normal transmission. Just the other way around, conventional Cooper pair splitters suppress transmission and local Andreev reflection by energy filtering or by Coulomb repulsion. In this case, nonlocal crossed Andreev reflection competes with local ordinary reflection. By this reasoning, Cooper pair splitting is not expected to work if the two local processes, i.e., ordinary reflection and local Andreev reflection compete. And in fact, it does not work, either, if the two nonlocal processes, transmission and crossed Andreev reflection, compete. To see this, as well as the singlet nature of the resulting pairs, I will repeat the argument in a formal way.

As I argued before, due to the chemical potential in the leads attached to the left and to the right normal regions, all incoming holes up to energy $\delta\mu$ are filled in the scattering state

$$|\Psi\rangle = \prod_{\substack{0<\varepsilon<\delta\mu \\ \alpha s}} h^{\alpha\dagger}_{s,\mathrm{in}}(\varepsilon)\,|\rangle \equiv \prod_{\substack{0<\varepsilon<\delta\mu \\ \alpha s}} c^{\alpha}_{s,\mathrm{in}}(-\varepsilon)\,|\rangle\,, \tag{2.1.1}$$

where $|\rangle$ denotes the quasiparticle vacuum with respect to the chemical potential of the superconductor and $h^{L/R\dagger}_{s,\mathrm{in}}(\varepsilon) \equiv s c^{L/R}_{-s,\mathrm{in}}(-\varepsilon)$ creates an incoming hole with spin s at energy ε in the left/right region. This is the same as removing an electron with opposite spin $-s$ at energy $-\varepsilon$. The valley index is implicit by the requirement that the incoming modes move towards the superconducting region and momentum is unambiguously related the energy ε. If there was no superconductor, all incoming holes would be transmitted as holes through the central region, $h^{\alpha\dagger}_{s,\mathrm{in}} = h^{\bar{\alpha}\dagger}_{s,\mathrm{out}}$, where $\bar{\alpha}$ is the side opposite of α. So in the state $|\Psi\rangle$ all electronic states between $-\delta\mu < \varepsilon < 0$ are empty and $|\Psi\rangle$ really is a Fermi sea with the chemical potential $-\delta\mu$. Prada and Sols [141] and Samuelsson et al. [142] realized independently that this redefinition of the Fermi sea is a key ingredient to connect Cooper pair splitting and Andreev reflection. We define this state as

$$|\rangle_{\delta\mu} := \prod_{\substack{0<\varepsilon<\delta\mu \\ \alpha s}} c^{\alpha}_{s}(-\varepsilon)\,|\rangle\,. \tag{2.1.2}$$

Here and in the following I drop the subscript 'out' if it is clear from the context. In the general case, the superconducting region allows

for the four scattering processes transmission (t_{ee}, t_{hh}), reflection (r_{ee}, r_{hh}), local Andreev reflection (r_{he}, r_{eh}), and crossed Andreev reflection (t_{he}, t_{eh}) and the relation between the incoming-state basis and the outgoing-state basis is more complicated,

$$\begin{pmatrix} c^L_{s,\mathrm{out}} \\ h^L_{s,\mathrm{out}} \\ c^R_{s,\mathrm{out}} \\ h^R_{s,\mathrm{out}} \end{pmatrix} = \begin{pmatrix} r_{ee} & r_{eh} & t_{ee} & t_{eh} \\ r_{he} & r_{hh} & t_{he} & t_{hh} \\ t_{ee} & t_{eh} & r_{ee} & r_{eh} \\ t_{he} & t_{hh} & r_{he} & r_{hh} \end{pmatrix} \begin{pmatrix} c^L_{s,\mathrm{in}} \\ h^L_{s,\mathrm{in}} \\ c^R_{s,\mathrm{in}} \\ h^R_{s,\mathrm{in}} \end{pmatrix}. \tag{2.1.3}$$

Because the scattering matrix S is unitary, from

$$\begin{pmatrix} c_{\mathrm{out},1} \\ c_{\mathrm{out},2} \\ \cdots \end{pmatrix} = S \begin{pmatrix} c_{\mathrm{in},1} \\ c_{\mathrm{in},2} \\ \cdots \end{pmatrix} \tag{2.1.4}$$

generally follows

$$S^{\mathrm{T}} \begin{pmatrix} c^\dagger_{\mathrm{out},1} \\ c^\dagger_{\mathrm{out},2} \\ \cdots \end{pmatrix} = \begin{pmatrix} c^\dagger_{\mathrm{in},1} \\ c^\dagger_{\mathrm{in},2} \\ \cdots \end{pmatrix}. \tag{2.1.5}$$

So the general normal/superconducting/normal scattering state written in the outgoing basis is

$$|\Psi\rangle = \prod_{\varepsilon s \alpha} \left(t_{hh} h_s^{\bar{\alpha}\dagger}(\varepsilon) + t_{eh} c_s^{\bar{\alpha}\dagger}(\varepsilon) + r_{hh} h_s^{\alpha\dagger}(\varepsilon) + r_{eh} c_s^{\alpha\dagger}(\varepsilon) \right) |\rangle \,. \tag{2.1.6}$$

Expressing $|\rangle$ in terms of the new Fermi sea $|\rangle_{\delta\mu}$ as defined in Eq. (2.1.2), we obtain

$$\begin{aligned} |\Psi\rangle = \prod_{\varepsilon s} \Big\{ & (t_{hh}^2 + r_{hh}^2) + (r_{eh}^2 - t_{eh}^2) c_s^{R\dagger}(\varepsilon) c_{-s}^{R\dagger}(-\varepsilon) c_s^{L\dagger}(\varepsilon) c_{-s}^{L\dagger}(-\varepsilon) \\ & + s(r_{eh} r_{hh} - t_{hh} t_{eh}) [c_s^{L\dagger}(\varepsilon) c_{-s}^{L\dagger}(-\varepsilon) + c_s^{R\dagger}(\varepsilon) c_{-s}^{R\dagger}(-\varepsilon)] \\ & + s[t_{eh} r_{hh} - t_{hh} r_{eh}) (c_s^{R\dagger}(\varepsilon) c_{-s}^{L\dagger}(-\varepsilon) + c_s^{L\dagger}(\varepsilon) c_{-s}^{R\dagger}(-\varepsilon)] \Big\} |\rangle_{\delta\mu} \,. \end{aligned} \tag{2.1.7}$$

By looking at the superscripts $\alpha = L, R$, we can distinguish three contributions: the first line contains product states, the second line contains local pairs, and the third line contains nonlocal pairs. Conventional Cooper pair splitters operate in the reflection-dominated limit,

$|r_{hh}|^2 \sim 1$. Then, in leading order,

$$|\Psi\rangle = \Big[1 + \sum_{\varepsilon s} \Big\{ r_{eh} s [c_s^{L\dagger}(\varepsilon) c_{-s}^{L\dagger}(-\varepsilon) + c_s^{R\dagger}(\varepsilon) c_{-s}^{R\dagger}(-\varepsilon)] + t_{eh} s [c_s^{R\dagger}(\varepsilon) c_{-s}^{L\dagger}(-\varepsilon) + c_s^{L\dagger}(\varepsilon) c_{-s}^{R\dagger}(-\varepsilon)] \Big\} \Big] |\rangle_{\delta\mu} , \quad (2.1.8)$$

so local Andreev reflection produces local pairs whereas crossed Andreev reflection produces nonlocal pairs. The bilayer graphene Cooper pair splitter has $|r_{hh}|^2 \sim 0$, so we have to seek the opposite limit, $|t_{hh}|^2 \sim 1$. Then the situation is reversed: in leading order

$$|\Psi\rangle = \Big[1 - \sum_{\varepsilon s} \Big\{ t_{eh} s [c_s^{L\dagger}(\varepsilon) c_{-s}^{L\dagger}(-\varepsilon) + c_s^{R\dagger}(\varepsilon) c_{-s}^{R\dagger}(-\varepsilon)] + r_{eh} s [c_s^{R\dagger}(\varepsilon) c_{-s}^{L\dagger}(-\varepsilon) + c_s^{L\dagger}(\varepsilon) c_{-s}^{R\dagger}(-\varepsilon)] \Big\} \Big] |\rangle_{\delta\mu} \quad (2.1.9)$$

and local Andreev reflection produces nonlocal pairs, whereas crossed Andreev reflection produces local pairs.

In the case of the valley-chiral channel, crossed Andreev reflection vanishes exactly, $t_{eh} = 0$, and the scattering state becomes

$$|\Psi\rangle = \Big\{ 1 + \sum_{\varepsilon\alpha} r_{eh} \Big[c_\downarrow^{\alpha\dagger}(\varepsilon) c_\uparrow^{\bar{\alpha}\dagger}(-\varepsilon) - c_\uparrow^{\alpha\dagger}(\varepsilon) c_\downarrow^{\bar{\alpha}\dagger}(-\varepsilon) \Big] + \mathcal{O}(r^2) \Big\} |\rangle_{\delta\mu} , \quad (2.1.10)$$

with a nonlocal spin singlet explicitly on top of the redefined Fermi sea $|\rangle_{\delta\mu}$. This limit of a small Andreev amplitude r_{eh} is the desired regime, in which it is meaningful to talk about individual entangled pairs. The differential conductance between the superconducting contact and the normal-state contact at the bias voltage V is $G(V) \propto 4e^2/h \times |r_{eh}(eV)|^2$, where the constant of proportionality depends on the number of channels the one-dimensional mode has. Also note that only the singlet contributes to the shot noise of the scattering state.

Andreev reflection is strongest when the energy ε of the hole incident from the normal region lies within the superconducting gap, $\varepsilon < \Delta$, because there are no propagating solutions in the superconducting region and the wave function decays exponentially on the superconducting coherence length $\hbar v_\mathrm{F}/\Delta$, where v_F is the normal-state Fermi velocity.

So the length of the interface between the bulk superconductor and the one-dimensional channel and the distance of the bulk superconductor to the one-dimensional channel, which determines the strength of the induced gap Δ, have to be adjusted such that the length of the proximity-induced superconducting region falls below the induced coherence length. Aiming for small r_{eh} sets the stage for treating the influence of the superconductor perturbatively when building the microscopic model.

Notably, in the often-sought limit of unit-strength crossed Andreev reflection, $|t_{eh}|^2 = |t_{he}|^2 = 1$ and all other amplitudes vanishing, no entanglement results. In this limit, all available outgoing modes are filled resulting in a product state. In general, having strong reflection as well as strong local Andreev reflection and having strong transmission as well as strong crossed Andreev reflection are both undesirable when building a Cooper pair splitter useful for entangled-pair production.

2.2 Topological modes in bilayer graphene in proximity to a superconductor

To describe the hybrid structure of the bilayer graphene sheet and the superconductor, I will proceed in two steps: first, I model the one-dimensional topological channel and account for the superconductor perturbatively. This is justified because, as I already argued, the superconductor is weakly coupled to the channel in the regime of interest. The second step will be to describe the subgap conductance with a rate equation, which is equivalent to the lowest order of the scattering approach discussed above. Again, this level of accuracy is sufficient because the influence of the superconductor is weak.

The bilayer graphene sheet with a nonuniform layer voltage $U(\mathbf{r})\pm V(\mathbf{r})$ is described by the usual low-energy Hamiltonian [129, 133],

$$H_{\mathrm{BLG}}^{\chi_\nu,s} = \alpha\hbar^2\left[2\chi_\nu\partial_x\partial_y\sigma_y + \left(\partial_x^2 - \partial_y^2\right)\sigma_x\right] + U(\mathbf{r}) + V(\mathbf{r})\sigma_z, \quad (2.2.1)$$

where $\alpha = v_F^2/\gamma_1$ with γ_1 the dominant direct interlayer hopping matrix element of the underlying tight-binding model. Because Eq. (2.2.1) is

diagonal in valley $\chi_\nu = \pm 1$ and real spin $s = \pm 1 \equiv \uparrow, \downarrow$, they enter only as parameters. The Pauli matrices σ_i act in (A_1, B_2) space. This is the model within which Martin et al. discovered valley-chiral edge states [133]. In order to include superconductivity, H_{BLG} is promoted to the Bogoliubov–de Gennes Hamiltonian [121, 122]

$$H_{\mathrm{BdG}}^{\chi_\nu,s} = H_{\mathrm{BLG}}^{\chi_\nu,s}\tau_z + \Delta(\mathbf{r})\tau_x, \tag{2.2.2}$$

with the s-wave pairing amplitude $\Delta(\mathbf{r})$. The Pauli matrices τ_i act in electron–hole space. In writing Eq. (2.2.2), I used that H_{BLG} is time-reversal symmetric (it commutes with the time-reversal operator $T = i\tau_x s_y K_0$, where K_0 denotes complex conjugation) and I chose the Fermi energy $E_F = 0$.

Assuming translational invariance along the y direction we can distinguish three regions: at $x > 0$, we choose $U = 0$ and $V = -V_0 < 0$, so the bilayer graphene sheet is insulating with a band gap $2V_0$. The influence of the superconductor is negligible, $\Delta = 0$. At $-d < x < 0$, the interlayer voltage is reversed, $V = V_0$. So the guided modes will emerge at $x = 0$ and propagate in the y direction. In reality, the voltage step will be smooth but because of the topological nature of the guided modes, this is inessential. This region is insulating, too, and serves as a tunnel barrier to the superconductor at $x < -d$. There, the pairing amplitude is finite, $\Delta > 0$. The interlayer voltage vanishes, $V = 0$ but the metallic superconductor causes higher doping, which is described by a band shift $U = -U_S < 0$. The steplike onset of superconductivity is justified by the short Fermi wavelength in the metallic superconducting bulk [121]. The Hamiltonian, Eq. (2.2.2), can hence be decomposed into two parts, $H_{\mathrm{BdG}}^{\chi_\nu,s} = H_0 + H_1$, where $H_0 = H_{\mathrm{BLG}}^{\chi_\nu,s}\tau_z$ describes the system without the superconductor, and the perturbation $H_1 = \Theta(-x-d)[(-U_S - V_0\sigma_z)\tau_z + \Delta\tau_x]$ is finite only in the superconducting region $x < -d$.

An analytic solution exists for H_{BLG} [133], which easily extends to H_0. The four-component spinor $\Phi_{\chi_\nu,s}(\mathbf{r}) = [\mathbf{u}_{\chi_\nu,s}(\mathbf{r}), \mathbf{v}_{\chi_\nu,s}(\mathbf{r})]^{\mathrm{T}}$ has electron components $\mathbf{u}_{\chi_\nu,s}(\mathbf{r}) = [u_{A_1,\chi_\nu,s}(\mathbf{r}), u_{B_2,\chi_\nu,s}(\mathbf{r})]^{\mathrm{T}}$ and hole components ($u \to v$), which decouple. In the electron sector, the solutions of the Schrödinger equation $H_0\Phi^0_{\chi_\nu,s} = \varepsilon\Phi^0_{\chi_\nu,s}$ have the form

$\mathbf{u}^0_{\chi_\nu,s}(\mathbf{r}) = \mathbf{u}^0_{\chi_\nu,s} e^{(i/\hbar)(p_x x + p_y y)}$, $\mathbf{v}^0_{\chi_\nu,s}(\mathbf{r}) = 0$ with

$$\mathbf{u}^0_{\chi_v,s} = \begin{pmatrix} -\varepsilon - V \\ \alpha^2 (p_x + i\chi_v p_y)^2 \end{pmatrix}. \tag{2.2.3}$$

The energy ε and the momentum along the channel p_y are good quantum numbers and fix the transverse momentum

$$p_x = \pm\sqrt{\pm i\sqrt{V_0^2 - \varepsilon^2}/\alpha - p_y^2}. \tag{2.2.4}$$

At subgap energies, $|\varepsilon| < V_0$, propagating modes do not exist and p_x is complex. For $x < 0$ and $x > 0$ two solutions each have the correct asymptotic behavior, $\Phi^0_{\chi_\nu,s}(x \to \mp\infty) \to 0$. Since H_0 is a second-order differential operator, the wave function $\Phi^0_{\chi_\nu,s}(\mathbf{r})$ and its derivative are continuous at $x = 0$. Applied to the two nontrivial components of the electronlike wave function, this yields two subgap bands $1, 2$ with the dispersion relation

$$\varepsilon^{0,1/2}_{\chi_v,s,p_y} = \pm\frac{\sqrt{2}V_0 - \alpha p_y^2}{2} - \frac{\chi_v p_y}{2}\sqrt{2\sqrt{2}\alpha V_0 + \alpha^2 p_y^2}, \tag{2.2.5}$$

and the corresponding coefficients which determine the wave functions $\Phi^{0,1/2}_{\chi_\nu,s}$. Both branches of the dispersion relation are valley chiral as expected (Fig. 2.3, inset). The solutions in the hole sector, $\Phi^{0,3/4}_{\chi_v,s,p_y}(x) = [0, \mathbf{v}^0_{\chi_v,s}(\mathbf{r})]^{\mathrm{T}}$ are obtained by time and energy reversal, $p_y \to -p_y$ and $\chi_\nu \to -\chi_\nu$, and $\varepsilon \to -\varepsilon$. There are four electron–hole crossings in the spectrum: two at the Fermi energy, $\varepsilon = 0$ and $p_y = \pm 2^{-3/4}\sqrt{V_0/\alpha}$, and two at zero momentum, $p_y = 0$ and $\varepsilon = \pm V_0/\sqrt{2}$. The superconductive pairing amplitude will mix electron and hole states and open gaps at the crossings. I already argued that Cooper pair transport is particularly important at energies where the spectrum is gapped because transmission, the process competing with Andreev reflection, is exponentially small in the length of the superconducting region. For later use, it is convenient to linearize the spectrum around these points of interest, i.e.,

$$E \approx -\frac{4}{3}2^{1/4}\sqrt{V_0\alpha}\Big(\chi_v p_y \mp 2^{-3/4}\sqrt{V_0/\alpha}\Big) \tag{2.2.6}$$

close to the Fermi points and

$$E \approx \pm\frac{V_0}{\sqrt{2}} - \chi_v 2^{-1/4}\sqrt{V_0\alpha}p_y \tag{2.2.7}$$

close to zero momentum. For consistency, we can check that the relevant momenta along the channel are still close to the Dirac points: with $|\varepsilon| \lesssim V_0$ the dispersion relation, Eq. (2.2.5), implies $|p_y| \lesssim \sqrt{V_0/\alpha}$ but the Dirac points are at $\frac{4\pi\hbar}{3a} \sim 10^2\sqrt{V_0/\alpha}$ when $V_0 \sim 10\Delta \sim 10$meV. More interesting is another estimate: the length on which the guided modes decay in the bulk is roughly $\hbar/|p_x| \sim \sqrt{\hbar^2\alpha/V_0}$, which is several tens of nanometers with the same parameters. This gives the separation d between the channel and the superconductor at which a sizable proximity effect can be expected.

The bilayer graphene model, Eq. (2.2.2), does not (effectively) include the skew-interlayer couplings between the A_1 and B_2 lattice sites of the underlying tight-binding model. At the bottom of the conduction band and at the top of the valence band, the bulk dispersion relation of gapless bilayer graphene experiences trigonal warping, i.e., it loses the rotational invariance around the Dirac points in momentum space. Instead, there are three additional pockets with zero-energy points symmetrically arranged around the Dirac point [129]. When the Fermi energy is sufficiently low, $\varepsilon \lesssim 1$ meV, a Lifshitz transition occurs, i.e., the topology of the Fermi surface changes from one circle to four circles. If the band gap is finite, a residual effect remains at energies close above the gap. Being topological, the subgap states are not broken but their dispersion relation changes if the gap V_0 becomes comparable to the Lifshitz energy ε_L [143]. Importantly, this can weaken the valley chirality at certain energies. The difference between the number of right-moving modes and left-moving modes is a topological constant so there will always be two more, say, right movers than left movers. But the dispersion of one or both bands can become nonmonotonic. This is not a severe restriction because of three reasons. First, since there is no protection against scattering within a valley, we can assume that to zeroth order all possibilities to distribute a Cooper pair onto one of the branches in each valley are equally likely. If there are N_0 right-moving modes and $N_0 + 2$ left-moving in valley K_+ but $N_0 + 2$ right-moving modes and N_0 left-moving modes in valley

K_-, there are $N_{\mathrm{NL}} = (N_0+2)(N_0+2) + N_0N_0$ possibilities to split a Cooper pair and there are $N_L = (N_0+2)N_0 + N_0(N_0+2)$ possibilities to emit a local pair. This gives an estimate of the splitting efficiency $N_{\mathrm{NL}}/(N_L+N_{\mathrm{NL}}) = 1-(N_0^2+2N_0)/(2N_0^2+4N_0+2) > 1/2$, which is still higher than the efficiency of most interaction-based Cooper pair splitters built so far. Second, even with a very small gap, i.e., strong influence of trigonal warping on the subgap dispersion, the states remain valley chiral in a certain energy range [143]. By tuning the Fermi energy into this range and limiting the applied bias voltage, the transport window is completely chiral and unit efficiency is restored. And third, there is no reason why not to choose the band gap substantially larger than the Lifshitz energy, such that the subgap bands are only distorted slightly but do not change qualitatively.

The next step is to include the influence of the superconductor. The simplest approach would be to start from the subgap modes $\varepsilon(p_y)$ and introduce a constant electron–hole coupling $\Delta(p_y) \equiv \tilde{\Delta}$. This opens gaps $2\tilde{\Delta}$ at the Fermi energy. The physical realization corresponding to this approach is the bilayer graphene sheet being covered with a superconducting metal everywhere, such that all of the translational symmetries are preserved. Quite generally, a time-reversal-invariant Hamiltonian with the spectrum $E_n(k)$ will produce a Bogoliubov–de Gennes spectrum $\sqrt{E_n(k)^2+|\tilde{\Delta}|^2}$. This is because when diagonalizing the Bogoliubov–de Gennes Hamiltonian, the off-diagonal couplings between the electron and hole sectors, $\tilde{\Delta}\mathbb{I}$, stay invariant. The meaning of $\tilde{\Delta}$ is that of an effective superconductive pairing which is proximity induced. Clearly, if it exceeds the band gap V_0, the subgap modes are completely suppressed.

While being simple, this ad-hoc approach misses some interesting aspects and even entire transport channels contained in the microscopic model, Eq. (2.2.2), in which the superconductor is more realistically placed at a distance d from the topological mode. To account for this, I will use quasidegenerate perturbation theory [144] to add the influence of H_1 to the four-by-four low energy (subgap) space of $H_0(p_y)$ we considered so far. In this way, the entire geometrical structure is taken into account. The bulk gap Δ in the superconducting region, $x < -d$, will be substantially larger than the resulting proximity gap in

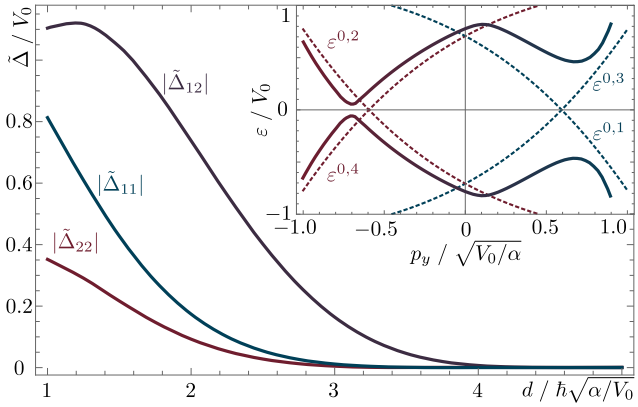

Figure 2.3: Induced intraband superconductivity $\tilde{\Delta}_{11}$ ($\tilde{\Delta}_{22}$) in the one-dimensional channel at the respective Fermi point $p_y = \pm 2^{-3/4}\sqrt{V_0/\alpha}$ and induced interband superconductivity $\tilde{\Delta}_{12}$ at $p_y = 0$. For illustrative purposes we choose the bulk superconducting gap $\Delta = V_0$ and the doping $U_S = 10V_0$ ($\Delta < V_0$ is equally feasible). The amplitudes decay exponentially with the distance d to the superconductor because the $V > 0$ region acts as a tunnel barrier. Inset: In the normal state dispersion (dashed) two different-sized gaps open at the Fermi energy because $\tilde{\Delta}_{11} \neq \tilde{\Delta}_{22}$, shown for $d = 1.5\sqrt{\hbar^2\alpha/V_0}$. Additionally, $\tilde{\Delta}_{12}$ opens a gap at $p_y = 0$. This point contributes significantly to Cooper pair transport because, compared to the Fermi points, the normal density of states is higher and because the energy is larger so the bound states extend further into the bulk, increasing the coupling to the superconductor. Figure and caption reproduced from the original publication, Ref. 115.

the subgap spectrum because of the tunnel barrier, $-d < x < 0$. Bound states exist only at $|\varepsilon| < \min(\Delta, V_0)$ since modes above Δ propagate in the superconductor and modes above V_0 propagate in the normal state graphene regions. Because H_1 conserves spin and valley, I now suppress the indices χ_v and s. The first order corrections in H_1 are

$$H^{(1)}_{nn'}(p_y) = \int dx \Phi^{0,n\dagger}_{p_y}(x) H_1(x) \Phi^{0,n'}_{p_y}(x). \tag{2.2.8}$$

We are interested in the matrix elements proportional to τ_x, which mix electron and hole states, at the respective band crossings because they allow for particle number nonconserving processes, i.e., Cooper pair transport. I will discuss this in more detail in the next section. They involve either one band, $\tilde{\Delta}_{11} = H^{(1)}_{1,3}(p_F)$ and $\tilde{\Delta}_{22} = H^{(1)}_{2,4}(-p_F)$, or both, $\tilde{\Delta}_{12} = \tilde{\Delta}^*_{21} = H^{(1)}_{1,4}(0)$, where $\pm p_F$ are the Fermi points of the unperturbed dispersion, Eq. (2.2.5). To first order, a result very similar to the ad-hoc model with a uniform effective pairing $\tilde{\Delta}$ is obtained: only the electron and hole states belonging to the same subgap band mix, $\tilde{\Delta}_{11} = \tilde{\Delta}_{22}$, $\tilde{\Delta}_{12} = 0$. New effects are revealed by the second order corrections,

$$\begin{aligned} H^{(2)}_{nn'}(p_y) = \frac{1}{2} \sum_{p_x} \int dx \Phi^{0,n\dagger}_{p_y}(x) H_1(x) \tilde{\Phi}^0_{p_x,p_y}(x) \\ \times \left[(\varepsilon^{0,n}_{p_y} - \tilde{\varepsilon}^0_{p_x,p_y})^{-1} + (\varepsilon^{0,n'}_{p_y} - \tilde{\varepsilon}^0_{p_x,p_y})^{-1} \right] \\ \times \int dx \tilde{\Phi}^{0\dagger}_{p_x,p_y}(x) H_1(x) \Phi^{0,n'}_{p_y}(x), \end{aligned} \tag{2.2.9}$$

where $\tilde{\Phi}^0_{p_x,p_y}(x)$ are the unperturbed free scattering states with real p_x and p_y and energy $\tilde{\varepsilon}^0_{p_x,p_y} = \sqrt{\alpha^2(p_x^2 + p_y^2)^2 + V_0^2} > V_0$ as obtained by standard wave function matching at the domain wall. I impose the quantization condition $p_x = 2\pi n/L$ and normalize the extended wave functions according to $\int_{-L/2}^{L/2} dx \tilde{\Phi}^{0\dagger}_{p_x,p_y}(x) \tilde{\Phi}^0_{p_x,p_y}(x) = 1$. The sum as well as the overlap integrals are evaluated numerically. The quantization length L and the cutoff of the momentum p_x are increased until the second order corrections converge, making sure that the model is in the tunnel regime, i.e., the overlap integrals are small compared to the excitation energies.

Including the second-order corrections, the electron–hole overlap turns out to be different in both bands, $\tilde{\Delta}_{11} \neq \tilde{\Delta}_{22}$ (Fig. 2.3). The difference between the bands is that one lives mostly on the layer with potential $+V_0$ and the other lives mostly on the layer with potential $-V_0$ on either side of the domain wall. The doping U due to the superconductor breaks the particle–hole symmetry, so $+V_0$ is not equivalent to $-V_0$. This leads to one of the bands decaying on a shorter scale in the superconductor than the other and consequently having a weaker electron–hole coupling. In the perturbative treatment, the modification of the wave functions enters only in second order. Another important effect is that there is finite band mixing, $\tilde{\Delta}_{12} \neq 0$, which means that there is an additional transport channel in which the electrons of a Cooper pair are injected into different bands. This happens at the band crossing, $p_y = 0$, i.e., at energy $\varepsilon = \pm V_0/\sqrt{2}$. At this point, the normal-state density of states is higher than at zero energy (the dispersion is flatter) and the energy is closer to the superconducting gap energy, so the contribution to the Cooper pair conductance will be particularly strong. The perturbative results are confirmed when calculating the full dispersion relation of H_{BdG} by matching the four-component spinor and its derivatives at both interfaces numerically (Fig. 2.3, inset): two gaps of different size open at zero energy ($\tilde{\Delta}_{11}$ and $\tilde{\Delta}_{22}$) and two gaps open at zero momentum where electron and hole states from different subgap bands cross ($\tilde{\Delta}_{12} = \tilde{\Delta}_{21}^*$). The advantage of the perturbative approach over the fully numerical one is that the effective pairing amplitudes $\tilde{\Delta}_{nn'}$ are readily used in a transport calculation. This will be the next and final step.

2.3 Cooper pair transport

To calculate the Cooper pair conductance, I will use Fermi's golden rule in an electron-only picture. This is similar to the original Cooper pair splitter proposal [44] but different from what most other authors do, i.e., a Bogoliubov–de Gennes scattering calculation. The latter does not require second quantization because Andreev reflection converts one electron into one hole or the other way around. But as we have seen at the beginning of the chapter, some work is required to relate Andreev

reflection to Cooper pair splitting. The rate equation approach, on the other hand, makes the emitted Cooper pairs explicit. In the perturbative regime the graphene Cooper pair splitter is designed to work in, the additional complexity due to second quantization is marginal.

We express the current

$$I = 2e \sum_{fi} (W^{+}_{fi} - W^{-}_{fi}) \rho_i \tag{2.3.1}$$

by the transition rates $W^{\pm}_{fi} = \frac{2\pi}{\hbar} |\langle f_{\pm} | H_T | i \rangle|^2 \delta(\varepsilon_f - \varepsilon_i)$ from the initial state i, which is realized with probability ρ_i and has the energy ε_i, to the final state $f_{\pm}$ with two more or two less electrons and energy ε_f. The tunnel Hamiltonian $H_T = \tilde{H}^{(1)} + \tilde{H}^{(2)} + \dots$ contains the influence of the superconductor on the normal-state guided modes and I denote by $\tilde{H}^{(i)}$ the second-quantized version of $H^{(i)}$, the i-th order of the effective Bogoliubov–de Gennes model obtained in the last section. More precisely,

$$\begin{aligned}
\tilde{H}^{(i)} = \sum_{\chi_\nu s k} \Big[& H^{(i)}_{\chi_\nu, s\ 1,1}(k) c^{1\dagger}_{\chi_\nu,s}(k) c^{1}_{\chi_\nu,s}(k) + H^{(i)}_{\chi_\nu, s\ 1,2}(k) c^{1\dagger}_{\chi_\nu,s}(k) c^{2}_{\chi_\nu,s}(k) \\
& + H^{(i)}_{\chi_\nu, s\ 1,3}(k) c^{1\dagger}_{\chi_\nu,s}(k) h^{1}_{\chi_\nu,s}(k) + H^{(i)}_{\chi_\nu, s\ 1,4}(k) c^{1\dagger}_{\chi_\nu,s}(k) h^{2}_{\chi_\nu,s}(k) \\
& + \dots \Big] \\
\equiv \sum_{\chi_\nu s k} \Big[& H^{(i)}_{\chi_\nu, s\ 1,1}(k) c^{1\dagger}_{\chi_\nu,s}(k) c^{1}_{\chi_\nu,s}(k) + H^{(i)}_{\chi_\nu, s\ 1,2}(k) c^{1\dagger}_{\chi_\nu,s}(k) c^{2}_{\chi_\nu,s}(k) \\
& + H^{(i)}_{\chi_\nu, s\ 1,3}(k) s c^{1\dagger}_{\chi_\nu,s}(k) c^{1\dagger}_{-\chi_\nu,-s}(-k) \\
& + H^{(i)}_{\chi_\nu, s\ 1,4}(k) s c^{1\dagger}_{\chi_\nu,s}(k) c^{2\dagger}_{-\chi_\nu,-s}(-k) + \dots \Big],
\end{aligned} \tag{2.3.2}$$

where I have introduced the shorthand $k \equiv p_y$, the electron field operators $c^{n}_{\chi_v,s}(k)$, and the hole operators $h^{n}_{\chi_v,s}(k) \equiv s c^{n\dagger}_{-\chi_v,-s}(-k)$. From the structure of the transition rate $W^{\pm}_{fi}$, it is clear that only the particle-number-nonconserving parts matter as anticipated in the last section. Dropping everything else, the tunnel Hamiltonian becomes

$$H_T = \sum_{\chi_v n n' k s} \tilde{\Delta}_{n n'}(k) s c^{n}_{\chi_v,s}(k) c^{n'}_{-\chi_v,-s}(-k) + \text{H.c.} \tag{2.3.3}$$

Before using the tunnel Hamiltonian, one further step is required. The interface between the superconductor and the guided modes has a finite width w, which I account for by setting the real-space transform of the pairing amplitudes $\tilde{\Delta}(x,x')$ to zero unless $x,x' \in [-w/2, w/2]$. Suppressing all indices other than position and momentum, this means

$$\begin{aligned}\sum_k \tilde{\Delta}(k)c(k)c(-k) &= \frac{1}{L}\int dxdx' \sum_k \tilde{\Delta}(k)e^{-ik(x-x')}\psi(x)\psi(x') \\ \longrightarrow \frac{1}{L}\int_{-w/2}^{w/2} dxdx' \sum_k \tilde{\Delta}(k)e^{-ik(x-x')}\psi(x)\psi(x') &= \sum_{kk'} \Delta_{kk'}c(k)c(k')\end{aligned} \tag{2.3.4}$$

with

$$\begin{aligned}\Delta_{kk'} &= \sum_l \frac{\sin\left[(l-k)\frac{w}{2}\right]}{(l-k)\frac{L}{2}} \frac{\sin\left[(l+k')\frac{w}{2}\right]}{(l+k')\frac{L}{2}} \tilde{\Delta}(l) \\ &\approx \tilde{\Delta}\Big(\frac{k-k'}{2}\Big)\frac{L}{2\pi}\int dl \frac{\sin\left[(l-k)\frac{w}{2}\right]}{(l-k)\frac{L}{2}} \frac{\sin\left[(l+k')\frac{w}{2}\right]}{(l+k')\frac{L}{2}},\end{aligned} \tag{2.3.5}$$

where I have exploited that the sum is peaked around $k \approx l \approx -k'$. The length of the system, L, which enters in the Fourier transformation, will not not be present in the final results. What happens in Eq. (2.3.4) has a straight-forward physical interpretation: an infinitely long tunnel interface does not break translational invariance and hence the Cooper pair electrons are put exactly at momenta k and $-k$. A long but finite interface provides only approximate momentum conservation, $k \approx -k'$. Energy conservation, however, is still exact: the energy of both of the electrons needs to sum to twice the normal-state chemical potential of the superconductor. Momentum and energy combined restrict the emission of Cooper pairs to the vicinity of the electron-hole crossings in the normal-state electron–hole spectrum (Fig. 2.3, inset).

With this, the rate W_{fi}^{+} for adding a Cooper pair, $|i\rangle \rightarrow |f\rangle =$

$c^{n\dagger}_{\chi_\nu,s}(k)c^{n'\dagger}_{-\chi_\nu,-s}(-k)\,|i\rangle$, becomes

$$W^{+}_{fi} = 4\pi|\Delta^{nn'}_{kk'}|^2\Big[1-\big\langle n^{n}_{\chi_\nu,s}(k)\big\rangle_i\Big]\Big[1-\Big\langle n^{n'}_{-\chi_\nu,-s}(k')\Big\rangle_i\Big] \times\delta\Big[\varepsilon^{n}_{\chi_\nu}(k)+\varepsilon^{n'}_{-\chi_\nu}(k')-2E_F\Big], \tag{2.3.6}$$

where $\big\langle n^{n}_{\chi_\nu,s}(k)\big\rangle_i$ is the occupation probability in state i. Similarly,

$$W^{-}_{fi} = 4\pi|\Delta^{nn'}_{kk'}|^2\big\langle n^{n}_{\chi_\nu,s}(k)\big\rangle_i\Big\langle n^{n'}_{-\chi_\nu,-s}(k')\Big\rangle_i \times\delta\Big[2E_F-\varepsilon^{n}_{\chi_\nu}(k)-\varepsilon^{n'}_{-\chi_\nu}(k')\Big]. \tag{2.3.7}$$

At low temperatures, the distribution function is steplike, $\big\langle n^{n}_{\chi_\nu,s}(k)\big\rangle_i \approx \Theta\Big[E_F-\delta\mu-\varepsilon^{n}_{\chi_\nu}(k)\Big]$, where $\delta\mu$ is the voltage applied between the superconductor and the channel. Making use of the symmetry between the valleys K and K', the current becomes

$$\begin{aligned} I &= \frac{32e}{\hbar}\pi\sum_{nn'kk'}|\Delta^{nn'}_{kk'}|^2\delta\Big[\varepsilon^{n}_{K}(k)+\varepsilon^{n'}_{K'}(k')\Big] \\ &\quad\times\Big\{1-\Theta\Big[E_F-\delta\mu-\varepsilon^{n}_{K}(k)\Big]-\Theta\Big[E_F-\delta\mu-\varepsilon^{n'}_{K'}(k')\Big]\Big\} \\ &= \frac{32e}{\hbar}\pi\frac{L^2}{(2\pi)^2}\sum_{nn'}\int_{-\delta\mu}^{\delta\mu}d\varepsilon\Big|\frac{\partial k^{n}_{K}(E_F+\varepsilon)}{\partial\varepsilon}\Big|\Big|\frac{\partial k^{n'}_{K'}(E_F-\varepsilon)}{\partial\varepsilon}\Big| \\ &\quad\times|\Delta^{nn'}(E_F+\varepsilon,E_F-\varepsilon)|^2. \end{aligned} \tag{2.3.8}$$

As a function of ε, the pair-tunneling probability $|\Delta_{nn'}(E_F+\varepsilon,E_F-\varepsilon)|^2$ has a single peak for each band configuration n,n', the position of which can be read off immediately from the electron–hole dispersion. Injection into the same subgap band, $n=n'$, requires $\varepsilon\approx\varepsilon^{nn}_0=E_F$, and injection into different subbands, $n\neq n'$, requires $\varepsilon\approx\pm\varepsilon^{12}_0 := \mp\varepsilon^{21}_0 := \pm E_F+V_0/\sqrt{2}$. This is shown schematically in Fig. 2.1(b). To make further analytical progress, I use the linearized subgap dispersion, Eqs. (2.2.6) and (2.2.7), $\varepsilon=\varepsilon^{nn'}_0+\hbar v^{nn'}_0(k-k^{nn'}_0)$, and the tunnel amplitude becomes

$$\Delta^{nn'}=\frac{\tilde\Delta(k^{nn'}_0)}{L}\frac{\sin\Big[(\varepsilon-\varepsilon^{nn'}_0)\frac{w}{\hbar v^{nn'}_0}\Big]}{\varepsilon-\varepsilon^{nn'}_0}. \tag{2.3.9}$$

Finally, the conductance is

$$G = \frac{\partial I}{\partial(\delta\mu/e)} \approx 4G_0 \sum_{nn'} T_{nn'} \Big[\delta_w(\delta\mu - \varepsilon_0^{nn'}) + \delta_w(\delta\mu + \varepsilon_0^{nn'})\Big], \quad (2.3.10)$$

with the conductance quantum $G_0 = 2e^2/h$ and the effective tunneling strength $T_{nn'} = 2\pi w|\tilde{\Delta}(k_0^{nn'})|^2/(\hbar v_0^{nn'})$. In the limit of a long interface, $w \to \infty$, the shorthand $\delta_w(\varepsilon) = \hbar v_0^{nn'} \sin^2\left[\varepsilon w/(\hbar v_0^{nn'})\right]/(\pi w \varepsilon^2)$ becomes the delta function, i.e., momentum conservation becomes exact and, together with energy conservation, completely fixes the orbital degrees of freedom in the splitting process. The conductance contains a factor of 4 due to spin and valley degeneracy and another factor of 2 because we are considering pair transport. Whether the latter is present or not depends on whether the current is measured at the superconducting terminal or at one of the normal state terminals. Also note that the conductance increases when the length of the interface w is increased. In contrast, the conventional Cooper pair splitters viewed as normal/superconducting/normal structures rapidly become inefficient once the length of the superconducting region exceeds its coherence length. This is a direct consequence of local Andreev reflection being the driving force instead of crossed Andreev reflection. Here, a long interface suppresses normal transmission exponentially on the scale of the coherence length ξ making the only alternative, local Andreev reflection, i.e., Cooper pair splitting, strong. The linear increase is hence the lowest order contribution to $|r_{eh}|^2 \sim 1 - \exp(-w/\xi)$. Clearly, perturbation theory breaks down when w exceeds ξ. This regime is in conflict with entanglement production, too, as I have argued before. More microscopically, Cooper pairs tunnel locally into the channel along the whole length of the interface and only then are they split kinematically, so a longer interface increases the current. Given that the length of the interface, i.e., the momentum uncertainty, is such that the different points of injection, $k = 0$ and $k = \pm k_F$, can be resolved, the conductance has a central zero-bias peak and two side peaks (Fig. 2.4), which are directly caused by the special subgap two-band structure of bilayer graphene domain walls. The peak height is proportional to the induced superconducting pairings. The characteristic peak structure may serve as an easily accessible indicator of Cooper pair splitting if more sophisticated detection schemes are not available.

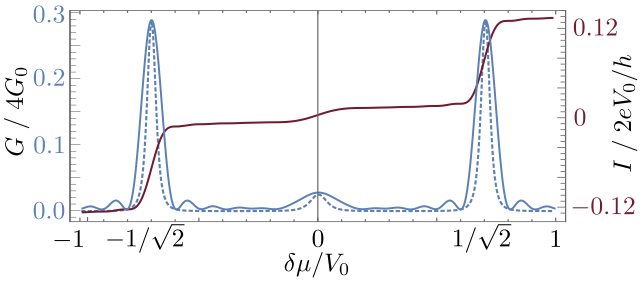

Figure 2.4: Subgap conductance G and Cooper pair current I of a $w = 25\hbar\sqrt{\alpha/V_0}$ long interface between the superconductor and the one-dimensional channel at a distance $d = 3\sqrt{\hbar^2\alpha/V_0}$ with $\Delta = U_S = V_0$. The peaks reflect simultaneous energy and approximate momentum conservation. The sharp boundary of the superconductor region causes oscillations which vanish if an exponential cutoff is used instead (dashed). Figure and caption reproduced from the original publication, Ref. 115.

This concludes the discussion of the bilayer graphene Cooper pair splitter. It might be pointed out that the scattering picture presented in the beginning does not include the subgap band index but, really, this just introduces an additional quantum number, which is always summed over and can be dealt with if desired [115].

3

Entanglement Detection via Josephson Transport

The first entanglement detection scheme I describe is based on a recent experimental setup investigated by Deacon et al. of the Tarucha group [92]. They placed two self-assembled indium-arsenide quantum dots in parallel into a nanometer-scale gap between two aluminum electrodes such that the quantum dots are a few 10 nm apart, much less than the superconducting coherence length. Driving the leads into the normal state by applying a magnetic field, they characterized the device. The quantum dots are clearly in the single-level regime, where the level-spacing and the Coulomb energy are on the order of a few millielectronvolts whereas the level broadening is below 1 meV. There is no relevant direct interdot tunneling and no capacitive coupling. Coherent transport through the structure was demonstrated by Aharonov–Bohm oscillations at high magnetic fields.

The setup differs from a Cooper pair splitter by substituting the two normal-state leads by one additional superconductor. This defeats the purpose of actually splitting the Cooper pairs since, once both of the electrons enter the second superconductor, there is no spatial separation any longer. But while still on separate quantum dots, they can be regarded as being split if only on a microscopic scale. What we gain is a new handle on transport: the Josephson effect [145, 146]. Being a ground-state property, the Josephson effect is robust and easy to measure. I will discuss how we can identify nonlocal contributions to the Josephson current, i.e., contributions by Cooper pairs the electrons of which are transported via one quantum dot each through the

junction. The Josephson effect is coherent and so if such contributions are present, the Cooper pair has to remain an entangled singlet when split across the quantum dots. Better still, Deacon et al. find strong indications that in order to detect the nonlocal contributions, it is sufficient to consider only the critical current I_c, i.e., the highest current which can flow through the junction without dissipation. The rationale is as follows: by integrating the Josephson equations, the (free) energy $E(\Delta\varphi)$ stored in the junction if a supercurrent flows due to a phase difference $\Delta\varphi$ is found to be

$$E(\Delta\varphi) = E_J\Big[1 - \cos(\Delta\varphi)\Big] \tag{3.0.1}$$

with the Josephson energy $E_J = \Phi_0 I_c/2\pi$, where $\Phi_0 = h/2e$ is the flux quantum. It follows that the critical current

$$I_c = \frac{2e}{\hbar} \max_{\Delta\varphi} \frac{\partial E(\Delta\varphi)}{\partial \Delta\varphi} \tag{3.0.2}$$

is proportional to the Josephson energy and that the critical current is taken at the critical phase difference $\Delta\varphi = \pm\pi/2$. Deacon et al. argue that the Josephson energy should be decomposable into local contributions E_{J1} and E_{J2} which involve only one of the two quantum dots 1 and 2 and into a nonlocal contribution E_{J12}. Because there is no cross-talk between the quantum dots, the local contributions depend on, say, the on-site energy of only one of the quantum dots, whereas the nonlocal contribution depends on both,

$$E_J = E_{J1}(\varepsilon_1) + E_{J2}(\varepsilon_2) + E_{J12}(\varepsilon_1, \varepsilon_2). \tag{3.0.3}$$

By virtue of Eq. (3.0.2), the critical current immediately inherits this decomposition. In essence, the experiment shows that the critical current *cannot* be understood as a sum of only two local contributions by varying the gate voltages and hence the on-site energies of the quantum dots independently. We will see that the actual decomposition of the Josephson energy is more complicated than Eq. (3.0.3) whenever both of the quantum dots have an odd occupation and that the simple relation $I_c \propto E_J$ breaks down. The qualitative features observed experimentally are, however, reproduced by the more rigorous model I discuss so it supports the hypothesis of nonlocal Cooper pair transport put forward by Deacon et al. In addition, precisely the deviation

from the simple expectation $I_c \propto E_J$ can be turned into an additional signature of nonlocal transport.

Quantum-dot Josephson junctions have enjoyed attention for a long time. Before the advent of nanofabrication, they were studied as *Anderson-impurity* Josephson junctions. When the impurity is magnetic, i.e., when it is occupied by one electron, there is a competition between superconductive ordering, which builds spin-singlet Cooper pairs within the leads, and Kondo screening, which builds a spin singlet from the impurity electron and the lead electrons. In the weak coupling limit, $k_B T_K \ll \Delta$, where T_K is the Kondo temperature, which increases with the level broadening Γ of the impurity, and Δ is the superconducting gap energy, the Kondo effect is negligible and the impurity remains magnetic. In the opposite limit, $k_B T_K \gg \Delta$, the Kondo cloud screens the magnetic moment on the impurity. This has immediate consequences for the Josephson current. Already in 1966, Kulik noticed that Josephson tunneling through magnetic barriers involves processes which contribute a negative Josephson current [147]. Specifically, this happens if both of the two Cooper pair electrons are spin flipped while tunneling from one superconductor to the other. The same thing happens in the case of magnetic Kondo impurities [148], although, microscopically, four single-particle tunnel events are needed to transfer a Cooper pair. Spivak and Kivelson gave a clear interpretation for this effect in terms of fermion-exchange signs [149]: if the entire Cooper pair is transferred past the localized electron on the impurity, no exchange sign results. But it is also possible that one electron of the Cooper pair is left behind on the impurity, while the electron which was originally on the impurity is incorporated into a new Cooper pair in the other superconductor. In this case, only one fermion exchange happens and the contribution to the Josephson current picks up a negative sign. The Kondo effect suppresses the magnetization, so, somewhat paradoxically, it can enhance the supercurrent. In the opposite extreme case, where the spin-flip processes dominate, the supercurrent $I(\Delta\varphi)$ changes sign and so does the energy of the junction, $E(\Delta\varphi) \propto \cos(\Delta\varphi) + \text{const}$. The energy is then minimized at $\Delta\varphi = \pi$ instead of at $\Delta\varphi = 0$, which is why the transition is called 0–π transition. I will discuss a similar mechanism of the double-quantum-dot junction in more detail later on with explicit examples of sign-changing

processes. Indeed, we will see that the double-quantum-dot Josephson junction, too, behaves either as a 0 junction, as π junction, or even goes to an intermediate regime depending on the energies and on the parity of the quantum-dot wave functions.

The 0–π transition is a convenient handle to detect the cross-over between the weak-coupling regime, where magnetic moments are present, and the strong-coupling regime, where magnetic moments are screened. It has been employed in several theoretical studies which treat the Anderson-impurity Josephson junction. In general, it is a formidable task to solve the model because there are necessarily interactions on the impurity and because of the competition between the superconducting ordering and the Kondo effect. The methods which have been applied to the problem include the Hartree–Fock approximation [150, 151], the slave-boson representation of the impurity at infinite Coulomb repulsion together with the non-crossing approximation [152], perturbation theory in the Coulomb repulsion [151], exact diagonalization in the limit of zero-bandwidth leads [151, 153], the numerical renormalization group [154], Monte-Carlo simulations [155], and real-time density-matrix diagrammatics [156]. The treatments agree that the π phase emerges at sufficiently small coupling and at odd occupation, so, in this regime, the Kondo effect is negligible and a perturbative treatment of the Josephson effect in terms of single-electron tunneling is valid. This is the regime the device of Deacon et al. appears to be in and it is the regime to which I limit the model I discuss.

Conclusive experiments followed soon after. The 0–π transition was observed both in nanowire [157] and in carbon-nanotube quantum dots [158]. The measurement strategy is to lock the superconducting phase difference by constructing a SQUID which includes the magnetic quantum dot in one arm and a 0-phase *pilot Josephson junction* in the other. The pilot junction has a much higher critical current and hence locks the phase difference to $\Delta\varphi = \pm\pi/2$ close to the critical current of the SQUID. Then regimes can be identified in which the magnetic quantum dot *increases* the critical current and regimes in which it *decreases* the critical current, indicating that its Josephson current changes sign [159]. In the double-quantum-dot device, the same may happen. More interestingly, the nonlocal transport channel, which is relevant, too,

since the quantum dots are much closer than in a SQUID, can flow opposite to the local ones.

With the advance of fabrication techniques, Josephson junctions containing more than one quantum dot have become a popular subject of theoretical studies. In these systems, magnetic correlations among the quantum dots come into play. This was investigated for Hubbard chains of two [160] and more sites [161] and in the limiting case of a Tomonaga–Luttinger liquid [153]. Choi et al. were the first to study a *parallel* configuration of two quantum dots and to suggest using it to probe spin entanglement [162]. Since the quantum dots are coupled by the superconducting leads, there are superexchange processes which mediate a magnetic coupling between them. Choi et al. discovered that deep in the single-level regime, i.e., when the level spacing, the Coulomb repulsion, the bandwidth of the leads, and the superconducting gap are much larger then the level broadening, at odd occupation, the system can be described effectively by a Heisenberg model with a phase-dependent coupling strength,

$$H_{\text{eff}} \approx J\Big[1+\cos(\Delta\varphi)\Big]\Big[\mathbf{S}_1\cdot\mathbf{S}_2-\frac{1}{4}\Big], \tag{3.0.4}$$

where $\mathbf{S}_1$ and $\mathbf{S}_2$ are the spin-1/2 low-energy degrees of freedom of the electrons localized on the quantum dots and $J>0$. This equation can be read in two ways: first, depending on the phase difference, the system has a spin-degenerate ground state ($\Delta\varphi=\pi$) or a unique singlet ground state ($\Delta\varphi\neq\pi$). Second, if the system is in the triplet state, it cannot support any supercurrent because $\mathbf{S}_1\cdot\mathbf{S}_2-\frac{1}{4}=0$ and so the ground-state energy is phase independent. Choi et al. proposed to employ this feature to detect the spin-singlet state, i.e., the entanglement between the quantum dots. Threading a magnetic flux through a SQUID with the double quantum dot and a pilot junction, the phase at the double-quantum-dot Josephson junction is set to $\Delta\varphi=\pi$ such that a mixture between the singlet and the triplet states result. Afterwards, the flux through the SQUID is removed and a current is driven through the SQUID which is larger than the critical current of the pilot junction but smaller than the combined critical currents of the pilot junction and of the singlet-state double-quantum-dot Josephson junction. If the spin-relaxation time is sufficiently long, the system can be observed to

switch into the nondissipative state and hence to establish a nonlocal singlet state on the double quantum dot.

It is instructive to investigate the physical behavior behind Eq. (3.0.4). The effective model H_{eff} contains processes up to fourth order in the single-particle tunnel amplitude. There are processes in which both the first two tunnel events involve the same superconductor and the third and fourth tunnel event involve the same superconductor. I will call this kind of process *second-order Cooper pair tunneling* because a typical example is that the two electrons of a Cooper pair are injected onto one of the quantum dots (or one electron is injected onto each quantum dot) and afterwards they tunnel back into one of the superconductors. Second-order Cooper pair tunneling is possible if the electrons localized on the quantum dots form a spin singlet but it is blocked in the triplet state. The reason is clear: only if the electrons on the quantum dots are a spin singlet, they can build a Cooper pair in a superconductor. And due to Pauli's principle it is neither possible to add two electrons of a Cooper pair from a superconductor locally on one of the already singly-occupied quantum dots, nor to put a nonlocal spin singlet to a nonlocal spin triplet. More formally, second-order Cooper pair tunneling restores the ground state of the superconducting leads in one of the three intermediate virtual states of the fourth-order process. There are other processes, which I will refer to as *genuine fourth-order processes*, with excitations of the superconducting leads in all three intermediate virtual states. We will see that genuine fourth-order processes *can* favor a triplet ground state and *can* support a supercurrent in the triplet state. But since they are suppressed at least by Δ^{-1} compared to Cooper pair tunneling, they are irrelevant in the limit of a large superconducting gap energy Δ, in which Eq. (3.0.4) was derived. So, a physical interpretation of what Choi et al. found is that only the singlet can gain energy by hybridizing with the superconducting leads (so there is a singlet ground state) and only with a spin singlet on the quantum dots, second-order Cooper pair tunneling can transport Cooper pairs from one superconductor to the other (so there is no supercurrent in the triplet state).

The double-quantum-dot Josephson junction itself can be viewed as a SQUID, although, due its small area, rather large fields are required to obtain a sizable Aharonov–Bohm effect. This is likely to be in con-

flict with superconductivity but would offer a way to detect nonlocal transport by observing half-period oscillations in the critical current [163], very similar to what was already suggested in the Cooper pair splitter proposal by Recher et al. [44]. Signatures of nonlocal transport in the Aharonov–Bohm effect are predicted to be still present in other quantum-dot charging states and at strong coupling [164]. When including tunneling between the quantum dots [165], rather complicated Aharonov–Bohm patterns result because three different closed-loop paths through the structure interfere. The double-quantum-dot Josephson junction was also studied in the Kondo regime although not in the context of entanglement [166].

Closely related to two quantum dots is one quantum dot with two levels. It, too, exhibits 0–π transitions, Kondo screening, and a spin-dependent Josephson current. An interlevel exchange coupling can induce a triplet ground state [167].

The model I present to describe the device investigated by Deacon et al. is very similar to the one by Choi et al. As dictated by the experimental findings, it contains two spin-degenerate single-level quantum dots, $i = 1, 2$, $\sigma = \uparrow, \downarrow$, with on-site energies ε_i and Coulomb repulsion U_i. Both of them in parallel are connected to two superconducting leads, $\nu = L, R$, with the tunnel couplings $t_{\nu i}$ [Fig. 3.1(a)]. There is no direct coupling between the quantum dots or between the superconducting leads. Formally,

$$H = H_1 + H_2 + H_L + H_R + H_T, \tag{3.0.5}$$

where the quantum-dot Hamiltonians are

$$H_i = \sum_\sigma \varepsilon_i d_{i\sigma}^\dagger d_{i\sigma} + U_i d_{i\uparrow}^\dagger d_{i\downarrow}^\dagger d_{i\downarrow} d_{i\uparrow}, \tag{3.0.6}$$

where the lead Hamiltonians are

$$H_\nu = \sum_{\mathbf{k}\sigma} \varepsilon_{\nu\mathbf{k}} c_{\nu\mathbf{k}\sigma}^\dagger c_{\nu\mathbf{k}\sigma} + \sum_{\mathbf{k}} \Delta_\nu e^{-i\varphi_\nu} c_{\nu\mathbf{k}\uparrow}^\dagger c_{\nu-\mathbf{k}\downarrow}^\dagger + \text{H.c}, \tag{3.0.7}$$

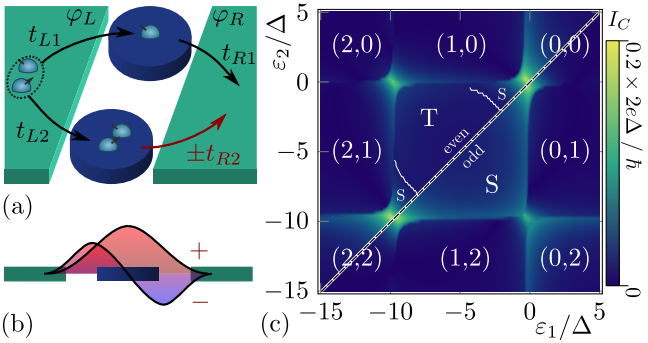

Figure 3.1: Double-quantum-dot Josephson junction. (a) The Josephson current is carried by Cooper pairs which tunnel coherently between two superconducting leads with superconducting phases φ_L and φ_R. Microscopically, this involves four single-particle tunneling events with amplitudes $t_{\nu i}$. Local transport (both electrons of a Cooper pair tunnel through a single quantum dot) can be distinguished from nonlocal transport (the two electrons of a Cooper pair tunnel through different quantum dots). (b) The symmetry of the orbital wave functions on the quantum dots is captured in the total tunnel parity $\mathcal{P} = \mathrm{sgn}(t_{L1}t_{L2}t_{R1}t_{R2})$, or, equivalently, in $\pm t_{R2}$, and has distinctive signatures in the critical current. (c) Critical current across the junction at zero temperature as a function of the quantum-dot level energies $\varepsilon_{1,2}$. The upper-left half of the plot shows the critical current at *even* tunnel parity and the lower-right half at *odd* tunnel parity. The critical current becomes large close to ground-state transitions, where the charge of the quantum dots (N_1, N_2) fluctuates. At even tunnel parity, a transition between a nonlocal singlet (S) and a triplet (T) ground state in the $(1, 1)$ sector emerges. The parameters are $|t| = 0.5\Delta$ and the Coulomb repulsion $U = 10\Delta$, where Δ is the magnitude of the superconducting gap in the leads. Figure and caption reproduced from the original publication, Ref. 116.

and where the tunnel Hamiltonian is

$$\begin{aligned} H_T &= \sum_{i\nu\sigma} t_{\nu i} d_{i\sigma}^\dagger \psi_{\nu\sigma}(\mathbf{x}_{\nu i}) + \text{H.c.} \\ &= \sum_{i\nu\mathbf{k}\sigma} t_{\nu i} e^{i\mathbf{k}\cdot\mathbf{x}_{\nu i}} d_{i\sigma}^\dagger c_{\nu\mathbf{k}\sigma} + \text{H.c.} \end{aligned} \tag{3.0.8}$$

The operators $d_{i\sigma}$ describe the electrons localized on the quantum dots and the operators $c_{\nu\mathbf{k}\sigma}$ and $\psi_{\nu\sigma}(\mathbf{x})$ describe the spin-σ electrons of momentum $\mathbf{k}$ or at position $\mathbf{x}$ in the superconductors. The normal-state dispersion of the superconductors is $\varepsilon_{\nu\mathbf{k}}$, which implies that they have the ordinary Bardeen–Cooper–Schrieffer spectrum $E_{\nu\mathbf{k}} = \sqrt{\varepsilon_{\nu\mathbf{k}} + \Delta_\nu^2}$. Since both of the superconductors are of the same material and have a similar geometry, I will assume that they have the same energy gaps, $\Delta_L = \Delta_R \equiv \Delta$, and the same normal-state dispersion, $\varepsilon_{L\mathbf{k}} = \varepsilon_{R\mathbf{k}}$. Obviously, there may be a finite phase difference between the superconductors, $\Delta\varphi = \varphi_L - \varphi_R$. In the absence of magnetic fields, the tunnel couplings $t_{\nu i}$ can be chosen real. It is, however, convenient to gauge the superconducting phase difference into the electron operators, $\Delta_\nu e^{-i\varphi_\nu} \to \Delta_\nu$ and $c_{\nu\mathbf{k}\sigma} \to e^{i\varphi_\nu/2} c_{\nu\mathbf{k}\sigma}$, because this is equivalent to replacing $t_{\nu i} \to t_{\nu i} e^{i\varphi_\nu/2}$. The phase difference then takes the role of a counting field and we recover Eq. (3.0.2) with $E(\Delta\varphi)$ the phase-dependent ground-state energy of the Hamiltonian H.

It will turn out that the critical current depends strongly on the orbital parity of the quantum-dot wave functions. This was already investigated experimentally [157] and theoretically in the context of the single-multilevel-quantum-dot Josephson junction [167]. If the localized wave function has odd parity, the tunnel amplitudes to the superconducting leads have opposite sign, $t_{Li} t_{Ri} < 0$ [Fig. 3.1(b)]. All signs cancel if entire Cooper pairs are transported through the quantum dot. But nonlocal Cooper pair transport picks up a sign if the quantum dots have opposite parities. Following Ref. 167, we can capture all possible combinations of signs in the *total tunnel parity*, $\mathcal{P} = \text{sgn}(t_{L1} t_{L2} t_{R1} t_{R2})$, which is $\mathcal{P} = +1$ if the quantum dots have the same parity and $\mathcal{P} = -1$ if the quantum dots have opposite parity. To make this explicit, in the following, I will arbitrarily substitute $t_{R2} \to \mathcal{P} t_{R2}$ and assume all tunnel couplings to be positive, $t_{\nu i} > 0$.

In the experiment, the level broadening $\Gamma_{\nu i} = 2\pi N(\varepsilon_F)|t_{\nu i}|^2$, with $N(\varepsilon_F)$ the normal-state energy density of states at the Fermi level, tends to be larger than the superconducting gap $\Gamma_{\nu i} \gtrsim \Delta$, whereas I will mostly investigate the case of $\Gamma_{\nu i} \lesssim \Delta$. The physical situation is the same since we remain in the regime where $\Gamma_{\nu i}$ is much smaller than the level spacing and than the Coulomb repulsion but perturbation theory in $\Gamma_{\nu i}$ becomes more stable [154], and it is from perturbation theory that we can gain most insight about the microscopic processes in the device.

In the weakly-coupled single-level regime, the charging state (N_1, N_2), where N_i is the number of electrons localized on quantum dot i, is well defined except close to where two levels are degenerate and the particle numbers fluctuate because of Josephson transport [Fig. 3.1(c)].

Deacon et al. argue that there is a sizable nonlocal current only if the quantum dots are closer than the superconducting coherence length in the leads. This is true but, from Eq. (1.2.1), an additional algebraic suppression by $(k_F r)^2$ is expected. It will be substantial even with a separation r on the order of 10 nm since the wave length in the metallic aluminum superconductors is less than a nanometer. Still, the nonlocal signatures observed on the experiment are comparable to the local ones, just like the splitting efficiency is much stronger than expected in the Cooper pair splitter experiments and with similar possible reasons. Since we are not interested in device-specific details we can choose the tunnel points in the leads to be identical, $\mathbf{x}_{\nu i} = 0$.

Except for the parity $\mathcal{P}$, the model, Eq. (3.0.5), is equivalent to the one Choi et al. investigated. Nevertheless, the results I present go beyond previous work. In contrast to Choi et al., all charging states will be investigated, including those only possible at finite Coulomb repulsion, and the central assumption of a large superconducting gap will be relaxed. The signatures of nonlocal transport I will discuss are based only on the critical current, which is, essentially, a macroscopic quantity, and require neither SQUIDs, nor magnetic fields, nor intradot couplings. In particular, there is a regime in the $(1, 1)$ charge sector in which the critical current is carried by a nonlocal *triplet* ground state. This is rather surprising in a singlet-driven system (and is, e.g., dismissed right away in Ref. 92). Even more intriguingly, this intrinsic

singlet–triplet phase transition gives rise to a new feature in the critical current which is present only if there is nonlocal transport. Finally, the model reproduces the experimental measurements in good qualitative agreement.

3.1 Cooper pair splitter regime

Due to the small superconducting gap, $\Delta \gtrsim \Gamma$, the device is not in the Cooper pair splitter regime and it is to be expected that sequential transport channels are highly relevant. Indeed, in the experiment, the transport resonances in the superconducting state coincide with the transport resonances in the normal state, i.e., they are single-particle resonances. Nevertheless, it is instructive to consider the Cooper pair splitter regime, $\Delta \to \infty$ and large U_i, first.

In the Cooper pair splitter regime, only virtual excitations of the superconducting leads are allowed because the temperature is much lower than Δ and because there is no bias voltage. When Δ is very large, the analysis may further be restricted to the leading order contributions in $t_{\nu i}/\Delta$, i.e., to second order. This allows two kinds of processes to happen: first, an electron tunnels from one of the quantum dots into a superconductor and back onto the same quantum dot (or the other way around), which shifts the on-site energy, or it tunnels onto the other quantum dot, which realizes cotunneling. This type of process is not specific for superconducting leads, although it has been argued that the superconducting gap might be helpful to establish long-range correlations between the quantum dots [168]. Second, two electrons of a Cooper pair can be injected simultaneously onto one of the quantum dots or, nonlocally, one onto each quantum dot. The other way around, the electrons may be absorbed as a Cooper pair into one lead if they form a spin singlet.

This is described by the effective model

$$\begin{aligned} H_{\text{eff}} = &\sum_{i\sigma} \varepsilon_i d_{i\sigma}^\dagger d_{i\sigma} + \sum_i U_i d_{i\uparrow}^\dagger d_{i\downarrow}^\dagger d_{i\uparrow} d_{i\downarrow} \\ &+ \sum_{ij\sigma\nu} \tilde{\Delta}_{ij} \mathcal{P}_\nu e^{-i\varphi_\nu} \sigma d_{i\sigma}^\dagger d_{j\bar{\sigma}}^\dagger + \text{H.c.} \\ &+ \sum_{ij\sigma\nu} \tilde{t} \mathcal{P}_\nu d_{i\sigma}^\dagger d_{j\sigma}, \end{aligned} \tag{3.1.1}$$

which can be derived formally from Eq. (3.0.5), assuming $|\varepsilon_i|, U_i, t_{\nu i} \ll \Delta$, as I will demonstrate in detail in Chap. 4. The effective amplitude to inject a local ($i = j$) or a nonlocal ($i \neq j$) Cooper pair is $\tilde{\Delta}_{ij}$ and the amplitude of cotunneling is $\tilde{t}$. Both are real because the phase dependence is written out explicitly in Eq. (3.1.1). The shorthand notation $\mathcal{P}_\nu = 1$ if $\nu = L$ and $\mathcal{P}_\nu = \mathcal{P}$ if $\nu = R$ captures the influence of parity. I absorbed the level shifts into ε_i.

I already argued that, under these conditions, the singlet is the only ground state possible in the $(1,1)$-charge sector because it gains energy by hybridizing with the Cooper pair condensates in the superconducting leads. This is reflected by the effective model, Eq. (3.1.1), where the triplet states decouple completely: both Cooper pair injection and cotunneling are in conflict with the exclusion principle.

The critical current is found by using Eq. (3.0.2) after having obtained the ground-state energy by exact diagonalization of the low-dimensional effective model (Fig. 3.2). This amounts to a partial resummation including what I defined as Cooper pair tunneling processes, whereas, e.g., genuine fourth-order processes are neglected. The benefit is that the result is regular even at the transport resonances.

The critical current exhibits steplike features at the charging state transitions (Fig. 3.2). They could be mistaken for asymmetric single-particle resonances but, as I already discussed, there is no single-particle transport in the limit of $\Delta \to \infty$. The two-particle resonances, on the other hand, are localized in the corners of the $(1,1)$-charge sector in the ε_1–ε_2 plane: when the Coulomb repulsion is large, the level broadening is small compared to the level spacing, so it is meaningful to consider sharp resonance conditions. The $(1,1)$ ground state

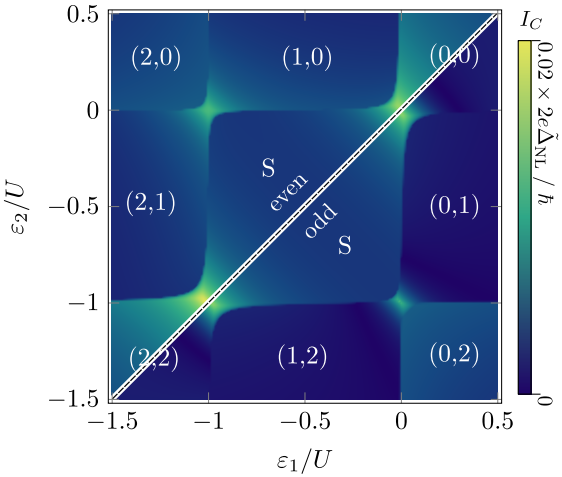

Figure 3.2: Critical current in the limit of large Δ_ν, where $U_1 = U_2 \equiv U$, $\tilde{\Delta}_{\mathrm{L}} = 0.05U$, $\tilde{\Delta}_{\mathrm{NL}} = 0.025U$, and $\tilde{t} = 0.01U$. The plot for even and the plot for odd parity are separated by a dashed line. Electrons can leave or enter the superconducting leads only in pairs, so sequential transport is not possible and the single particle resonances at the ground-state transitions are suppressed. In turn, two-particle resonances with the ground state are possible only at four points, where $\varepsilon_i = 0$ or $\varepsilon_i = -U_i$ is fulfilled simultaneously for both quantum dots $i = 1, 2$. At these points, nonlocal transport dominates. Parity has only quantitative influence. In particular, the singlet ground state is stable. Figure and caption reproduced from the original publication, Ref. 116.

exhibits strong nonlocal transport if it is almost degenerate with the $(0,0)$ state, which requires $\varepsilon_1 + \varepsilon_2 = 0$, or with the $(2,2)$ state, which requires $\varepsilon_1 + \varepsilon_2 = 2(\varepsilon_1 + \varepsilon_2) + U_1 + U_2$. But, in addition, for the $(1,1)$ state to be the ground state in the first place, both $\varepsilon_i \leq 0$ and $\varepsilon_i \leq 2\varepsilon_i + U_i$ need to hold. This can be fulfilled simultaneously only if $\varepsilon_1 = \varepsilon_2 = 0$ or if $\varepsilon_i = -U_i$. Nonlocal transport is possible, too, when the $(0,1)$ ground state is almost degenerate with the $(1,2)$ state, i.e., when $\varepsilon_2 = \varepsilon_1 + 2\varepsilon_2 + U_2$. This is compatible with the corresponding ground-state condition, $\varepsilon_1 \geq 0$, $\varepsilon_2 \leq 0$, and $\varepsilon_2 \leq 2\varepsilon_2 + U_2$, only if $\varepsilon_1 = 0$ and $\varepsilon_2 = -U_2$. The same argument holds under exchange of quantum dot 1 and quantum dot 2. These conditions define the four localized transport resonances in Fig. 3.2.

On the other hand, the condition for local transport, i.e., that the $(N_1, 0)$ ground state is almost degenerate with the $(N_1, 2)$ state or that the $(0, N_2)$ state is almost degenerate with the $(2, N_2)$ state, is $0 = 2\varepsilon_i + U_i$. But because $U_i > 0$, it is never fulfilled in a ground state in which quantum dot i is either empty or doubly occupied.

Localized features in the ε_1–ε_2 plane are, by definition, clear indications of nonlocality, making them interesting candidates for entanglement detection. In fact, they have been observed experimentally (Fig. 5 in Ref. 92) but since that particular device is *not* in the Cooper pair splitter regime a more careful analysis is required, which I will present in the remainder of this chapter.

3.2 Zero-bandwidth approximation

Of the numerous strategies which have been employed to solve the interacting quantum-dot Josephson junction [150–156, 162], the zero-bandwidth approximation [153] is well suited for the double-quantum-dot Josephson junction. It amounts to replacing the lead Hamiltonians, Eq. (3.0.7), by a single-site model,

$$H_\nu \to H_\nu^{\mathrm{zbw}} = \Delta_b c_{\nu\uparrow}^\dagger c_{\nu\downarrow}^\dagger + \mathrm{H.c.} \tag{3.2.1}$$

with a renormalized gap energy Δ_b and to renormalizing the tunnel couplings $t_{\nu i} \to t_{\nu i}^b$. In contrast to the Cooper pair splitter limit,

Eq. (3.1.1), the lowest-lying electronlike and holelike excitations in the superconducting lead are retained. This enables the model to capture the regime of a small superconducting gap energy and hence, in particular, sequential Cooper pair transport. At 2^8 dimensions, the Hilbert space is still sufficiently small to obtain the ground-state energy by exact diagonalization.

The validity of the zero-bandwidth approximation for quantum-dot Josephson junctions is well established in the regime of $\Gamma \lesssim \Delta$ [151, 161]. In particular, it is able to describe the competition between superconductivity and the Kondo effect, i.e., the cross-over between weak and strong coupling. In order to obtain quantitative predictions, the renormalized parameters Δ_b and $t^b_{\nu i}$ should be determined self-consistently. In the weak-coupling limit, however, we will see that already when using the bare parameters, the features are well reproduced qualitatively up to a global factor which is proportional to the normal-state energy density of states in the leads.

Using the zero-bandwidth approximation, the regime corresponding to the experiment can be accessed, where, in particular, the superconducting gap is small [Figs. 3.1(c) and 3.3]. There are three notable differences in comparison to the limit of $\Delta \to \infty$. First, the transport resonances are not localized points in the ε_1–ε_2 plane anymore but coincide with the single-particle resonances. This is expected because, when virtual excitations in the superconducting leads are acceptable, the electrons of a Cooper pair can be transported sequentially, i.e., one after another, through the double-quantum-dot structure. Whenever a *nonlocal* sequential transport channel is available, *local* sequential transport through only one of the dots is possible, too, which complicates the search for signatures of nonlocal transport. Second, there is a parameter regime in which the critical current is carried by a triplet state. More precisely, the spin-singlet Cooper pairs can be transferred past the spin triplet localized on the quantum dots. So we are dealing still with conventional s-wave superconductivity but, nevertheless, it is remarkable: there has to be a triplet ground state at some phase difference $\Delta\varphi$ in the first place and, in addition, it has to support a larger supercurrent than the (possibly singlet) ground state at any other phase difference, even though only sequential transport channels, i.e., genuine

fourth-order processes, are available. Third, there is a singlet–triplet transition only at even total parity.

3.3 Perturbation theory and microscopic processes

Understanding the phenomenology found in the zero-bandwidth approximation and confirming that it still applies in the more realistic case of dispersionful leads calls for additional investigation. Furthermore, thinking of entanglement detection, the nonlocal effects need to be identified. Perturbation theory in the tunnel couplings $t_{\nu i}$ is able to address all three issues. With dispersionful leads, the level broadening $\Gamma_{\nu i}$ takes the role of the tunnel probability $|t_{\nu i}|^2$ in the zero-bandwidth approximation. I will only discuss the wide-band limit, in which the normal-state density of states of the superconducting leads N can be assumed to be constant at all relevant quantum-dot energies. In this case, $\Gamma_{\nu i}$ and $|t_{\nu i}|^2$ differ only by the constant factor, $2\pi N(\varepsilon_F)$, and all perturbative corrections scale accordingly. In particular, the critical current scales by this factor.

It is sufficient to calculate the correction of the ground-state energy as a function of the phase difference $\Delta\varphi$ to obtain the critical current via Eq. (3.0.2). The unperturbed ground state, i.e., the ground state of the isolated double-quantum-dot system and the isolated superconducting leads, depends on the gate voltages applied to the quantum dots. Whereas the leads are always in the Bardeen–Cooper–Schrieffer ground state, the state of the double quantum dot is uniquely characterized by its charging state (N_1, N_2) and by the z component of the total spin S_z. Since the model, Eq. (3.0.5), conserves spin, the perturbation will not couple degenerate ground states except the nonlocal singlet and the nonlocal triplet with $S_z = 0$ in the $(1, 1)$-charge sector. Only even orders of the perturbative expansion are nonzero because the Bardeen–Cooper–Schrieffer ground state does not have overlap with states with an odd number of electron excitations or hole excitations. The second-order corrections are level renormalizations which can be absorbed into the tunable parameters ε_i and are not accessible in the

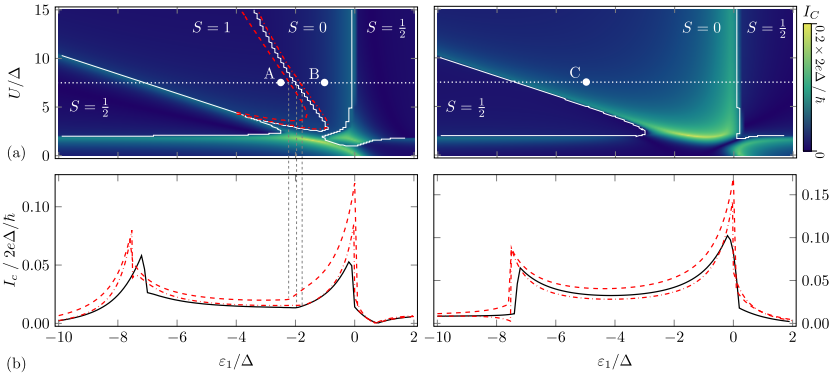

Figure 3.3: (a) Critical current and total spin of the Josephson junction depending on the on-site energy ε_1 on quantum dot 1 and on the Coulomb repulsion $U = U_1 = U_2$. Quantum dot 2 is kept at $\varepsilon_2 = -1.5\Delta$ and the tunnel couplings are $|t_{\nu i}| = 0.5\Delta$. Following the white dotted line from left to right, the quantum-dot occupation varies $(2,1) \to (1,1) \to (0,1)$. The critical current increases at each transition because the particle number fluctuates. Left: at even tunnel parity, $\mathcal{P} = 1$, an additional ground-state transition between a nonlocal singlet and a nonlocal triplet occurs in the $(1,1)$ sector. It is caused by competing cotunneling processes between the quantum dots via the superconducting leads which give rise to an exchange interaction (text). The red lines indicate the phase boundary obtained in perturbation theory in the zero-bandwidth approximation (dash dotted) and in the wide-band limit (dashed). Right: at odd tunnel parity, $\mathcal{P} = -1$, the singlet–triplet transition is absent. (b) Cuts across the ε_1–U plane at $U = 7.5\Delta$ reveal that the shape of the current peaks depends strongly on the tunnel parity. This can be traced back to the singlet–triplet transition (text), which also immediately manifests as a kink in the critical current. Since singlet and triplet can be distinguished only by nonlocal transport, this kink is immediate evidence of coherently split Cooper pairs. There is no qualitative difference between the zero-bandwidth approximation (exact: solid black, perturbative: dash-dotted red) and the wide-band limit (dashed red). In the wide-band limit, the critical current scales with the density of states, which is chosen to agree with the zero-bandwidth approximation. Figure and caption reproduced from the original publication, Ref. 116.

experiment. Transferring the two electrons of a Cooper pair across the double-quantum-dot Josephson junction requires at least four microscopic single-particle tunnel events. I will call a process which involves adding Cooper pairs to the condensate of the leads and removing them *Josephson process*. At the same order, superexchange enters via a *cotunneling process*, which transfers one electron from one quantum dot to another and transfers the same or another electron back. Both Josephson processes and cotunneling processes can either involve only one of the quantum dots, which makes them *local*, or both, in which case they are *nonlocal*. Formally, the perturbative corrections of the ground state energy δE are obtained from the matrix

$$\begin{aligned} H^{(4)}_{mm'} = -\frac{1}{2} \sum_{l,l',m''} & H_{ml} H_{lm''} H_{m''l'} H_{l'm'} \\ & \times \Big(\frac{1}{(E_m - E_l)^2 (E_m - E_{l'})} + \frac{1}{(E_m - E_l)(E_m - E_{l'})^2} \Big) \\ + \sum_{l,l',l''} & H_{ml} H_{ll'} H_{l'l''} H_{l''m'} \frac{1}{E_m - E_l} \frac{1}{E_m - E_{l'}} \frac{1}{E_m - E_{l''}}, \end{aligned} \tag{3.3.1}$$

where E_n is the energy of the unperturbed state n and H_{ij} is the matrix element for transitions between the states i and j due to the perturbation, Eq. (3.0.8) [144]. In the case of a unique ground state, $n = 0$, the correction of the ground-state energy is immediately given by $\delta E = H^{(4)}_{00}$. In the case of a degenerate ground state, the matrix $H^{(4)}_{mm'}$, where m and m' label the states which span the degenerate subspace, needs to be diagonalized as in conventional degenerate perturbation theory. Specifically, in the $(1,1)$-charge sector with two opposite-spin electrons, $S_z = 0$, it is possible for both cotunneling processes and Josephson processes to exchange the spins between the two quantum dots. This distinguishes spin-symmetric wave functions and spin-antisymmetric wave functions, i.e., $H^{(4)}_{mm'}$ is diagonal in the basis

of the nonlocal singlet and the nonlocal triplet,

$$|S\rangle = \frac{1}{\sqrt{2}}\Big(|\uparrow,\downarrow\rangle - |\downarrow,\uparrow\rangle\Big) \tag{3.3.2}$$

$$|T\rangle = \frac{1}{\sqrt{2}}\Big(|\uparrow,\downarrow\rangle + |\downarrow,\uparrow\rangle\Big), \tag{3.3.3}$$

where $|\uparrow,\downarrow\rangle$ denotes the state in which quantum dot 1 is occupied with one spin-up electron and quantum dot 2 is occupied with one spin-down electron. Since the singlet picks up a sign under spin exchange but the triplet does not, they are energetically split by spin-exchange processes as, e.g., in the Hubbard chain at half filling. The spin-triplet states with $S_z = \pm 1$ are statistically equivalent to the triplet with $S_z = 0$.

The amount of fourth-order processes is large. The primary challenge when calculating Eq. (3.3.1) is, first, not to miss any and, second, to find the correct fermion-exchange sign after the four tunnel events. The energy denominators are always negative for ground-state corrections. Both of the issues can be solved elegantly with a tailor-made diagrammatic formalism [116]. Irrespective of the individual processes, the energy correction is of the form

$$\begin{aligned}\delta E_0(\Delta\varphi) = {} & E^{\mathrm{loc}}_{\mathrm{CT},1} + E^{\mathrm{loc}}_{\mathrm{CT},2} + E^{\mathrm{loc}}_{J,1}(\Delta\varphi) + E^{\mathrm{loc}}_{J,2}(\Delta\varphi) \\ & + E^{\mathrm{nl}}_{\mathrm{CT,sc}} + E^{\mathrm{nl}}_{J,\mathrm{sc}}(\Delta\varphi) \pm \big[E^{\mathrm{nl}}_{\mathrm{CT,se}} + E^{\mathrm{nl}}_{J,\mathrm{se}}(\Delta\varphi)\big],\end{aligned} \tag{3.3.4}$$

where the first subscript distinguishes cotunneling processes (CT) from Josephson processes (J) and the superscript distinguishes local transport (loc) from nonlocal transport (nl). In the case of a local process, the second subscript denotes, which quantum dot is involved in the processes. Nonlocal processes are either spin conserving (sc) or spin exchanging (se). Obviously, spin-exchange processes are possible only in the degenerate singlet–triplet subspace. Then, the upper sign in Eq. (3.3.4) is the energy correction of the nonlocal triplet and the lower sign is the energy correction of the nonlocal singlet.

3.3.1 Ground state in the (1,1) sector

The ground state in the $(1,1)$ sector is determined by the sign of the spin-exchange contributions, $E^{\mathrm{nl}}_{\mathrm{CT,se}}$ and $E^{\mathrm{nl}}_{J,\mathrm{se}}(\Delta\varphi)$. The index ν of the

superconductor which is involved in any given microscopic process is an internal quantum number which is summed over in the perturbative expansion. Crucially, since the superconductors are identical, only the tunnel amplitudes $t_{\nu i}$ depend on ν. The energy correction hence factors into the tunnel couplings and a remainder $\mathcal{M}$, which is independent of the parity and of the phase difference because I associated both to the tunnel amplitudes.

In the case of the nonlocal spin-exchange Josephson processes, the decomposition reads

$$E^{\mathrm{nl}}_{J,\mathrm{se}}(\Delta\varphi) = \mathcal{M}^{\mathrm{nl}}_{J,\mathrm{se}}\Big[(t_{R1}t_{R2})^2 + (t_{L1}t_{L2})^2 + 2\mathcal{P}t_{R1}t_{R2}t_{L1}t_{L2}\cos(\Delta\varphi)\Big]. \tag{3.3.5}$$

The diagrammatic treatment reveals that the parity-independent and phase-independent factor is nonnegative, $\mathcal{M}^{\mathrm{nl}}_{J,\mathrm{se}} \geq 0$, such that $E^{\mathrm{nl}}_{J,\mathrm{se}}$, too, is nonnegative and favors the singlet ground state.

The case of the nonlocal spin-exchange cotunneling processes is less clear. The decomposition,

$$\begin{aligned} E^{\mathrm{nl}}_{\mathrm{CT,se}} &= \mathcal{M}^{\mathrm{nl}}_{\mathrm{CT,se}}\Big[(t_{R1}t_{R2})^2 + (t_{L1}t_{L2})^2 + 2\mathcal{P}t_{R1}t_{R2}t_{L1}t_{L2}\Big] \\ &= \mathcal{M}^{\mathrm{nl}}_{\mathrm{CT,se}}(t_{R1}t_{R2} + \mathcal{P}t_{L1}t_{L2})^2, \end{aligned} \tag{3.3.6}$$

shows that, again, the overall sign is governed by the sign of $\mathcal{M}^{\mathrm{nl}}_{\mathrm{CT,se}}$. Unfortunately, this time, there are microscopic processes of either sign. Very much like in the case of the 0–π transitions of single-quantum-dot Josephson junctions, it is a fermion-exchange sign, which makes the difference. If the electrons are exchanged exclusively through intermediate electronlike virtual excitations in the leads [Fig. 3.4(a)], the singlet ground state is favored but, if an electronlike excitation and a holelike excitation are involved [Fig. 3.4(b)], process are possible which favor the triplet ground state. So, ultimately, it is a question of the microscopic parameters, whether a triplet phase emerges or not. All possible spin-exchange processes are listed in Ref. 116.

As a rough estimate, the processes with only electronlike excitations, which favor the singlet ground state, put the double-quantum-dot system into an excited state at all intermediate virtual states unless

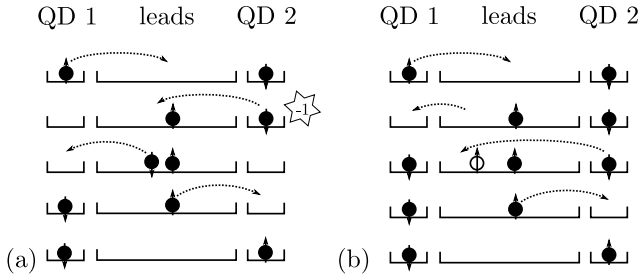

Figure 3.4: Two spin-exchange processes which have a different overall sign and hence energetically favor (a) singlet states and (b) triplet states. Initially, one of two electrons (filled circles) with opposite spin resides on each quantum dot (left and right narrow tray). A final state with the spins swapped can be reached via intermediate virtual states (arranged top to bottom) connected by four tunnel processes (dashed arrows) between the quantum dots and the superconducting leads (wide tray). Every time the left-to-right order of two fermions is changed, a sign results. (a) If only electronlike states in the leads are involved, the two initial electrons have to be swapped. This kind of process with a negative sign energetically favors the singlet state. (b) If the exchange process involves a hole (empty circle), it is possible to exchange the spins without anticommutation signs. This type of process energetically favors the triplet state. Figure and caption reproduced from the original publication, Ref. 116.

they involve doubly-occupied quantum dot states. So according to Eq. (3.3.1), they are weighted by

$$\frac{1}{(\varepsilon_{\mathrm{DQD}}+\Delta)^2}\frac{1}{2\varepsilon_{\mathrm{DQD}}+2\Delta}, \tag{3.3.7}$$

where $\varepsilon_{\mathrm{DQD}}$ is a typical quantum-dot energy scale set by the charging energy of the relevant transitions. Processes with electronlike and holelike excitations, which favor the triplet ground state, restore the initial charging state of the double quantum dot in one of the virtual states. Their strength is on the order of

$$\frac{1}{(\varepsilon_{\mathrm{DQD}}+\Delta)^2}\frac{1}{2\Delta}. \tag{3.3.8}$$

The ratio between the strength of the triplet-favoring processes and the strength of the singlet-favoring processes, $1+\varepsilon_{\mathrm{DQD}}/\Delta$, becomes large when the superconducting gap Δ is comparable with or smaller than the quantum-dot energy scale $\varepsilon_{\mathrm{DQD}}$, and the triplet ground state may emerge.

At even parity, $\mathcal{P}=1$, the triplet phase is readily found without tuning any parameters both in the zero-bandwidth approximation as and the wide-band limit. In the left panel of Fig. 3.3(a), the phase boundary obtained by exact diagonalization in the zero-bandwidth approximation is marked by a solid line. It agrees with the perturbative result in the zero-bandwidth approximation (dash-dotted line), demonstrating the validity of the perturbation expansion, and, more importantly, with the wide-band limit (dashed line). As anticipated, the transition occurs when the quantum-dot energy scale $\varepsilon_{\mathrm{DQD}} \sim |\varepsilon_1|$ is sufficiently large. It was already reported by Choi et al. that there is no triplet ground state in the wide-band limit if the Coulomb repulsion is assumed to be infinitely large, $U_i \to \infty$. If, however, either the band width or the Coulomb repulsion are not substantially larger than all of the remaining energy scales, a triplet ground state can be observed, so rather the *presence* than the *absence* of the triplet ground state is the rule.

This is not the case in the regime of odd parity, $\mathcal{P}=-1$. In Fig. 3.3(a), right panel, the triplet ground state is completely absent. This is because the tunnel couplings are chosen symmetrically, $t_{Li}=t_{Ri}$, and

so different paths of spin exchange through cotunneling interfere destructively: with $\mathcal{P} = -1$, Eq. (3.3.6) vanishes identically. Only the *Josephson* spin-exchange processes remain, which always lower the singlet state according to Eq. (3.3.5). If there is no perfect symmetry, there will be no perfect cancellation and, at some point, there might be a triplet ground state at odd parity, too. But it will always be more robust at even parity.

Although both the singlet ground state and the triplet ground state allow for Cooper pairs to flow across the junction, the supercurrent tends to be higher in the singlet phase because second-order Cooper pair tunneling provides another transport channel in addition to genuine fourth-order processes. Close to the resonance at $\varepsilon_1 = 0$ in the left panel of Fig. 3.3(b), second-order Cooper pair tunneling is particularly strong since the quantum-dot charging states $(1,1)$, $(1,0)$, $(0,1)$, and $(0,0)$ are almost degenerate. The supercurrent is mainly supported by the process depicted in Fig. 3.5(a). By checking all possible processes, it can be verified that, in the triplet ground state, there is no fourth-order Josephson process involving the $(0,0)$ state. This is most easily done by considering a fully-polarized triplet state with $S_z = \pm 1$, which is statistically equivalent to the triplet with $S_z = 0$. But at the second resonance in the left panel of Fig. 3.3(b), near $\varepsilon_1 = -U_1$, there *is* a Josephson process in the triplet ground state involving all of the four almost-degenerate charging states $(1,1)$, $(1,0)$, $(2,1)$, and $(2,0)$ [Fig. 3.5(b)]. All of the transport channels which are available in the triplet ground state are available in the singlet ground state, too. When ε_1 is increased along the horizontal axis in Fig. 3.3(b), the system first exhibits a resonance at the $(2,1)$–$(1,1)$ transition. Afterwards, it is in the triplet ground state, which does not have an equivalent resonance at the $(1,1)$–$(0,1)$ transition. Hence, the critical current decreases with increasing ε_1 until the singlet–triplet boundary is reached. After the boundary, which is located rather close to the $(1,1)$–$(0,1)$ transition, the critical current rises again because the singlet ground state *does* have a transport resonance at the $(1,1)$–$(0,1)$ transition. This produces a notable asymmetry between the two resonance peaks. At odd parity, there is no asymmetry because there is no singlet–triplet transition. The peak asymmetry can hence be employed to distinguish between even and odd orbital parity.

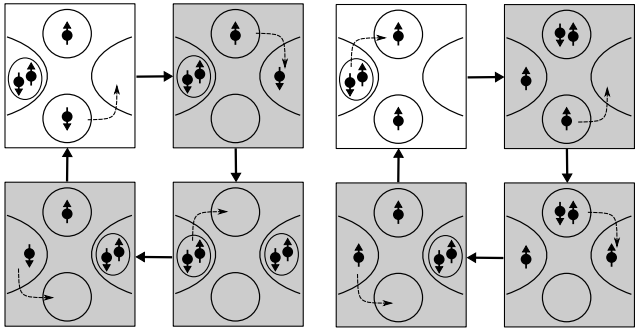

Figure 3.5: Typical Josephson transport processes via three intermediate virtual states (gray) in the $(1,1)$-charge sector. (a) In the singlet ground state, there are transport channels with intermediate states in which the two electrons of the transferred Cooper pair reside simultaneously on the double quantum dot. (b) In the triplet ground state (all triplets are equivalent by spin-rotation invariance), the electrons of the Cooper pair need to be transferred sequentially through the double quantum dot. Figure and caption reproduced from the original publication, Ref. 116.

But there is more to the singlet–triplet transition: directly at the phase boundary, the critical current has a kink. Again, the reason is that, in the singlet phase, different processes carry the critical current than in the triplet phase so, across the transition, the dependency of the critical current on the parameters, such as the gate voltages, changes. Note that the critical current is still continuous because, after all, it is simply the maximum of the largest possible current in the singlet state and the largest possible current in the triplet state, both of which depend on the parameters in a continuous fashion. The kink is caused by the transition between the *nonlocal* singlet ground state and the *nonlocal* triplet ground state. So none of the *local* currents are affected by the ground state transition. If the kink is observed, there have to be *nonlocal* currents. So the kink is evidence of nonlocal coherent Cooper pair transport, i.e., of split spin singlets.

3.3.2 Singlet–triplet transition and critical current

Due to the singlet–triplet transition, the simple relation between the Josephson energy and the critical current, Eq. (3.0.3), breaks down.

At the phase difference $\Delta\varphi = \pi$ (even parity) or $\Delta\varphi = 0$ (odd parity), the nonlocal spin-exchange Josephson processes vanish, as we can see from Eq. (3.3.5). An arbitrarily-small ferromagnetic superexchange coupling due to the nonlocal spin-exchange cotunneling processes, $E_{\mathrm{CT,se}}^{\mathrm{nl}} < 0$, is then sufficient for the triplet ground state to emerge. But if the observed quantity is the critical current, the phase difference is not going to be at $\Delta\varphi = 0$ or at $\Delta\varphi = \pi$. It is not even going to be always at $\Delta\varphi = \pm\pi/2$ as in ordinary Josephson junctions. This is because the simple form the ground state energy as a cosine of the phase difference with a fixed amplitude given by the Josephson energy, Eq. (3.0.3), is no longer valid. The distinction between the singlet and the triplet ground state in the correct expression, Eq. (3.3.4), means that the Josephson energy E_J itself depends on the phase difference $\Delta\varphi$. Both deep in the triplet phase and deep in the singlet phase, this distinction is irrelevant [Fig. 3.6(a)] but close to the transition, an interesting situation arises: there may be, e.g., a singlet ground state at $\Delta\varphi = \pi/2$ with the Josephson energy $E_J(\pi/2)$. But if there is a triplet ground

state at the phase difference $\Delta\varphi'$ and if it has has a larger Josephson energy $E_J(\Delta\varphi')$ such that $|E_J(\pi/2)\sin(\pi/2)| < |E_J(\Delta\varphi')\sin(\Delta\varphi')|$, the system will switch to the triplet ground state and the phase difference locks to a nonstandard value $\Delta\varphi' \neq \pi/2$ [Fig. 3.6(b)]. Again, we see that there is no triplet ground state for any phase difference at odd parity, where the cotunneling spin-exchange processes are absent [Fig. 3.6(c)].

In more physical terms, according to Eqs. (3.3.4) and (3.3.5), the sign of the nonlocal Josephson current in the $(1,1)$ state depends on the phase difference $\Delta\varphi$, on the parity $\mathcal{P}$, and on whether the ground state is a singlet or a triplet. There are configurations in which, at $\Delta\varphi = \pi/2$, the maximum nonlocal current flows opposite to the maximum local currents. So in order to maximize the supercurrent, the system might switch to $\Delta\varphi \neq \pi/2$ such that the total spin changes and the individual currents are decreased but flow in the same direction producing, overall, a larger critical current.

The piecewise nature of the current–phase relation $I(\varphi)$ shown in Fig. 3.6 is, of course, due to zero temperature. Considering that the critical phase difference may lock exactly to the discontinuity, I will temporarily relax the assumption of $T = 0$. At finite temperature, the Josephson current is calculated from the free energy $F(T, \Delta\varphi)$ instead of from the ground state energy [169], i.e.,

$$I(\Delta\varphi) = \frac{2e}{\hbar}\frac{\partial F(T,\Delta\varphi)}{\partial\Delta\varphi} = -\frac{2ekT}{\hbar}\partial_{\Delta\varphi}\ln\sum_n e^{-E_n/kT}. \tag{3.3.9}$$

At finite temperature, the discontinuities of $I(\Delta\varphi)$ are smoothed out such that the critical phase difference is slightly shifted. More importantly, the distinction between the singlet phase and the triplet phase is blurred since both of the states are realized with the relative thermal probability $e^{-E_n/kT}$ such that the expectation value of the total spin $\langle S\rangle$ lies between 0 and 1. We can, however, distinguish configurations in which the spin expectation value decreases and approaches 0 when decreasing the temperature, $\partial\langle S\rangle/\partial T > 0$, from configurations in which the spin expectation value increases towards 1 when decreasing the temperature $\partial\langle S\rangle/\partial T < 0$. The former case is realized in the situation

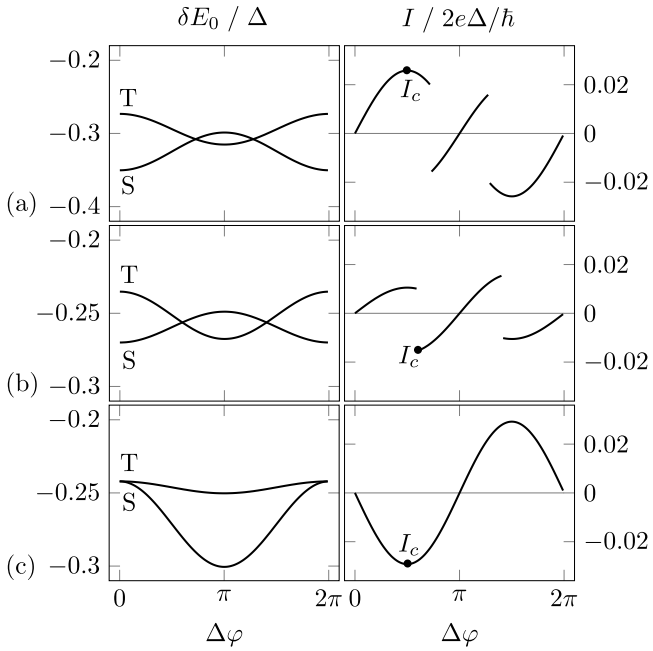

Figure 3.6: Phase dependence of the energy corrections δE_n of the two lowest-lying states in the $(1,1)$-charge sector and the resulting supercurrent I in the ground state evaluated in the zero-bandwidth approximation. (a) Point A in Fig. 3.3. The critical current I_c is carried by the singlet ground state (S) at $\Delta\varphi = \pm\pi/2$. (b) Point B in Fig. 3.3. The critical current is carried by the triplet ground state (T) at $\Delta\varphi \neq \pm\pi/2$. (c) Point C in Fig. 3.3. At odd total tunnel parity, $\mathcal{P} = -1$, the ground state is a singlet at all $\Delta\varphi$ and the critical current has the conventional sinusoidal dependence on $\Delta\varphi$. The junction is in the π phase. Figure and caption reproduced from the original publication, Ref. 116.

of Fig. 3.6(a) and corresponds to the singlet phase at zero temperature whereas the latter case is realized in the situation of Fig. 3.6(b) and corresponds to the triplet phase. So the total-spin transition is present also at finite temperature. In this example, the criterion is unambiguous once $kT \lesssim 0.1\Delta$, i.e., if the temperature is one order of magnitude below the superconducting transition temperature. This is experimentally accessible. Strictly speaking, Δ is renormalized because the data of Figs. 3.6(a) and (b) are obtained in the zero-bandwidth approximation. But it is a good estimate to use the bare value: with $\Delta = 0.1$ meV, which is the order of magnitude of aluminum, the critical current in Fig. 3.3, where $|t_{\nu i}| = 0.5\Delta$, is a few nanoampere in agreement with the experimental results of Ref. [92] so the quantitative size of the perturbative contributions is correct.

3.4 Comparison to experiments

Finally, the model can be applied directly to reproduce one of the experimental measurements performed by Deacon et al. To do so, an additional level is incorporated on quantum dot 2 such that the critical current can be studied across four successive resonances by continuously increasing the gate voltage of quantum dot 2 as has been done in Fig. 4 of Ref. 92. More precisely, H_2 is replaced by

$$H_2 = \varepsilon_2 d^\dagger_{21\sigma} d_{21\sigma} + (\varepsilon_2 + \delta) d^\dagger_{22\sigma} d_{22\sigma} + \sum_{(i\sigma)\neq(j\rho)} U_{ij} d^\dagger_{2i\sigma} d^\dagger_{2j\rho} d_{2j\rho} d_{2i\sigma}, \tag{3.4.1}$$

where δ is the separation between the two levels on quantum dot 2. The levels are coupled to the superconducting leads with amplitudes $t_{\nu 21}$ and $t_{\nu 22}$, respectively. The Coulomb repulsion U_{ij} is taken to be spin independent, i.e., the exchange interaction between the two levels is neglected. This is a valid approximation considering that the device is in the single-level regime. For the same reason, the physical behavior of the extended model is expected to be basically the same as the behavior of the single-level model, taking into account only the levels which are close to resonance. In particular, the total tunnel parity may be different for each of the two levels on quantum dot 2.

With the additional level, the Hilbert space has 1024 dimensions in the zero-bandwidth approximation, which is still sufficiently small for exact diagonalization but too large to determine the microscopic parameters in an automated fashion. A first indication how to choose them is provided by the shape of the conductance peaks: the two neighboring peaks at lower gate voltages (i.e., at higher level energies) are clearly more symmetric than the two neighboring resonances at higher gate voltages (i.e., at lower level energies). This is just one of the manifestations of orbital parity I discussed in the single-level case. It is, therefore, a reasonable assumption that the two lower peaks belong to an odd-parity level whereas the two higher peaks belong to an even-parity level. Another possible interpretation is, of course, that the measurement actually involves *three* levels on quantum dot 2, i.e., that the two inner resonances belong to one level and that the outer two resonances belong to a separate level each. There is incomplete experimental data based on the Zeeman splitting which points in this direction but two levels turn out to be sufficient to describe the experimental findings. Fig. 3.7 shows the critical current depending on the on-site energies ε_2 and ε_1 together with cuts at three different values of ε_1. This way of presenting the data is directly adapted to Ref. 92. Close to the resonance of quantum dot 1 (blue curve), the behavior of two mostly independent levels on quantum dot 2 is recovered as expected. Comparing this cut to another one with quantum dot 1 a bit further off resonance (green curve), the model recovers the signature of nonlocal Cooper pair transport proposed in the experiment: if a decomposition of the critical current into two local contributions were possible, the green curve could be obtained by shifting the blue curve along the vertical axis. The shaded areas under the curves serve as arbitrarily-chosen references which illustrate that this is not the case: the closer quantum dot 1 is brought to resonance, the more are the resonance peaks of quantum dot 2 increased in relation to the reference. This is caused by the additional nonlocal transport channel. Furthermore, there are nonlocal effects which *lower* the critical current when quantum dot 1 is brought closer to resonance and quantum dot 2 is fixed between its two levels. This is most likely caused by the competition of local and nonlocal supercurrents I discussed in detail for the simpler case of the single-level model. Still another behavior is found when quantum dot 1 is further detuned (yellow curve): the resonance

at $\varepsilon_2 \approx -18\Delta$ increases again. This indicates that the two levels on quantum dot 2 are more relevant for transport than quantum dot 1 and so the multi-level single-dot regime is approached [167].

The most important aspect in the context of entanglement detection is, however, that the model, which clearly has nonlocal transport channels, does reproduce the anomalous features observed in Ref. 92. This strongly supports their interpretation as being caused by nonlocal Cooper pair currents, although the decomposition of the Josephson energy, Eq. (3.3.4) turned out to be more complicated than assumed so far [Eq. (3.0.3)].

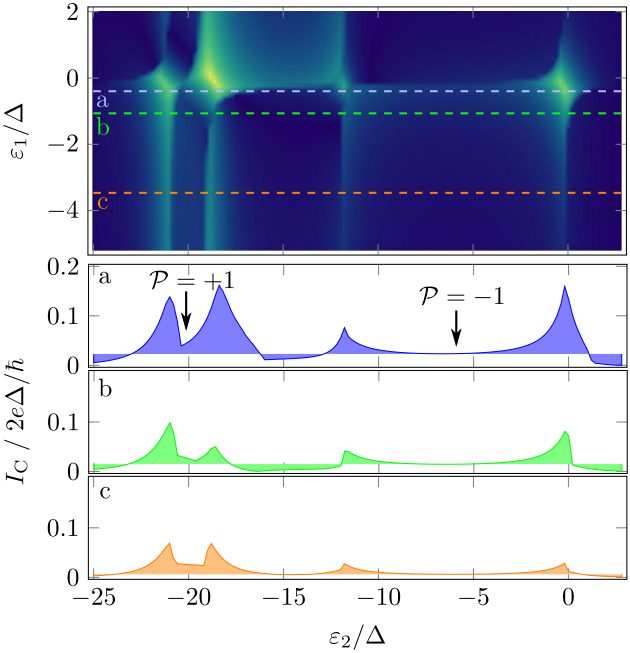

Figure 3.7: Critical current of the double-quantum-dot junction with two different levels of opposite parity on quantum dot 1. The parameters of the quantum dots are $\delta = 18.5\Delta$, $t_{R1} = t_{L1} = 0.45\Delta$, $t_{R21} = -t_{L21} = 0.45\Delta$, $t_{R22} = t_{L22} = 0.57\Delta$, $U_1 = 28\Delta$, $U_{11} = 12\Delta$, $U_{22} = 3\Delta$, and $U_{12} = 0.5\Delta$. Upper panel: critical current as a function of the gate-controlled on-site energies ε_1 and ε_2. Lower panel: cuts at (a) $\varepsilon_1 = -0.9\Delta$, (b) $\varepsilon_1 = -1.8\Delta$, and (c) $\varepsilon_1 = -4.2\Delta$. In the absence of nonlocal transport, the three curves are expected to differ only by a constant. Instead, when approaching the resonance, $\varepsilon_1 \searrow 0$, the critical current grows more strongly at the peaks and less strongly between the peaks. Within the model this behavior is clearly attributable to nonlocal coherent transport and it was already observed experimentally [92]. Figure and caption reproduced from the original publication, Ref. 116.

4

Entanglement Detection via Optical Conversion

I will now present another scheme which combines entanglement production and entanglement detection. Like the double-quantum-dot Josephson junction discussed in the preceding chapter, the Cooper pair splitter part of the device is straight forward: a superconductor coupled to two quantum dots. Unlike the rather indirect assessment of entanglement via specific features in the critical Josephson current, however, this time I aim at a full Bell test. As I discussed in Chap. 1, all-electronic Bell tests are very challenging so it may be beneficial to transfer the spin wave function of the Cooper pair to the polarization wave function of a pair of photons. Among the first kind of radiation which comes to mind in the context of superconductors is the Josephson radiation, which is emitted due to the current oscillating across a biased Josephson junction, i.e., due to the alternating current Josephson effect. Its frequency is, however, the same as the frequency of the alternating current, $\omega = 2eV/\hbar$, where the bias voltage V is limited by the superconducting band gap, $V < \Delta$. Hence the frequency of the electromagnetic radiation is restricted to the terahertz regime far from the optical range. A more quantum interpretation is that each time a Cooper pair tunnels from the source superconductor to the drain superconductor, a charge of $2e$ is transferred across the potential difference V, releasing the energy $E = 2eV$ as a photon. With Einstein's relation $E = \hbar\omega$, its frequency is again found to be the Josephson frequency. Unfortunately, terahertz radiation is of little use since we are aiming at a conventional optical Bell test, such that we can rely on the vast experience of the quantum-optics community. The alternative is to use a p–n

junction, i.e., two semiconductor quantum dots with a large direct band gap, and a source–drain voltage close to the band gap. Here, optical photons are emitted when the electrons relax from the conduction band into the valence band just like in an ordinary light-emitting diode. Crucially, the selection rules of the quantum dots provide a correspondence between the spin of the electrons and the polarization of the photons. As a bulk p–n junction termed *spin LED*, this type of device has been around experimentally for some time and has mostly been employed to detect spin-polarized electrons by detecting circular-polarized photons [170, 171]. Soon after its invention, Gywat et al. extended the concept to single quantum dots [172] and proposed to use two quantum-dot spin LEDs to convert pairs of electrons to pairs of photons [173]. They modeled the recombination process with a master equation which includes an effective rate to inject spin-entangled electrons and showed that the conversion scheme is highly efficient. Titov et al. pointed out, however, that it can transfer only *classical* correlations onto the photons [174], which I will discuss in more detail below. To bring Cooper pairs back into the picture, the leads could be semiconductors with proximity-induced superconductivity, or the quantum dots are directly coupled to metallic superconductors. Arguably, as an alternative to the all-electronic Bell test, this construction replaces one technological challenge by another but, intriguingly, once the conversion itself is done, all which remains is the standard task of photonic entanglement detection, and interfacing semiconductors with superconductors has already enjoyed a lot of attention. In particular, superconducting p–n junctions were successfully built [114, 175]. They have an enlarged luminous intensity at temperatures below the superconducting gap because Cooper pair recombination opens up an additional emission channel [176, 177]. For the application in the Cooper pair splitter, the p–n region has to be restricted to single quantum dots, e.g., in gallium-arsenide quantum dots, as proposed by Suemune et al. [178], or using the proximity effect in semiconducting nanowires as demonstrated experimentally by the Delft group [157, 179].

What is still missing, is a complete device which comprises the Cooper pair splitter, as well as an optical conversion mechanism, and a Bell test. It turns out that interesting side effects arise in the combined device such as electron–photon correlations and inevitable local photon

pair emission but that these issues can be dealt with. In addition, I will estimate the microscopic parameters including, e.g., the expected amount of imperfect splitting in a generic implementation. Since it involves an actual Bell test, this entanglement detection scheme can be viewed as the most fundamental one of the three I discuss. But while it is certainly true that the resulting photons can be proven to be entangled or not, it should be noted that we still need to make an assumption about how the photons are related to the electronic Cooper pairs, about which we want to make a statement. This scheme relies on the fact that if the photons are entangled, the only plausible source of entanglement are nonlocal pairs of electrons because the photons themselves do not interact.

A common problem in entanglement-generating devices, be it for photons or for massive particles, is that *which-path information* has to be avoided. The name probably goes back to the double-slit experiment, in which the coherent superposition fringes vanish if the experimenter knows which slit each particle went through, i.e., which path it took [180]. Similarly, entanglement as a special case of a superposition vanishes if certain pieces of information are gained. The obvious example is to use a spin-helical channel for Cooper pair splitting, where it is known in advance which spin leaves in which direction. But it can be more subtle: entangled photons created in a biexciton cascade are polarization entangled [181]. When the first electron–hole pair recombines, it leaves behind an exciton with opposite angular momentum than the emitted photon and, when the remaining exciton recombines, hence, a photon of opposite polarization is emitted. In this situation, two paths exist: either, first, a right-polarized photon $|\circlearrowright\rangle$ is emitted and, second, a left-polarized photon $|\circlearrowleft\rangle$ or the other way around. Because the intermediate-state exciton is spinful, it is subject to fine-structure splitting. If present, it implies that, say, the right-circular photon always comes at a lower energy than the left-circular photon. If this energy difference is resolved, the entanglement is lost. This problem is avoided in emission cascades with a different intermediate single-exciton state such that either two horizontally-polarized (H) or two vertically-polarized (V) photons are emitted, $|HH\rangle + |VV\rangle$. In this cascade, too, the intermediate state may be split (*anisotropic exchange splitting*), which causes the energy of the first emitted photon to be

higher if it is horizontally polarized, and the energy of the second electron to be higher by the same amount if it is vertically polarized (or the other way around). In either case, however, two photons with *different* energies but with the *same* polarizations are emitted, such that the orbital part and the polarization part of the wave function factorize and entanglement remains. But, unfortunately, there can be a finite biexciton binding energy, i.e., the two-exciton state has a lower energy than twice that of one exciton. Then, four different emission energies result and the two paths $|HH\rangle$ and $|VV\rangle$ *can* be told apart. A number of strategies have been demonstrated to remove either the fine-structure splitting, the anisotropic exchange splitting, or the biexciton binding energy by engineering the structure and the material of the quantum dots [182–185], by applying magnetic [186] or electric [187–192] fields, by strain [193], or by using special emission wavelengths [182]. Once the two photons have sufficient spectral overlap due to their (e.g., lifetime) broadening, it is possible to filter, i.e., postselect, pairs of photons with equal energy [194]. For the device I discuss, I will therefore assume this problem to be solved and neglect both the biexciton binding energy and the splitting of the intermediate state. But still, due to the electronic part of the device, there is another possible leak of information of a kind which was first discussed by Titov et al. [174]. The ideal biexciton cascade starts in the unique empty state, goes over into the biexciton state by laser pumping, and ends in the unique empty state after having emitted two photons. So if there is some which-path information to be gained, it is certainly contained in the degrees of freedom of the photons. With the superconducting p–n junction, we face a different situation. The spin-singlet electrons split across the two quantum dots relax into the valence band emitting two photons. The optical selection rules, i.e., conservation of angular momentum, ensure that, if a spin-3/2 heavy hole recombines with a spin-$-1/2$ electron, a right-circular photon is emitted along the quantization axis of angular momentum and that, if a spin-$-3/2$ heavy hole recombines with a spin-1/2 electron, a left-circular photon is emitted along the quantization axis of angular

momentum [195]. So, the system evolves as

$$\begin{aligned} & |\rangle_n \, |\rangle_p \, |\rangle_{\mathrm{ph}} \\ \longrightarrow\, & |\uparrow\downarrow\rangle_n \, |\rangle_p \, |\rangle_{\mathrm{ph}} - |\downarrow\uparrow\rangle_n \, |\rangle_p \, |\rangle_{\mathrm{ph}} \\ \longrightarrow\, & |\rangle_n \, |\uparrow\downarrow\rangle_p \, |\circlearrowleft\circlearrowleft\rangle_{\mathrm{ph}} - |\rangle_n \, |\downarrow\uparrow\rangle_p \, |\circlearrowleft\circlearrowleft\rangle_{\mathrm{ph}} \,, \end{aligned} \tag{4.0.1}$$

where the first arrow indicates the injection of a Cooper pair from the superconductor into the quantum dots on the n side and the second arrow indicates their relaxation into the valence band or, equivalently, their transition into the p side, emitting two photons. In the resulting state, the entanglement has not been transferred onto the photons but is only reflected by them: if information is gained about which spin ends up on which quantum dot, not only is the entanglement of the electrons lost but that of the photons is, too, because the electronic subsystem contains which-path information. In an open system, the abstract concept of information gain translates to decoherence, which is captured by the idea that "the environment performs measurements on the system". In other words, after the electrons enter the normal-state p-side lead, their spin wave function will soon decohere and, once this happened, the entanglement of the photons is lost. Formally, the degrees of freedom which are not observed have to be traced out,

$$\begin{aligned} \mathrm{tr}_{n,p}\Big[& \Big(|\rangle_n \, |\uparrow\downarrow\rangle_p \, |\circlearrowleft\circlearrowleft\rangle_{\mathrm{ph}} - |\rangle_n \, |\downarrow\uparrow\rangle_p \, |\circlearrowleft\circlearrowleft\rangle_{\mathrm{ph}} \Big) \\ & \times \Big(\langle|_n \, \langle\uparrow\downarrow|_p \, \langle\circlearrowleft\circlearrowleft|_{\mathrm{ph}} - \langle|_n \, \langle\downarrow\uparrow|_p \, \langle\circlearrowleft\circlearrowleft|_{\mathrm{ph}} \Big) \Big] \\ = & \, |\circlearrowleft\circlearrowleft\rangle \, \langle\circlearrowleft\circlearrowleft| + |\circlearrowleft\circlearrowleft\rangle \, \langle\circlearrowleft\circlearrowleft| \,, \end{aligned} \tag{4.0.2}$$

and a classical mixed state remains. In order to circumvent this problem, we have to make sure that, like in the biexciton cascade, the electronic subsystem returns to its initial state after the emission. Different strategies to do so are conceivable. E.g., Nigg et al. consider a different set of selection rules where the entangled states are not left-circularly and right-circularly polarized, but circularly and linearly polarized [110]. Their approach, however, comes at the expense of an active multi-step driving scheme, which has to be reset after each cycle, and the entanglement is partly leaked into the photon energy as with anisotropy-split biexcitons. Here, I will pursue a different approach: if

the p-side lead is superconducting, too, the spin singlet is absorbed coherently into the Bardeen–Cooper–Schrieffer ground state and (in the thermodynamic limit) the electronic system returns into the same state it started in,

$$\begin{aligned} &|\rangle_n\,|\uparrow\downarrow\rangle_p\,|\circlearrowleft\circlearrowleft\rangle_{\mathrm{ph}} - |\rangle_n\,|\downarrow\uparrow\rangle_p\,|\circlearrowleft\circlearrowleft\rangle_{\mathrm{ph}} \\ \longrightarrow\ &|\rangle_n\,|\rangle_p\,|\circlearrowleft\circlearrowleft\rangle_{\mathrm{ph}} + |\rangle_n\,|\rangle_p\,|\circlearrowleft\circlearrowleft\rangle_{\mathrm{ph}}\,. \end{aligned} \tag{4.0.3}$$

In an electron–hole picture, an electron singlet recombines with a hole singlet. Curiously, this produces a polarization *triplet*: note the + sign in Eq. (4.0.3), which arises because the fermionic electrons anticommute but the bosonic photons commute. Total angular momentum is not conserved because the rotational symmetry has to be reduced to mere azimuthal symmetry when imposing the selection rules, which are valid only for photons emitted along the quantization axis of angular momentum defined by the quantum dots.

Recher et al. calculated the spectral intensity of such an entirely superconducting p–n junction with a *single* quantum dot [196]. They found that, at certain frequencies, the junction emits optical photons in pairs, and already argue that these pairs should be entangled. From this perspective, the device is rather a source of entangled photons than a tool to proof Cooper pair splitting since, obviously, no Cooper pairs are split. This direction was investigated further by a number of follow-up publications, including coherent qubit-like manipulations on the quantum dot [197], the non-classical statistics of the emitted photons [198], and lasing [199–201]. All of these proposals, as well as the one by Nigg et al. [110], require p-type superconductivity simultaneously to the more common n-type superconductivity. To my knowledge, p-type superconductivity has not been demonstrated clearly, yet. In principle, no fundamental problems should arise since, considering only one relevant band, the theory of conventional superconductivity is electron–hole symmetric. When this relevant band, however, is the valence band instead of the conduction band, the effective parameters will be affected. When, e.g., the metallic superconductor is coupled to a semiconductor valence band, a large Schottky barrier might result and reduce the proximity effect. But then again, the quantum dots might even benefit from being only weakly coupled to the metallic leads. For

the device I consider, the required superconducting pairing is, in particular, ultimately limited only by thermal broadening and may be rather small.

A final ingredient is required for the device to work. Two problems arise if the emission of photons is completely unconstrained. First, only photons emitted along the quantization axis of angular momentum obey the selection rules needed to translate spin entanglement to polarization entanglement. Second, energy conservation dictates that the total energy of the electronic system changes by twice the source–drain voltage in one emission process. But, because the splitting process and the emission process happen in a coherent fashion, it may be that red-shifted photons are emitted while the electronic system is brought into an excited state. Depending on the charging energy, this applies to the quantum dots and certainly to the superconducting leads since quasiparticles are available already at the millielectronvolt scale [196]. A variant of quasiparticle poisoning results and ruins the correlation between the photons: it may happen that only one electron–hole pair recombines at a time while the other is stored on the quantum dots or in the leads, and that, later, two emission events happen simultaneously which are not related to the same Cooper pairs. Both problems can be solved elegantly when embedding the quantum dots into two photonic nanocavities, which, via the Purcell effect [202], constrain both the direction of emission and the emission frequency if they have a sufficiently narrow linewidth. The progress in embedding optical quantum dots into nanocavities was recently reviewed in Ref. 106. A system of two quantum dots in separate cavities initially charged with a pair of entangled electrons and with a pair of entangled holes but without leads was studied in some detail by Budich and Trauzettel [203] including a number of entanglement measures applied to the photons and different relaxation mechanisms.

The entire device is depicted in the left panel of Fig. 4.1. It comprises the superconducting leads on the n side and on the p side, the optically-active double quantum dot and the two nanocavities. In the remainder of the chapter, I will build a microscopic model of this rather complicated heterostructure by integrating out the electronic degrees of freedom piece by piece such that we end up with an effective model which contains only the photons, or, more precisely, polaritons. Then,

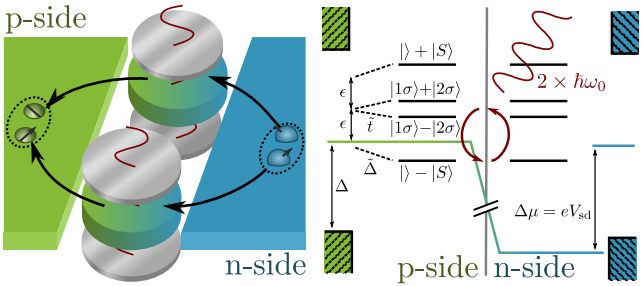

Figure 4.1: Left: two quantum dots (1,2) are tunnel coupled to superconducting p-type and n-type leads. Coulomb repulsion on the quantum dots splits the electrons or holes of incoming Cooper pairs, so each quantum dot contains one electron and one hole. Upon recombination polarization-entangled photons are emitted into two nanocavities (gray) with resonance frequency ω_0 and detected by an optical Bell test. Right: Lowest relevant energy levels of the double-quantum-dot system. The superconducting leads hybridize the empty state and the singlet state, $|\rangle \pm |S\rangle$, and the singly occupied states, $|1\sigma\rangle \pm |2\sigma\rangle$, creating a closed two-photon emission cycle. Figure and caption reproduced from the original publication, Ref. 117.

a suitable Bell measurement is devised to detect entanglement reliably even though we will see that exclusively-nonlocal emission is not possible even with infinitely strong Coulomb repulsion on the quantum dots.

4.1 Microscopic model

The n side of the electronic system consists of the conduction band levels of the two quantum dots $i = 1, 2$ coupled to the n-side superconducting lead. I will focus on the limit of one relevant spin-degenerate level ε_{ni} on each quantum dot with very large Coulomb repulsion, which is easily achieved experimentally, as we saw in the previous chapter, and which makes the discussion particularly transparent. If desired, finite Coulomb repulsion can be included perturbatively or numerically without conceptional changes [117]. In the Cooper pair splitter regime,

i.e., when the superconducting energy gap $\Delta_n = |\Delta_n| e^{i\phi}$ is the largest energy, $|\Delta_n| \gg |\varepsilon_{ni}|, k_B T$, the superconducting lead will provide an amplitude to inject nonlocal Cooper pairs into the quantum dots, $\tilde{\Delta}_n$, and an amplitude to remove a nonlocal Cooper pair from the quantum dots, $\tilde{\Delta}_n^*$. Because the large Coulomb repulsion suppresses double occupation, there is no need to consider local Cooper pair injection. But, like in Chap. 3, there are cotunneling processes, too, in which an electron tunnels from one quantum dot to the other through the superconducting lead with the amplitude $\tilde{t}$. All of the effects are summarized in the Hamiltonian

$$H_n = \sum_{i\sigma} \varepsilon_{ni} d_{i\sigma}^\dagger d_{i\sigma} + \sum_{\sigma} \Big[\tilde{\Delta}_n \sigma d_{1\sigma}^\dagger d_{2\bar{\sigma}}^\dagger + \tilde{t}_n d_{1\sigma}^\dagger d_{2\sigma} + \text{H.c.} \Big], \qquad (4.1.1)$$

where $d_{i\sigma}$ annihilates electrons with spin $\sigma = \uparrow, \downarrow \equiv \pm 1$ on quantum dot i. The energy gap $|\Delta_n|$, which is the lower bound on single-particle excitations in the Bardeen–Cooper–Schrieffer ground state of the lead, is the height of the tunnel barrier for the cotunneling process. So unless additional cancellations come into play, we can expect cotunneling to decay exponentially with the superconducting coherence length $\xi = \hbar v_F / (\pi |\Delta_n|)$, just like the Cooper pair splitting amplitude usually does [cf. Eq. (1.2.1)]. Indeed, in one of the first publications concerned with crossed Andreev reflection, Falci et al. already discovered that the crossed Andreev conductance and the cotunneling conductance are basically identical in the absence of, e.g., magnetization [204]. The reason why this is not important in the usual Cooper pair splitter setup is that the quantum dots are strongly coupled to metallic leads and are hence quickly depleted. So, even if cotunneling is possible, it will not happen because most of the time the quantum dots are empty and, once a Cooper pair is injected, it leaves the quantum dots on a much shorter time scale than the cotunneling rate. The p–n junction is a different situation because I will not assume optical recombination to be much stronger than the coupling between the superconducting lead and the quantum dots.

In order to obtain the amplitudes $\tilde{\Delta}_n$ and $\tilde{t}_n$, I now perform a Schrieffer–Wolff transformation [205] on a more fundamental model which still

includes the superconducting lead explicitly,

$$H = H_0 + H_T \tag{4.1.2}$$

$$H_0 = \sum_{\mathbf{k}\sigma} E_{\mathbf{k}} \gamma^\dagger_{\mathbf{k}\sigma}\gamma_{\mathbf{k}\sigma} + \sum_{i\sigma} \varepsilon_{ni} d^\dagger_{i\sigma} d_{i\sigma} + \sum_i U_i d^\dagger_{i\uparrow} d^\dagger_{i\downarrow} d_{i\downarrow} d_{i\uparrow} \tag{4.1.3}$$

$$H_T = \sum_{i\sigma} t_i d^\dagger_{i\sigma} \psi_\sigma(\mathbf{x}_i) + \text{H.c.}, \tag{4.1.4}$$

where $E_{\mathbf{k}} = \sqrt{(\varepsilon_k - \mu)^2 + |\Delta_n|^2}$ is the lead dispersion of the Bogoliubov quasiparticles annihilated by $\gamma_{\mathbf{k}\sigma}$. Tunneling from point $\mathbf{x}_i$ in the lead onto quantum dot i has the amplitude t_i. Without magnetic fields, t_i is real. The Coulomb repulsion U_i may be finite in Eq. (4.1.3) but in order to ensure a consistent separation of energy scales it should be either much larger or much smaller then the bulk superconducting gap. The operators $\psi_\sigma(\mathbf{x})$, which describe the *electrons* in the superconductor, are related to the operators $\gamma_{\mathbf{k}\sigma}$, which describe the *quasiparticle* excitations in the superconductor, through the Bogoliubov transformation $\psi_\sigma(\mathbf{x}) = \sum_{\mathbf{k}} \varphi_{\mathbf{k}}(\mathbf{x})(u^*_{\mathbf{k}}\gamma_{\mathbf{k}\sigma} + \sigma v_{\mathbf{k}} \gamma^\dagger_{-\mathbf{k}\bar{\sigma}})$, where the coherence factors obey $|v_{\mathbf{k}}|^2 = 1 - |u_{\mathbf{k}}|^2 = (1 - (\varepsilon_{\mathbf{k}} - \mu)/E_{\mathbf{k}})/2$ and $v^*_{\mathbf{k}} u_{\mathbf{k}} = -|v_{\mathbf{k}}||u_{\mathbf{k}}| e^{-i\phi}$, and where $\varphi_{\mathbf{k}}(\mathbf{x})$ is the normal-state electron wave function.

There is a very convenient operator-based formulation of the second-order Schrieffer–Wolff transformation which is applicable if the unperturbed low-energy space is degenerate. This method has been applied first probably by Hewson to derive the Kondo Hamiltonian from the Anderson impurity model in the symmetric and hence degenerate case [206]. It can be applied here as well because, in the Cooper pair splitter regime, the excitation energies are dominated by $E_{\mathbf{k}} \sim |\Delta_n|$ which is much larger than, e.g., the on-site energies ε_i. We define a complementary pair of projection operators

$$P = \prod_{\mathbf{k}\sigma} \left(1 - \gamma^\dagger_{\mathbf{k}\sigma}\gamma_{\mathbf{k}\sigma}\right) \qquad Q = 1 - P, \tag{4.1.5}$$

where P projects onto the low-energy space, in which the superconducting lead is in the ground state. A simple algebraic transformation [206] brings the Hamiltonian into the form

$$H_{\text{eff}} = PHP + PHQ(E - QHQ)^{-1}QHP. \tag{4.1.6}$$

Expanding the second term, which contains the contributions from the high-energy space, up to second order in the tunnel amplitude t_i, we obtain

$$H_{\text{eff}} = H_0 + \sum_{ij\sigma}\Big[\tilde{\Delta}_{ij}\sigma d^\dagger_{i\sigma}d^\dagger_{j\bar{\sigma}} + \text{H.c.} + \tilde{t}_{ij}d^\dagger_{i\sigma}d_{j\sigma}\Big] \tag{4.1.7}$$

with the Cooper pair injection amplitude

$$\tilde{\Delta}_{ij} = \sum_{\mathbf{k}} \frac{t_i t_j}{E_{\mathbf{k}}}\varphi_{\mathbf{k}}(\mathbf{x}_i)\varphi_{-\mathbf{k}}(\mathbf{x}_j)|u_{\mathbf{k}}||v_{\mathbf{k}}|e^{i\phi}, \tag{4.1.8}$$

and the cotunneling amplitude

$$\tilde{t}_{ij} = -\sum_{\mathbf{k}} \frac{t_i t_j}{E_{\mathbf{k}}}\varphi_{\mathbf{k}\sigma}(\mathbf{x}_i)\varphi^*_{\mathbf{k}\sigma}(\mathbf{x}_j)(|u_{\mathbf{k}}|^2 - |v_{\mathbf{k}}|^2). \tag{4.1.9}$$

In the energy denominators of Eqs. (4.1.8) and (4.1.9), the quantum-dot energies are neglected against the lead excitation energy $E_{\mathbf{k}}$ as anticipated. Higher-order terms can be derived by expanding Eq. (4.1.6) to higher orders in t_i/Δ_n but they do not contribute additional different effective processes, so it is safe to ignore them. Assuming the superconducting lead to be an isotropic electron gas, $\varphi_{\mathbf{k}}(\mathbf{x}) = e^{i\mathbf{k}\cdot\mathbf{x}}$, Eqs. (4.1.8) and (4.1.9) can be evaluated in the wide-band approximation, which amounts to replacing the sum over momenta by an integral over energies with infinite boundaries and linearizing the dispersion, i.e., assuming the density of states to be constant, $N(\varepsilon) \approx N(\varepsilon_F)$. The resulting Cooper pair splitting amplitude

$$\tilde{\Delta}_n \equiv \tilde{\Delta}_{i\neq j} = -\frac{\Gamma}{2}\frac{e^{-\frac{r}{\pi\xi}+i\phi}}{k_F r}\Big[\sin(k_F r) + \frac{1-\cos(k_F r)}{\pi k_F \xi}\Big] \tag{4.1.10}$$

and the cotunneling amplitude

$$\tilde{t}_n \equiv \tilde{t}_{i\neq j} = -\frac{\Gamma}{2}\frac{e^{-\frac{r}{\pi\xi}}}{k_F r}\Big\{\frac{\sin(k_F r)}{\pi k_F \xi} - [1-\cos(k_F r)]\Big\} \tag{4.1.11}$$

share the same characteristic exponential decay with the coherence length ξ, where $r = |\mathbf{x}_i - \mathbf{x}_j|$ is the distance between the tunnel contact to quantum dot 1 and the tunnel contact to quantum dot 2 measured

in the superconducting lead and $\Gamma = 2\pi N(\varepsilon_F)t_1t_2$ is the normal-state level broadening. The transformation also shifts the on-site energies by $\tilde{t}_{i=j}$, which can be absorbed into ε_{ni}, and allows for local Cooper pair injection with amplitude $\tilde{\Delta}_{i=j}$, which is suppressed by the Coulomb repulsion. Eqs. (4.1.10) and (4.1.11) are valid in the ballistic limit. Crossed Andreev reflection and cotunneling have been shown to be enhanced by moderate disorder, $l < r < \sqrt{\xi l}$, where l is the mean free path, but to keep their relative strength [47].

In the pointlike limit, $k_F r \to 0$, Cooper pair splitting becomes large compared to cotunneling, $\tilde{\Delta}_n/\tilde{t}_n = \pi k_F \xi$. This would be desirable because cotunneling delocalizes the electrons and hence reduces the Cooper pair splitting efficiency even at infinite Coulomb repulsion. The limit is, however, of doubtful practical relevance. At least in metallic leads, the Fermi wavelength $2\pi/k_F$ will be on the order of a nanometer whereas the distance between the quantum dots is more likely to exceed one hundred nanometers when taking the cavities in account. The situation might be different with semiconductor leads and proximity-induced superconductivity, which have a much larger Fermi wavelength, and geometric realization are conceivable which minimize the distance between the tunnel points [Fig. 4.2(a)]. Taking a conservative approach, in which the tunnel contacts are further apart than the Fermi wavelength but still closer than the coherence length, it is evident from Eqs. (4.1.10) and (4.1.11) and from Fig. 4.2(b) that, at best, $|\tilde{\Delta}_n| \sim |\tilde{t}_n|$ can be realized even if fine tuning via the oscillatory dependence on the Fermi vector k_F, i.e., on the carrier concentration, is taken into account. This opens a parasitic side channel: a Cooper pair is split and the electron on quantum dot 1 relaxes emitting a photon into cavity 1 as desired. But then, the second electron does not relax on quantum dot 2. It cotunnels onto quantum dot 1 and emits a photon into cavity 1, too. This is an inevitable source of local photon pairs which we will have to deal with when constructing the Bell test. The heavy holes on the p side are described by a Hamiltonian of the same form as Eq. (4.1.1) with the replacement $d_{i\sigma} \to h_{i\sigma} \equiv \sigma d^{\mathrm{HH}\dagger}_{i\bar{\sigma}}$, where the energies and amplitudes may differ between the n side and the p side, $\tilde{\Delta}_n \neq \tilde{\Delta}_p$, $\tilde{t}_n \neq \tilde{t}_p$, and $\varepsilon_{ni} \neq \varepsilon_{pi}$.

To describe the photoemission processes with the appropriate selection

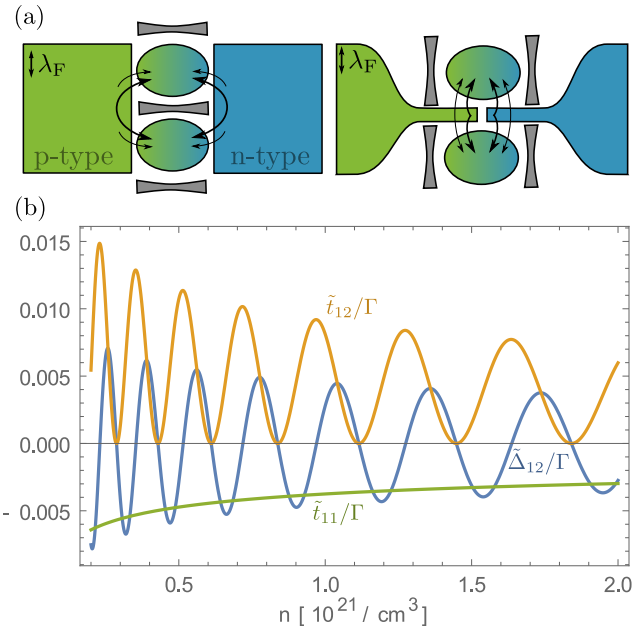

Figure 4.2: (a) Two different device geometries. Left panel: The tunnel contacts between the superconducting leads and the quantum dots are separated by several Fermi wavelengths. Cotunneling between the quantum dots is as strong as Cooper pair splitting. Right panel: Electrons can tunnel into both quantum dots from the same point in the superconducting leads. Cooper pair splitting dominates over cotunneling. (b) Proximity-induced amplitudes of Cooper pair splitting, $\tilde{\Delta}_{12}$, and cotunneling, $\tilde{t}_{12}$, and the renormalization of the on-site energy $\tilde{t}_{11}$ at different carrier concentrations n. When optimizing the Cooper pair splitting amplitude, cotunneling cannot be neglected. The quantum dots are separated by $r = 100$ nm and the superconducting coherence length is $\xi = 200$ nm (arbitrarily chosen). Figure and caption reproduced from the original publication, Ref. 117.

rules for heavy holes and cavity-enforced emission along the quantization axis of angular momentum, I use the standard rotating-wave-approximated Hamiltonian [195]

$$H_{\mathrm{RWA}} = \sum_{i\sigma} g_{i\sigma} e^{-ieV_{\mathrm{sd}}t/\hbar} d_{i\bar{\sigma}} h_{i\sigma} a_{i\sigma}^{\dagger} + \mathrm{H.c.}, \tag{4.1.12}$$

with the photons $a_{i\xi}$ of polarization ξ in cavity i and with the radiative dipole coupling $g_{i\xi}$. While the magnitude of the dipole matrix element depends on microscopic details, the shape of the recombination term H_{RWA} is fixed by the symmetry of the electron band and the heavy-hole band [196]. For brevity, I will identify $\sigma = \uparrow$ with $\xi = R$ and $\sigma = \downarrow$ with $\xi = L$. The exponential accounts for the different chemical potentials on the n side and on the p side due to the voltage bias V_{sd} across the junction. Gauging it into the photon field, $a \to e^{ieV_{\mathrm{sd}}t/\hbar}a$, the photonic contribution to the microscopic model is summarized in the Hamiltonian

$$H_P = \sum_{i\xi} (\hbar\omega_0 - eV_{\mathrm{sd}}) a_{i\xi}^{\dagger} a_{i\xi} + \sum_{i\sigma} g_{i\sigma} d_{i\bar{\sigma}} h_{i\sigma} a_{i\sigma}^{\dagger} + \mathrm{H.c.}, \tag{4.1.13}$$

where ω_0 is the resonance frequency of the cavities, which I assume to be equal for both. In general, having different resonance frequencies would not affect the entanglement because no additional information about the photons is gained: it is known which photon originates from which cavity anyway. The effective pair emission amplitudes will, of course, depend on the resonance frequencies via the detuning $\hbar\omega_0 - eV_{\mathrm{sd}}$, which enters in intermediate states in the perturbative treatment later on. But they are dominated by the excitation energies in the electronic system, which will be required to be larger than the line width of the cavities, anyway. In other words, as long as the difference of the resonance frequencies is smaller than the line width of the cavities, the results I present hold unmodified and, in any case, the quantum-dot on-site energies $\varepsilon_{n,p\,i}$ can be increased at the expense of lowering the emission rate.

Having set up the microscopic model, we can now turn to the emission process. Without the influence of the photonic subsystem, Eq. (4.1.13), the ground state $|0\rangle_n$ of the n-side electronic system is a superposition of the empty state $|\rangle_n$ and of the nonlocal singlet state $|S\rangle_n :=$

$2^{-1/2}(d^\dagger_{1\uparrow}d^\dagger_{2\downarrow} - d^\dagger_{1\downarrow}d^\dagger_{2\uparrow})\,|\rangle_n$, i.e., $|0\rangle_n = c^0_{n,0}\,|\rangle + c^0_{n,s}\,|S\rangle$. This reflects that Cooper pairs can tunnel onto the quantum dots from the superconductor. It is convenient to rewrite the quantum-dot on-site energies as $\varepsilon_{n\,1,2} =: \varepsilon_n \pm \delta_n$, where ε_n is the average on-site energy and δ_n is the difference between the two quantum dots. If the amplitude of Cooper pair injection is small, $|\tilde{\Delta}_n| \ll |\varepsilon_n|$, the quantum dots remain mostly empty, $c^0_{n,s} \to 0$, but in the limit of a strongly coupled superconductor, $|\tilde{\Delta}_n| \gg |\varepsilon_n|$, the admixture of singlets is substantial, $|c^0_{n,s}| \to |c^0_{n,0}|$. In an experiment, $\tilde{\Delta}_n$ is likely to be fixed because it is essentially given by the tunnel rate between the lead and the quantum dots, which depends on the sample fabrication. Nevertheless, the on-site energies, which are accessible via gate voltages, allow a large degree of control over the strength of Cooper pair injection: if the quantum-dot levels are brought in resonance with the chemical potential of the superconductor, $\varepsilon_n = 0$, it is as strong as possible, whereas if the quantum dots are lifted above the chemical potential, it decreases. The amplitudes $c^0_{n,0}$ and $c^0_{n,s}$ do not depend on δ_n because, as I discussed already in Chap. 2, Cooper pairs are always opposite-energy pairs with respect to the Fermi level. The ground-state energy is lowered by the hybridization with the superconductor and becomes $E^0_n = \varepsilon_n - (\varepsilon_n^2 + 2|\tilde{\Delta}_n|^2)^{1/2}$. Apart from the ground state, which has even parity, the photoemission cycle of the system includes four odd-parity excited states. They contain only one electron with either spin up or spin down and they are delocalized across the two quantum dots because of the cotunneling amplitude $\tilde{t}_n$. I will call them $|\sigma\pm\rangle_n = c^\pm_{n,1}\,|1\sigma\rangle + c^\pm_{n,2}\,|2\sigma\rangle$, where $|i\sigma\rangle := d^\dagger_{i\sigma}\,|\rangle_n$ is the state with one spin-σ electron on quantum dot i. Contrary to the ground state, the excited states are affected *only* by the energy difference δ_n, which controls how strongly the electrons are localized for any fixed cotunneling amplitude $\tilde{t}_n$: large δ_n imply a large energy difference between the two quantum dots and delocalization is unfavorable. Again, δ_n is a tunable parameter. The energies of the excited states are $E^\pm_n = \varepsilon_n \pm (\delta_n^2 + \tilde{t}_n^2)^{1/2}$. The very same considerations apply to the holes on the p side of the junction.

The photoemission process described by H_{RWA}, Eq. (4.1.12), changes the number of electrons and holes by one, so it induces transitions from the even–even ground state $|0\rangle_n\,|0\rangle_p$ to an odd–odd excited state $|\sigma\mu\rangle_n\,|\bar{\sigma}\nu\rangle_p$, where $\mu, \nu = \pm$. Because parity is conserved by all other

processes and protected by the superconducting bulk energy gap, the only way for the system to go back into the ground state is to reabsorb the photon or to emit a second one. The latter is possible ultimately because of the superconducting pairing in the leads, which breaks particle number conservation. There is, in fact, one more even-parity state, which is orthogonal to the ground state $|0\rangle$. But it turns out to reside at even higher energies than the odd states. It can only be reached by first exciting the even–even ground state into an odd–odd intermediate state followed by a second excitation back into the even–even sector. Similarly, two more events are required to complete the emission cycle. This means that the even-parity excited state participates only in at least four-photon processes and I will neglect it. The emission cycle is depicted in the right panel of Fig. 4.1. At this point, we see that, after having emitted a pair of photons, the electronic system returns to the very state it started in, so the entanglement must have been completely transferred onto the photons. The excitation energies between the initial even–even state and the intermediate odd–odd states, $\Delta E^{\mu\nu} = E_n^\mu + E_p^\nu - E_n^0 - E_p^0$, however, play a crucial role. Since the aim is to emit the photons only in pairs, the intermediate states should be virtual states. This requires the excitation energies $\Delta E^{\mu\nu}$ to be larger than the linewidth of the optical nanocavity. Now, there are competing interests: because $\Delta E^{\mu\nu} \gtrsim \varepsilon_n + \varepsilon_p$, it is desirable to increase the on-site energies. The drawback is that the admixture of singlets on the quantum dots, $c^0_{n,p\,s}$, is decreased. Similarly, the energy difference $\delta_{n,p}$ should be small to obtain large excitation energies $\Delta E^{\mu\nu}$ but this increases the delocalization and hence the emission of local pairs. In any case, the quantum-dot energies need to be smaller than the bulk superconducting gap. Otherwise, quasi-particle poisoning will spoil the entanglement (and the model will break down). As a side note, because of parity conservation, we can expect the photons to be entangled even if the linewidth of the cavities is larger than the excitation energy but still smaller than the bulk superconducting gap in the leads and than the Coulomb repulsion. But this leads to a different regime in which single photons can be emitted sequentially, which I will not consider here.

To be specific, I assume that the quantum dots are separated by more than the Fermi wavelength but still less than the coherence length,

$k_F r \sim 10$, $r/(\pi\xi) \sim 0.5$. With a typical superconductor–quantum dot coupling of $\Gamma = 500$ μeV observed with both nanowire [58] and nanotube [64] splitters, the Cooper pair splitting amplitude $\tilde{\Delta}_n$ and the cotunneling amplitude $\tilde{t}_n$ are on the order of 15 μeV. It has already been demonstrated that a linewidth on the order of 10 GHz, which is 40 μeV, is achievable with all common flavors of nanocavities [207–210]. Imposing electron–hole symmetry and dropping the subscript n, p for ease of notation, we need to apply a gate voltage to the quantum dots such that (i) $\varepsilon = 30$ μeV if pessimistically cotunneling is as strong as Cooper pair splitting, $\tilde{t} = \tilde{\Delta}$, or such that (ii) $\varepsilon = 20$ μeV if more optimistically cotunneling is only half as strong as Cooper pair splitting, $\tilde{t} = \tilde{\Delta}/2$. It will turn out not to be necessary to suppress cotunneling any further, so we can choose $\delta = 0$. This is a very conservative estimate. Already if Cooper pair splitting and cotunneling are twice as large, $\tilde{\Delta} \gtrsim 30$ μeV, maybe because the separation is smaller or because the Fermi wavelength is larger, the quantum dots can be brought into resonance with the superconducting leads, $\varepsilon = 0$, which optimizes the emission rate. This is possible because the hybridization between the leads and the quantum dots lowers the ground state and hence increases the excitation energies $\Delta E^{\mu\nu}$. Conversely, when the coupling is reduced, both Cooper pair splitting and cotunneling are decreased by the same factor, c.f. Eqs. (4.1.10) and (4.1.11), so there is no immediate impact on the relative strength between local emission, which is bad for entanglement detection, and nonlocal emission, which is what we want.

Quantitatively, I describe the emission cycle in quasidegenerate perturbation theory [144]. Then, the low-energy sector, in which the electronic system is in the ground state $|0\rangle_n |0\rangle_p$, decouples from the high-energy sector, in which the electron–hole system is in any other state, up to second order in the electron–hole recombination $g_{i\xi}$. The resulting model is

$$H_{\mathrm{ph}} = \sum_{i\xi} (\hbar\omega_0 - eV_{\mathrm{sd}}) a_{i\xi}^\dagger a_{i\xi} + \sum_{ij\xi} M_{ij\xi} a_{i\xi}^\dagger a_{j\xi} + \sum_{ij\xi} \frac{\tilde{M}_{ij\xi}}{2} a_{i\xi} a_{i\bar{\xi}} + \mathrm{H.c.}, \tag{4.1.14}$$

where

$$M_{ij\xi} = g_{i\xi} g^*_{j\xi} \sum_{\mu\nu=\pm} \Big(\frac{|c^0_{n,0}|^2 |c^0_{p,0}|^2 c^{\mu}_{n,i} c^{\mu *}_{n,j} c^{\nu}_{p,i} c^{\nu *}_{p,j}}{(\hbar\omega_0 - eV_{\mathrm{sd}}) - \Delta E^{\mu\nu}} - \frac{1}{4} \frac{|c^0_{n,s}|^2 |c^0_{p,s}|^2 c^{\mu *}_{n,\bar{i}} c^{\mu}_{n,\bar{j}} c^{\nu *}_{p,\bar{i}} c^{\nu}_{p,\bar{j}}}{(\hbar\omega_0 - eV_{\mathrm{sd}}) + \Delta E^{\mu\nu}} \Big) \tag{4.1.15}$$

$$\tilde{M}_{ij\xi} = g^*_{i\xi} g^*_{j\bar{\xi}} \sum_{\mu\nu=\pm} \frac{c^{0*}_{n,s} c^0_{n,0} c^{0*}_{p,s} c^0_{p,0} c^{\nu *}_{p,j} c^{\nu}_{p,\bar{i}} c^{\mu *}_{n,j} c^{\mu}_{n,\bar{i}} \Delta E^{\mu\nu}}{(\Delta E^{\mu\nu})^2 - (\hbar\omega_0 - eV_{\mathrm{sd}})^2}. \tag{4.1.16}$$

At symmetric gating, $\delta = 0$, the excited state amplitudes $c^{\pm}_{n/p,i}$ are on the order of 1 and the ground state amplitudes fulfill $|c^{0*}_{n/p,s} c^0_{n/p,0}| = |\tilde{\Delta}|/(2|\varepsilon|) + \mathcal{O}(|\tilde{\Delta}|^2/\varepsilon^2)$, so the pair-emission amplitudes are $\tilde{M}_{ij\xi} \sim g(g/\Delta E)(\tilde{\Delta}/\varepsilon)^2$. This yields a total emission rate on the order of $10^{-3} g/\hbar$. Although it is not obvious from Eqs. (4.1.15) and (4.1.16), intercavity hopping, $M_{i\neq j}$, and local pair emission, $\tilde{M}_{i=j}$, would vanish exactly if there was no electron cotunneling, $\tilde{t} = 0$, which is what we expect from the qualitative considerations of how the device works.

4.2 Photoemission and Bell test

I will restrict the remainder of the discussion to a highly symmetric situation, where both cavities are identical, both quantum dots are identical, and the radiative coupling is polarization independent. The motivation is not to achieve, e.g., particular cancellations but simply that it reduces the number of indices and tidies up the notation a lot, while there is no reason to assume that any interesting physical effects are lost. Renaming $\hbar\omega := \hbar\omega_0 - eV_{\mathrm{sd}} + M_{i=j}$, $t_{\mathrm{ph}} := M_{i\neq j}$, $\Lambda_{\mathrm{ph}} := \tilde{M}_{i=j}$, and $\Delta_{\mathrm{ph}} := \tilde{M}_{i\neq j}$, the effective model, Eq. (4.1.14), becomes

$$H_{\mathrm{ph}} = \sum_{\substack{i=1,2 \\ \xi=R,L}} \hbar\omega a^{\dagger}_{i\xi} a_{i\xi} + t_{\mathrm{ph}} a^{\dagger}_{i\xi} a_{\bar{i}\xi} + \Big(\frac{\Delta_{\mathrm{ph}}}{2} a_{i\xi} a_{\bar{i}\bar{\xi}} + \frac{\Lambda_{\mathrm{ph}}}{2} a_{i\xi} a_{i\bar{\xi}} + \mathrm{H.c.} \Big). \tag{4.2.1}$$

The mode energy $\hbar\omega$ now contains the frequency pull caused by the quantum dots and is measured relative to the source–drain voltage.

Two photons of opposite polarizations ξ and $\bar{\xi}$ are emitted or absorbed nonlocally, i.e., in different cavities i and $\bar{i}$, with the amplitude Δ_{ph}, whereas the amplitude to inject two photons locally into the same cavity, Λ_{ph}, is always finite, too, as we have seen in the microscopic treatment. Both nonlocal emission Δ_{ph} and local emission Λ_{ph} involve the transfer of one Cooper pair from the n side to the p side of the junction, which means that if there is a phase difference between the superconductors, both pick it up equally. We will see that, because of this, the phase drops out when calculating the photon correlations, which is why I will not distinguish the amplitudes Δ_{ph} and Λ_{ph} from their complex conjugates. The intercavity coupling t_{ph} does not pick up superconducting phases because, on the microscopic level, it involves only cotunneling. In the absence of external magnetic fields, t_{ph} can hence safely be assumed to be real, too.

The reason to introduce the cavities was to restrict the emission to pairs of photons. This requires a sufficiently narrow linewidth, i.e., cavities of a high quality factor. The higher the quality factor, the better are the cavities isolated from the environment. This, together with the assumption of extremely low temperatures, implies that the Bell measurement will mostly probe the ground state of the effective model H_{ph}, Eq. (4.2.1). The effective model is a noninteracting bosonic system with pairing terms similar to the ones known from spin waves or from superfluidity. There is, however, an additional complication: because of the hopping amplitude t_{ph}, the kinetic part and the pairing part are not simultaneously diagonal with respect to the cavity index i, which corresponds to momentum in the usual situation. This means that eliminating the pairing and diagonalization need to be done simultaneously. It turns out to be convenient to approach this problem from the equations of motion,

$$i\hbar\partial_t a_{i\xi} = \left[a_{i\xi}, H\right] = \hbar\omega a_{i\xi} + t_{\mathrm{ph}} a_{\bar{i}\xi} + \Delta_{\mathrm{ph}} a^\dagger_{\bar{i}\bar{\xi}} + \Lambda_{\mathrm{ph}} a^\dagger_{i\bar{\xi}} \tag{4.2.2}$$

$$i\hbar\partial_t a^\dagger_{i\xi} = \left[a^\dagger_{i\xi}, H\right] = -\hbar\omega a^\dagger_{i\xi} - t_{\mathrm{ph}} a^\dagger_{\bar{i}\xi} - \Delta_{\mathrm{ph}} a_{\bar{i}\bar{\xi}} - \Lambda_{\mathrm{ph}} a_{i\bar{\xi}}, \tag{4.2.3}$$

which can be expressed as a Nambu-like matrix equation, $i\hbar\partial_t \mathbf{a} = M\mathbf{a}$, where $\mathbf{a} = (a_{1R}, a_{1L}, \ldots, a^\dagger_{1R}, a^\dagger_{1L}, \ldots)^{\mathrm{T}}$. The dynamical matrix M is diagonalized by a transformation U, which can be found analytically. This yields a new set of operators $U\mathbf{a}$ with corresponding eigenvalues

E_i of M, which come in pairs of opposite sign. We can choose to identify all operators with positive E_i as new bosonic creation operators $\pi_i^\dagger$, whereas the operator π_j with $E_j = -E_i$ is automatically the respective annihilation operator π_i. Hence, the additional degrees of freedom introduced artificially when constructing the Nambu vector drop out again, very similar to discarding all negative-energy solutions of the Bogoliubov–de Gennes equation. In fact, M *is* the Bogoliubov–de Gennes matrix up to a sign in the lower left quadrant due to Bose–Einstein statistics. Normalizing the new operators π_i such that they fulfill the proper bosonic commutation relations and replacing the four values i by a more convenient index pair $\mu, \nu = \pm 1$, we obtain, up to an inessential additive constant,

$$H_{\mathrm{ph}} = \sum_{\mu\nu} E_\nu \pi_{\mu\nu}^\dagger \pi_{\mu\nu} \tag{4.2.4}$$

with the dispersion $E_\pm = \sqrt{(\hbar\omega \pm t_{\mathrm{ph}})^2 - |\Delta_{\mathrm{ph}} \pm \Lambda_{\mathrm{ph}}|^2}$. The new bosons are related to the original ones by $\pi_{\mu\nu} = [u_\nu(a_{1\mu}^\dagger + \nu a_{2\mu}^\dagger) + v_\nu(\nu a_{1\bar{\mu}} + a_{2\bar{\mu}})]/(v_\nu^2 - |u_\nu|^2)^{1/2}$ with $u_\pm = \Delta_{\mathrm{ph}} \pm \Lambda_{\mathrm{ph}}$ and $v_\pm = (\hbar\omega \pm t_{\mathrm{ph}}) + E_\pm$. Interestingly, a Bogoliubov transformation exists only if $|\hbar\omega \pm t_{\mathrm{ph}}| > |\Delta_{\mathrm{ph}} \pm \Lambda_{\mathrm{ph}}|$, where $E_\pm > 0$. This is precisely the offresonant regime I investigate. A similar situation arises in the effective spin-wave Hamiltonian of the antiferromagnet, where an equivalent instability signals the transition to the spin-flop phase [211]. Here, it appears that if the offresonant condition were not fulfilled, the system could gain energy by producing more and more pairs of photons. Then the effective model, Eq. (4.2.1), is not meaningful: in reality, the production of photons will be limited by the electronic subsystem, too, e.g., by the rate of Cooper pair injection from the leads into the quantum dots. This is neglected in the Schrieffer–Wolff transformation. The problem is generally absent in fermion systems because the Pauli principle limits the maximum occupation of all modes which are not off resonance.

Now the ground state $|G\rangle$ of H_{ph} is the one without any excitation, i.e., it is defined by the condition $\pi_{\mu\nu}|G\rangle = 0$ for all μ, ν. But to formulate the Bell test, the ground state has to be expressed in terms of the original photons. Because H_{ph} creates and destroys photons in local

pairs and in nonlocal pairs, we can guess that it will be of the form

$$|G\rangle = \mathcal{N} \exp\Big[A\Big(a^\dagger_{1R}a^\dagger_{1L} + a^\dagger_{2R}a^\dagger_{2L}\Big) + B\Big(a^\dagger_{1R}a^\dagger_{2L} + a^\dagger_{1L}a^\dagger_{2R}\Big)\Big]. \quad (4.2.5)$$

To verify this assumption, I will use that the state $|G\rangle$ has the interesting property that taking out a photon is equivalent to adding a photon with opposite polarization,

$$a_{i\xi}\,|G\rangle = (Aa^\dagger_{i\bar{\xi}} + Ba^\dagger_{\bar{i}\bar{\xi}})\,|G\rangle\,. \quad (4.2.6)$$

A similar property is easy to see for a state with only two independent bosons a and b,

$$\begin{aligned} a \exp\Big[a^\dagger b^\dagger\Big]\,|\rangle &= a\sum_{i=0}^{\infty} \frac{(a^\dagger)^i(b^\dagger)^i}{i!}\,|\rangle = \sum_{i=1}^{\infty} \frac{(a^\dagger)^{i-1}(b^\dagger)^i}{(i-1)!}\,|\rangle \\ &= \sum_{i=0}^{\infty} \frac{(a^\dagger)^i(b^\dagger)^{i+1}}{i!}\,|\rangle = b^\dagger \exp\Big[a^\dagger b^\dagger\Big]\,|\rangle\,. \end{aligned} \quad (4.2.7)$$

To generalize it to $|G\rangle$, we first rearrange the operators

$$\begin{aligned} a_{i\xi}\,|G\rangle &= a_{i\xi}\mathcal{N} \exp\Big[\Big(Aa^\dagger_{i\bar{\xi}} + Ba^\dagger_{\bar{i}\bar{\xi}}\Big)a^\dagger_{i\xi} + Aa^\dagger_{\bar{i}\xi}a^\dagger_{\bar{i}\bar{\xi}} + Ba^\dagger_{\bar{i}\xi}a^\dagger_{i\bar{\xi}}\Big]\,|\rangle \\ &= \mathcal{N} \exp\Big[Aa^\dagger_{\bar{i}\xi}a^\dagger_{\bar{i}\bar{\xi}} + Ba^\dagger_{\bar{i}\xi}a^\dagger_{i\bar{\xi}}\Big]a_{i\xi} \exp\Big[\Big(Aa^\dagger_{i\bar{\xi}} + Ba^\dagger_{\bar{i}\bar{\xi}}\Big)a^\dagger_{i\xi}\Big]\,|\rangle\,, \end{aligned} \quad (4.2.8)$$

where we have used that $a_{i\xi}$ commutes with all creation operators except $a^\dagger_{i\xi}$, and then identify $a := a_{i\xi}$ and $b := Aa_{i\bar{\xi}} + Ba_{\bar{i}\bar{\xi}}$ to find Eq. (4.2.6). Now, in the defining property of the ground state,

$$0 = \pi_{\mu\nu}\,|G\rangle \propto \Big[u_\nu(a^\dagger_{1\mu} + \nu a^\dagger_{2\mu}) + v_\nu(\nu a_{1\bar{\mu}} + a_{2\bar{\mu}})\Big]\,|G\rangle \quad (4.2.9)$$

the annihilation operators can be substituted with creation operators by virtue of Eq. (4.2.6),

$$0 = \Big[\Big(u_\nu + v_\nu(\nu A + B)\Big)a^\dagger_{1\mu} + \nu\Big(u_\nu + v_\nu(\nu A + B)\Big)a^\dagger_{2\mu}\Big]\,|G\rangle\,. \quad (4.2.10)$$

But this can only be true if $A + \nu B = -\nu u_\nu / v_\nu$, so A and B are fixed and we find

$$|G\rangle = \frac{1}{v_+ v_-} \exp\Big[-\frac{1}{2}\Big(\frac{u_+}{v_+} - \frac{u_-}{v_-}\Big)(a_{1R}^\dagger a_{1L}^\dagger + a_{2R}^\dagger a_{2L}^\dagger) \\ -\frac{1}{2}\Big(\frac{u_+}{v_+} + \frac{u_-}{v_-}\Big)(a_{1R}^\dagger a_{2L}^\dagger + a_{1L}^\dagger a_{2R}^\dagger)\Big] |\rangle \,. \qquad (4.2.11)$$

This state has an interesting structure. It is a coherent superposition of any number of pairs of photons. This distinguishes it from ordinary coherent states, which are a superposition of any number of *single* photons. Instead, $|G\rangle$ is a squeezed state [212] and so the double-quantum-dot system is a nonclassical light source. In fact, the effective model, Eq. (4.2.1), closely resembles the quantum parametric amplifier, which describes, e.g., parametric down conversion [213]. But, again, the device is not actually optimized to be operated as a light source but to test for Cooper pair splitting. Also note that for fermionic operators, the exponential function becomes $\exp(x) = 1 + x$ and the structure of the well-known Bardeen–Cooper–Schrieffer ground state is recovered.

I will now construct a CHSH Bell test. As explained in Chap. 1, this requires four observables, two acting on each cavity. All of the observables can take only the two values ± 1. In the standard Bell test, individual pairs of photons are postselected. In the language of quantum mechanics, the quantum state under consideration, i.e., $|G\rangle$, is projected onto the subspace with exactly one photon in each cavity. If we do this, $|G\rangle$ collapses to the Bell state $(u_+/v_+ - u_-/v_-)(a_{1R}^\dagger a_{1L}^\dagger + a_{2R}^\dagger a_{2L}^\dagger)$, which gives a maximum violation of the standard CHSH inequality unless $u_+/v_+ - u_-/v_- = 0$. The problem is that this scheme works only if single photons can be uniquely identified. On the one hand, this is a rather strict requirement on the physical photodetectors, although one that can be dealt with. But on the other hand, it would work only if the photons could be measured *inside* the cavities. It is difficult to imagine how to achieve this. The best which can probably be done is to detect all photons which leak out of the cavities, while the detector effectively misses all photons which remain inside. So regardless of the actual quality of the physical photodetectors, I will describe the Bell measurement with perfect vacuum detectors, which have the property that the detector will never click in vacuum but may not click even if pho-

tons are present. In particular, the number of photons is not resolved. Formally, I use a positive-operator-valued measure: the probability to detect at least one photon in cavity i with polarization ξ if $n_{i\xi}$ photons are present is $P^+_{i\xi} = 1-(1-\gamma)^{n_{i\xi}}$, where $\gamma \in [0,1]$ is the single-photon detection efficiency or the single-photon escape probability from the cavity. It follows that there is a probability $P^-_{i\xi} = 1 - P^+_{i\xi}$ not to detect any photon. This special choice of operators turns out to have convenient analytical properties when applied to squeezed states [214], which I will make use of when calculating the expectation values which enter the CHSH inequality. More generally, a photon with the arbitrary polarization α is detected with probability $P^+_{i\alpha} = 1-(1-\gamma)^{\tilde{a}^\dagger_{iR}\tilde{a}_{iR}}$, where $\tilde{a}_{1R} = a_{1R}\cos\alpha - a_{1L}\sin\alpha$ and $\tilde{a}_{1L} = a_{1R}\sin\alpha + a_{1L}\cos\alpha$. I will not distinguish between the basis of circularly-polarized photons and the basis of linearly-polarized photons because they are equivalent up to a unitary transformation, which may be realized by a quarter wave plate in the experiment. At each detection angle α and for each cavity i, there are four possible measurement outcomes: (i) no photon is detected. This event is discarded as in the usual Bell test. (ii) Only photons of polarization α are detected. This event is assigned the measurement result $+1$. (iii) Only photons of the orthogonal polarization $\alpha+\pi/2$ are detected. This event is assigned the measurement result -1. (iv) Both polarizations are detected. This event cannot happen in the standard Bell test, where individual pairs are selected. But here it is possible that two photons of opposite polarization leak out of the same cavity and are both detected. This is an indication that the state has a nonentangled admixture and we discard the event. This is an important ingredient to construct a feasible Bell test: because all events are averaged over to find the correlators which make up the CHSH inequality, each nonentangled pair which is not discarded necessarily reduces the violation of the Bell inequality. Like in the original CHSH test, we now construct two observables for cavity 1 by setting $\alpha = 0$ or $\alpha = \pi/4$ and two observables for cavity 2 by setting $\alpha = \pi/8$ or $\alpha = 3\pi/8$. Note that in the experiment there are, in total, four physical photodetectors, two for each cavity. One detects photons with polarization α and the other detects photons with the orthogonal polarization $\alpha + \pi/2$. Together, they make up *one* observable defined by the angle α. There are four photodetectors in the experiment and four observables in the CHSH

inequality but they are not in one-to-one correspondence. This applies to the scheme I discuss just as is applies to the standard two-photon Bell test. Coming back to the formal description, the Bell parameter is

$$\mathcal{B}_\alpha = \mathcal{C}(0,\alpha) + \mathcal{C}\Big(0,\alpha+\frac{\pi}{4}\Big) + \mathcal{C}\Big(\frac{\pi}{4},\alpha\Big) - \mathcal{C}\Big(\frac{\pi}{4},\alpha+\frac{\pi}{4}\Big), \qquad (4.2.12)$$

with the nonlocal correlations $\mathcal{C}(\alpha,\beta) = \sum_{\mu\nu}\mu\nu P^{\mu\nu}_{\alpha\beta} / \sum_{\mu\nu} P^{\mu\nu}_{\alpha\beta}$, where $P^{\mu\nu}_{\alpha\beta}$ is the probability to obtain the measurement result μ at cavity 1 when the polarization detector 1 is set to the angle α and to simultaneously obtain the measurement result ν at cavity 2 when the polarization detector 2 is set to the angle β. We can calculate the probabilities using the perfect-vacuum-detector observables, $P^{\mu\nu}_{\alpha\beta} = \langle G|\, P^{\mu}_{1\alpha} P^{\bar{\mu}}_{1\alpha+\pi/2} P^{\nu}_{2\beta} P^{\bar{\nu}}_{2\beta+\pi/2}\, |G\rangle$. They decompose into sums of expressions of the form

$$\begin{aligned} P_\eta &= \langle G|\, \eta_{1R}^{\tilde{a}^\dagger_{1R}\tilde{a}_{1R}} \eta_{1L}^{\tilde{a}^\dagger_{1L}\tilde{a}_{1L}} \eta_{2R}^{\tilde{a}^\dagger_{2R}\tilde{a}_{2R}} \eta_{2L}^{\tilde{a}^\dagger_{2L}\tilde{a}_{2L}}\, |G\rangle \\ &\propto \Big| \eta_{1R}^{\frac{1}{2}\tilde{a}^\dagger_{1R}\tilde{a}_{1R}} \eta_{1L}^{\frac{1}{2}\tilde{a}^\dagger_{1L}\tilde{a}_{1L}} \eta_{2R}^{\frac{1}{2}\tilde{a}^\dagger_{2R}\tilde{a}_{2R}} \eta_{2L}^{\frac{1}{2}\tilde{a}^\dagger_{2L}\tilde{a}_{2L}} \\ &\qquad \times \exp\Big[A(a^\dagger_{1R}a^\dagger_{1L} + a^\dagger_{2R}a^\dagger_{2L}) + B(a^\dagger_{1R}a^\dagger_{2L} + a^\dagger_{1L}a^\dagger_{2R})\Big]\, |\rangle \Big|^2, \end{aligned} \qquad (4.2.13)$$

where $\eta_{i\xi} = 1-\gamma$ or $\eta_{i\xi} = 1$. This expression still contains photon operators a in the cavity basis and photon operators $\tilde{a}$ in the measurement basis defined by the detection angles. After using the unitary transformation

$$\begin{pmatrix} \tilde{a}_{1R} \\ \tilde{a}_{1L} \\ \tilde{a}_{2R} \\ \tilde{a}_{2L} \end{pmatrix} = U \begin{pmatrix} a_{1R} \\ a_{1L} \\ a_{2R} \\ a_{2L} \end{pmatrix}, \qquad (4.2.14)$$

where

$$U = \begin{pmatrix} \cos\alpha & -e^{i\phi}\sin\alpha & 0 & 0 \\ e^{-i\phi}\sin\alpha & \cos\alpha & 0 & 0 \\ 0 & 0 & \cos\beta & -e^{i\theta}\sin\beta \\ 0 & 0 & e^{-i\theta}\sin\beta & \cos\beta \end{pmatrix}, \qquad (4.2.15)$$

to eliminate $a_{i\xi}$ in favor of $\tilde{a}_{i\xi}$, we can apply the operator identity [215] $x^{a^\dagger a} f(a^\dagger) = f(xa^\dagger) x^{a^\dagger a}$ together with $x^{a^\dagger a} |\rangle = |\rangle$ to express the observables and the ground state as a single exponential,

$$P_\eta \propto \left| \exp[\frac{1}{2} \begin{pmatrix} \tilde{a}_{1R}^\dagger & \tilde{a}_{1L}^\dagger & \tilde{a}_{2R}^\dagger & \tilde{a}_{2L}^\dagger \end{pmatrix} D^{\mathrm{T}} U^{\mathrm{T}} M U D \begin{pmatrix} \tilde{a}_{1R}^\dagger \\ \tilde{a}_{1L}^\dagger \\ \tilde{a}_{2R}^\dagger \\ \tilde{a}_{2L}^\dagger \end{pmatrix}] \, |\rangle \right|^2 \tag{4.2.16}$$

where

$$D = \begin{pmatrix} \sqrt{\eta_{1R}} & 0 & 0 & 0 \\ 0 & \sqrt{\eta_{1L}} & 0 & 0 \\ 0 & 0 & \sqrt{\eta_{2R}} & 0 \\ 0 & 0 & 0 & \sqrt{\eta_{2L}} \end{pmatrix} \tag{4.2.17}$$

and

$$M = \begin{pmatrix} 0 & A & 0 & B \\ A & 0 & B & 0 \\ 0 & A & 0 & B \\ A & 0 & B & 0 \end{pmatrix}. \tag{4.2.18}$$

The bilinear argument of the exponential is expressed by the matrix $D^{\mathrm{T}} U^{\mathrm{T}} M U D$, which is symmetric, so we can find another transformation to four independent bosons b_i, such that

$$P_\eta \propto \left| \exp[\frac{1}{2} \sum_{i=1}^{4} \lambda_i b_i^\dagger b_i] \, |\rangle \right|^2, \tag{4.2.19}$$

where λ_i are the eigenvalues of $D^{\mathrm{T}} U^{\mathrm{T}} M U D$. This expression can be evaluated by inserting the definition of the exponential as a series,

$$P_\eta \propto \prod_{i=1}^{4} \langle | \, e^{\frac{1}{2}\lambda_i^* b_i b_i} e^{\frac{1}{2}\lambda_i b_i^\dagger b_i^\dagger} \, | \rangle = \prod_{i=1}^{4} \Big(1 - |\lambda_i|^2 \Big). \tag{4.2.20}$$

In this way, the infinite-dimensional problem involving arbitrarily large numbers of photons is reduced to finding the eigenvalues of a 4×4 matrix, which can always be done, at least numerically, to arbitrary precision. The phases of A and B, which are the superconducting phase

picked up during the transport of one local or one nonlocal Cooper pair, are equal and drop out because only the absolute value of the eigenvalues λ_i enters the final result, Eq. (4.2.20).

The situation is somewhat easier in the actual experiment: the probabilities are estimated by counting the corresponding coincidence events. When normalizing the correlation functions, we assume that we cover all possible outcomes of the experiment, so, strictly speaking, the dichotomy required by the Bell test is put in by hand. At least within the model this is certainly correct.

In the hypothetical limit of perfect photodetection, $\gamma = 1$, the standard Bell test is recovered asymptotically. If a local pair is present in one of the cavities, both polarizations will be detected and the measurement is discarded. The measurement scheme is sensitive to single pairs of photons and to several nonlocal pairs which occur with an exponentially-small amplitude, cf. Eq. (4.2.11). This means that for almost all parameters of the effective model the maximal Bell parameter $\mathcal{B}_{\max} := \max_\alpha \mathcal{B}_\alpha$ exceeds the classical boundary, $\mathcal{B}_{\max} > 2$ [colored regions in Fig. 4.3(a)]. So the entanglement is detected reliably. The situation becomes more interesting with lossy detection. To get an order-of-magnitude estimate of the detection efficiency γ, assume that during the coincidence interval Δt of the measurement, the probability for a single photon to leave its cavity (and hence to be detected) is $\gamma \lesssim 1 - e^{-\kappa \Delta t}$. The loss rate κ is commonly expressed through the quality factor Q as $\kappa = (\hbar\omega + eV_{\mathrm{sd}})/Q$. In a conservative estimate where the quality factor is high, $Q = 10^6$, the light frequency is low, $f = \omega/2\pi = 10$ THz, and the coincidence interval is short, $\Delta t = 1$ ps, the efficiency is reduced to $\gamma \sim 10^{-4}$. Accordingly, although the parameter region in which entanglement detection *is* possible is still large, the region in which the Bell test fails is substantially enlarged [black region in Fig. 4.3(b)]. What happens is that only one photon of a *local pair* is detected and believed to belong to a *nonlocal pair*. If this happens too often, i.e., if Λ_{ph} is too large, the Bell parameter is reduced below the classical threshold, $\mathcal{B}_{\max} < 2$ and the entanglement, although present, cannot be detected any more. The good news is that, even within this estimate, the effective parameters obtained in the preceding section fall right into the region where entanglement detection does work [blue curves in Fig. 4.3(b)], no matter whether cotunneling

is (i) half as strong as Cooper pair injection, (ii) as strong as Cooper pair in injection, or (dashed) as strong as Cooper pair injection with the additional complication of weak Coulomb repulsion in the quantum dots [117].

Apart from affecting the detection probability, cavity losses modify the steady state. For one thing, this breaks up entangled pairs leaving behind single photons. If they are detected and believed to belong to an entangled pair, the Bell parameter is reduced. On the other hand, the admixture of states with more photons is reduced such that if one photon from each cavity is detected, the likelihood for them to stem from a nonlocal pair, which involves only two photons, is increased in proportion to the likelihood for them to stem from two unrelated local pairs, involving four photons in total. To quantify this, we can employ a quantum master equation [216],

$$\dot{\rho} = \mathcal{L}\rho = -\frac{i}{\hbar}[H_{\mathrm{ph}}, \rho] + \sum_{i\xi} \kappa \left(2a_{i\xi}\rho a_{i\xi}^{\dagger} - a_{i\xi}^{\dagger} a_{i\xi}\rho - \rho a_{i\xi}^{\dagger} a_{i\xi} \right), \quad (4.2.21)$$

where the Liouvillian $\mathcal{L}$ includes both the coherent behavior of the system and a Lindblad loss mechanism with rate κ. With a loss term of Lindblad form the microscopic details of the loss mechanism are eliminated as far as possible, which is fine because we are interested in the universal behavior, but the master equation is still hard to solve. Whereas the coherent evolution is easily described in a Bogoliubov picture, the loss term is naturally treated in terms of the original photons. What can be exploited, however, is the fact that we are interested in small numbers of photons. With a cutoff of $N_{\mathrm{max}} = 4$ photons per mode, the Fock space is N_{max}^4 dimensional and accessible by exact diagonalization. The steady state $\dot{\rho} = 0$ is found numerically either by propagating an arbitrary initial state in time until convergence or by finding the smallest eigenvalue of the Liouvillian, which is always numerical zero. Artifacts possibly introduced by the cutoff are ruled out by checking the limit $\kappa \to 0$, increasing the cutoff to $N_{\mathrm{max}} = 5$ photons, and by solving in a basis of up to N_{max} Bogoliubov excitations instead of photons. The resulting occupation probability distribution [Fig. 4.3(a), left inset] shows the two expected effects. More importantly, the CHSH inequality is violated for $\kappa > 0$ except in configurations, where the Bell parameter is very close to the classical boundary, $\mathcal{B}_{\mathrm{max}} \gtrsim 2$, already

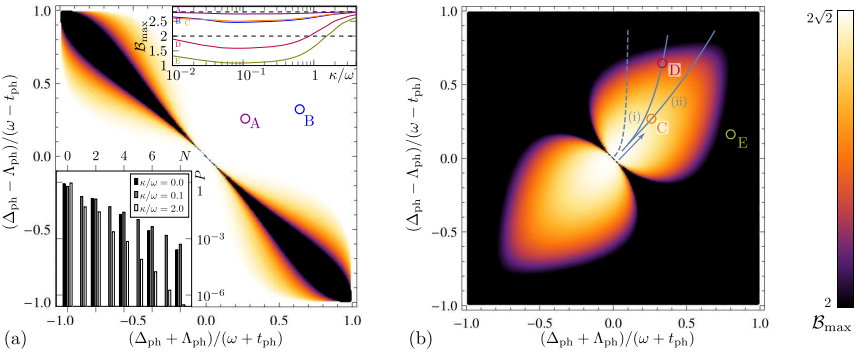

Figure 4.3: Maximum violation of the CHSH Bell inequality depending on the local and nonlocal pair creation amplitudes Λ_{ph} and Δ_{ph}. In the black regions, entanglement cannot be detected, $\mathcal{B}_{max} \leq 2$, but, in the white regions, $\mathcal{B}_{max} \geq 2\sqrt{2}$. (a) Perfect detectors, $\gamma = 1$, isolate the contribution of a single nonlocal pair and entanglement is detectable for almost all parameters. Right inset: Cavity losses affect $\mathcal{B}_{max}$ [shown at different points A, B ($\gamma = 1$) and C–E ($\gamma = 10^{-4}$) in the parameters space], possibly reducing it below the critical value of 2 (lower dashed line). At high losses, however, all surviving coincidences are due to nonlocal pairs and $\mathcal{B}_{max}$ approaches the two-particle maximum value $2\sqrt{2}$ (upper dashed line). Left inset: Probabilities P to find N photons in the cavities at point B/D, and at different loss rates κ. At finite cavity losses, odd-number states are populated, because photon pairs are broken up. (b) Lossy detectors, $\gamma = 10^{-4}$ (see text), are able to detect entanglement if the admixture of local pairs is sufficiently small. The lines indicate the parameters obtained from the microscopic model if cotunneling is (i) as strong as Cooper pair splitting at infinite (solid) or finite charging energy 2 meV (dashed) on both quantum dots, or (ii) if cotunneling is half as strong as Cooper pair splitting. Following these lines in the direction of the arrow corresponds to different cavity detunings, $eV_{sd}/\hbar = \omega_0 + \delta\omega$, where $\hbar\delta\omega$ increases from $-0.1g$ to $0.1g$. Figure and caption reproduced from the original publication, Ref. 117.

at $\kappa = 0$. When the loss rate κ dominates over the pairing amplitudes $|\Delta_{\mathrm{ph}}|$ and $|\Lambda_{\mathrm{ph}}|$, in total, $\mathcal{B}_{\max}$ is even increased since the standard two-photon situation is approached.

In summary, we can expect the CHSH-like test for entanglement to succeed reliably in a large range of configurations, but only if the nonlocal pairing amplitude Δ_{ph} is nonzero. This amplitude is, in turn, closely related to Cooper pair splitting. In this setup, unlike in Ref. 44, Cooper pair splitting can also involve cotunneling between the quantum dots because there are no strongly-coupled leads to deplete the quantum dots immediately after injection. But the effective amplitude of nonlocal emission Δ_{ph} is finite only if at some point two spin-entangled electrons reside on two different quantum dots. In particular, local pair emission alone does not suffice to violate the Bell inequality even if the photons can tunnel from one cavity into another. Depending on the geometry of the device, which is fundamentally restricted by the superconducting coherence length, and on the emission rates, the two electrons on the two quantum dots do not necessarily fulfill the criterion of being spacelikely separated, which would be required in a fundamental Bell test. But as I already pointed out in Chap. 1, the aim is not to proof or to disproof quantum mechanics. Instead, taking for granted the laws of quantum mechanics and the model I presented, observing $\mathcal{B}_{\max} > 2$ is an experimental proof of coherent Cooper pair splitting.

5

Entanglement Detection via Spin–Charge Separation

In all of the preceding chapters, electron–electron interactions mediated by the Coulomb force were largely being ignored, with the notable exception of the repulsion between two electrons on the same quantum dot. Intuitively, we expect that, if several electrons or holes are confined to a small space such as a quantum dot, their mutual interaction is highly relevant, whereas they can easily avoid one another in the bulk of a conductor making interactions less of an issue. Indeed, charging diagrams of quantum dots [217] give immediate access to the Coulomb force, whereas many other transport phenomena are successfully described by noninteracting theories, e.g., the conductance of two-dimensional electron gas structures, including the Aharonov–Bohm effect [93], and many topological properties [134]. The remarkable predictive power of noninteracting theories goes well beyond what could be justified by the influence of Coulomb repulsion merely being small (in whatever sense). In 1957, Landau came up with an explanation [218–220], the (Landau–)Fermi-liquid theory. Coulomb interactions preserve the translational symmetry of the noninteracting Fermi gas, so it is to be expected that the single-particle excitations $E_{\mathbf{k}\sigma}$ of the noninteracting theory, labeled by momentum $\mathbf{k}$ and spin σ, are adiabatically connected to excitations of the interacting theory with the same quantum numbers as long as there is no phase transition such as Wigner crystallization [221]. Landau further argued that these quasiparticle excitations decay into the exact eigenstates of the interacting system only slowly if they are sufficiently close to the Fermi level, $E_{\mathbf{k}} \ll E_F$. Close to the Fermi level, there is little phase space for scattering: the

quasiparticle (if it is electronlike) is required to stay above the Fermi sea by the exclusion principle, so it cannot lose too much of its momentum. Its scattering partner, on the other hand, has to be lifted out of the Fermi sea, which would be favored by a *large* momentum transfer. Landau estimated that the quasiparticle lifetime is therefore larger than $\hbar E_F/E_k^2$ in three dimensions [218]. Note that this argument does not require the interactions to be weak. It relies, however, on the Fermi sea staying more or less unaffected by the interactions. If this is the case, quasiparticles are a good concept for excitations of the interacting electron gas. But it is not always true. Fermi-liquid theory does not only break down in zero-dimensional quantum dots, but already in one-dimensional systems, such as nanowires, carbon nanotubes, quantum-Hall edge states, and cleaved-edge overgrowths. In dimensions larger than one, the electric potential of a particle which moves through a solid causes density fluctuations. Density fluctuations are of bosonic nature so the original fermion together with the cloud of fluctuations is still a fermion. In one dimension, on the other hand, there is no way for an electron to circumvent its neighbors — in order to transport charge, it can only push them into the desired direction. This kind of excitation is necessarily a collective, bosonic one. This precludes us from mapping the noninteracting fermions to interacting fermions as it is done in Fermi-liquid theory. On the other hand, one-dimensional systems have a very special Fermi surface which consists of two isolated points $\pm p_F$, around which the dispersion relation may be linearized, $\varepsilon_\pm(p) = \pm v_F(p \mp p_F)$. This means that an electron–hole pair created by applying some fixed momentum q to an arbitrary Fermi-sea electron has a well defined energy $\varepsilon_{eh\pm}(q) = \varepsilon_\pm(p+q) - \varepsilon_\pm(p) = \pm v_F q$. This is quite different in a higher-dimensional system: applying a momentum $\mathbf{q}$ with a fixed direction results in a variety of different energies $\varepsilon(|\mathbf{p}+\mathbf{q}|) - \varepsilon(|\mathbf{p}|)$ for different momenta $\mathbf{p}$ from the Fermi sea. Since they have a proper dispersion relation $\varepsilon_{eh}(q)$, the bosonic excitations of one-dimensional systems may very well behave as quasiparticles [222]. This is the basis for bosonization [223], which rewrites the excitations of a one-dimensional system in terms of bosonic electron–hole pairs, i.e., density fluctuations. Density is what the Coulomb repulsion couples to, so the good news is that, although interactions add a great deal of complexity, the fully-interacting problem, called Tomonaga–Luttinger liquid [224, 225], is analytically solvable using bosonization.

One of various unusual properties of the Tomonaga–Luttinger liquid is fractionalization: because the basic excitations are density fluctuations, their charge is not necessarily a multiple of the elementary charge but depends on the interaction strength. An electron injected into a Tomonaga–Luttinger liquid decomposes into a left-moving part and into a right-moving part which, only together, sum up to the charge of the original electron [226]. This is particularly important in the fractional quantum Hall effect. A related phenomenon is spin–charge separation. The injected electron does not only decay into two charge excitations but in a spin excitation, too, which propagates *separately* from either of the charge excitations. In the experiment, spin–charge separation gives rise to two distinct branches in the excitation spectrum, which has been observed by momentum-resolved tunneling [227] and by angle-resolved photoemission spectroscopy [228, 229].

Coming back to entanglement, the unusual interaction-induced properties open up an exciting possibility: as I discussed in Chap. 1, there is a close link between entanglement and interactions. So we can hope that novel effects emerge if we consider entanglement detection in the context of this non-Fermi-liquid system. A most natural candidate system is the electronic beam splitter proposed by Burkard et al. [41]. First of all, because entanglement detection by bunching and antibunching is conceptionally relatively straight forward and yet reasonably significant. But second, the whole idea of a beam splitter is tailor made for one-dimensional conductors: imagine a crossing between two nanowires or between two carbon nanotubes. Where they touch, a tunnel junction is formed, and the structure becomes a beam splitter. Crossings of two carbon nanotubes have been realized early by several groups [230–233]. As predicted by the Tomonaga–Luttinger model, the voltage dependence and the temperature dependence of the conductance are power laws. Alternatively, when two edge states of quantum-Hall systems come sufficiently close to each other at a constriction of the host sample, tunneling between them is possible. Quantum-Hall edge states have the additional benefit of extremely large coherence lengths exceeding several micrometers, as witnessed by selfinterference of single electrons in a Mach–Zehnder setup [234] and by antibunching of independent electrons in a Hanbury Brown–Twiss setup [100, 101]. For our purposes, we need spinful channels, i.e., two copropagating quantum-

Hall edge states of opposite spin. This, too, has already been realized [235], including spin–charge separation [236]. I will discuss both of the approaches, nanowires and edge states, later on in more detail. There have been attempts to build beam splitters from two-dimensional leads, e.g., cutting them out from graphene. Unfortunately, their rough edges induce strong scattering which spoils probably the entanglement and certainly its detection although recently there has been some progress by guiding the electrons via total internal reflection at p–n boundaries in the bulk of graphene, similar to optical waveguides [237].

So far, the theoretical studies on beam splitters as proposed by Burkard et al. found signatures of entanglement only in the current noise but not in the current itself. This is intuitive: entanglement is a two-particle property, so in the case of noninteracting particles, the current, which is a single-particle property, should not know about entanglement but correlation measurements, such as noise, can very well. This argument, however, is not complete because it ignores the exchange interactions, which even noninteracting fermions are subject to. Nevertheless, the statement is true for any Fermi-liquid system and any device geometry. To show this, I will give a stronger argument based on the scattering matrix formalism (cf. Chap. 1). The current flowing away from the beam splitter in lead i is

$$\hat{I}_i(t) = \frac{e}{2\pi\hbar} \sum_{\varepsilon\varepsilon' n\sigma} e^{i(\varepsilon-\varepsilon')t/\hbar} \left[\overrightarrow{c}^{\dagger}_{in\sigma}(\varepsilon) \overrightarrow{c}_{in\sigma}(\varepsilon') - \overleftarrow{c}^{\dagger}_{in\sigma}(\varepsilon) \overleftarrow{c}_{in\sigma}(\varepsilon') \right] \tag{5.0.1}$$

where $\overrightarrow{c}_{in\sigma}(\varepsilon)$ destroys outgoing quasiparticles of energy ε and spin σ in mode n of lead i and $\overleftarrow{c}_{in\sigma}(\varepsilon)$ destroys ingoing quasiparticles [238]. As I discussed already in Chap. 1, the outgoing modes are related to the ingoing modes by a unitary transformation, $\overleftarrow{c}_{in\sigma} = \sum_{jm\rho} s_{in\sigma,jm\rho} \overrightarrow{c}_{jm\rho}$, where s is the scattering matrix. The physical statement is that, if all which goes in is known, all which goes out is determined, too. What is important here is, first, that Eq. (5.0.1) is a completely general expression for the current under the assumption of free quasiparticles, i.e., it is valid for Fermi-liquid systems, and, second, that it is bilinear in the field operators c. Strictly speaking, Eq. (5.0.1) uses that at all relevant energies $\varepsilon, \varepsilon'$ the quasiparticle velocity is equal but this assumption only simplifies the coefficients and, without it, the current

operator is still bilinear. Now we want to calculate the current of a state which is initially a nonlocal spin triplet or a nonlocal spin singlet, $|\Psi(t=0)\rangle = 2^{-1/2}(|in\uparrow; jm\downarrow\rangle \pm |in\downarrow; jm\uparrow\rangle)$. The expectation value of any operator $\mathcal{O}(t)$ with respect to this state is

$$\begin{aligned}
&\langle\Psi\,|\,\mathcal{O}\,|\,\Psi\rangle \\
&= \frac{1}{2}\langle in\uparrow; jm\downarrow|\,\mathcal{O}(t)\,|\,in\uparrow; jm\downarrow\rangle + \frac{1}{2}\langle in\downarrow; jm\uparrow|\,\mathcal{O}(t)\,|\,in\downarrow; jm\uparrow\rangle \\
&\pm \frac{1}{2}\langle in\uparrow; jm\downarrow|\,\mathcal{O}(t)\,|\,in\downarrow; jm\uparrow\rangle \pm \frac{1}{2}\langle in\downarrow; jm\uparrow|\,\mathcal{O}(t)\,|\,in\uparrow; jm\downarrow\rangle \\
&= \underbrace{\langle in\uparrow; jm\downarrow|\,\mathcal{O}(t)\,|\,in\uparrow; jm\downarrow\rangle}_{\langle\mathcal{O}\rangle_{\mathrm{dir}}} \pm \underbrace{\langle in\uparrow; jm\downarrow|\,\mathcal{O}(t)\,|\,in\downarrow; jm\uparrow\rangle}_{\langle\mathcal{O}\rangle_{\mathrm{exc}}}.
\end{aligned} \tag{5.0.2}$$

In the last step I assumed spin-rotation invariance because, after all, one of the benefits of the bunching-and-antibunching approach is that spin-dependent devices such as spin filters are *not* required to detect spin entanglement. Assuming spin-rotation invariance at this point is merely for convenience because, instead of keeping all of the four terms, the expectation value of $\mathcal{O}$ decomposes into one *direct* contribution $\langle\mathcal{O}\rangle_{\mathrm{dir}}$ and one *exchange* contribution $\langle\mathcal{O}\rangle_{\mathrm{exc}}$. Whereas the direct contribution is just the same as that of an ordinary product state $|in\uparrow\rangle\,|jm\downarrow\rangle$, the exchange contribution tells about entanglement. This distinction was already made by Burkard et al. in their beam-splitter proposal for entanglement detection [41] and it is a very useful one. To see if the current can carry a signature of entanglement, we need to investigate whether the exchange contribution of the current expectation value in lead k, $\langle I_k(t)\rangle_{\mathrm{exc}}$, is finite. Because I_k is bilinear, we can express the exchange contribution as

$$\begin{aligned}
\langle I_k(t)\rangle_{\mathrm{exc}} &= \sum_{ab\sigma\rho} a_{ab\sigma\rho}(t)\,\langle in\uparrow; jm\downarrow|\,c^\dagger_{ka\sigma}c_{kb\rho}|in\downarrow; jm\uparrow\rangle \\
&= \sum_{ab\sigma\rho} a_{ab\sigma\rho}(t)\,\langle|c_{in\uparrow}c_{jm\downarrow}c^\dagger_{ka\sigma}c_{kb\rho}c^\dagger_{jm\uparrow}c^\dagger_{in\downarrow}|\rangle\,.
\end{aligned} \tag{5.0.3}$$

Since we are dealing with a Fermi-liquid system, we are allowed to decompose the correlator using Wick's theorem. There are only two contributions (at $T=0$) but already by simply counting the number of

operators we see that we always get a contraction involving both in and jm, e.g., $\langle c_{in\uparrow} c^\dagger_{jm\uparrow}\rangle = \langle in|jm\rangle$, which vanishes because we assume the two spins to be spatially separated initially. So, indeed, the current does not know about two-particle entanglement in a Fermi-liquid system with a general scattering matrix. There is a shortcut if the spin is conserved in the scattering process: the current operator, Eq. (5.0.1), can then be expressed as the sum of two operators acting exclusively on different spins, $I_k = I_{k\uparrow} + I_{k\downarrow}$. So the exchange contribution of the current expectation value is

$$\begin{aligned}\langle I_k\rangle &= \langle in\uparrow; jm\downarrow | \, I_{k\uparrow} + I_{k\downarrow} \, | in\downarrow; jm\uparrow\rangle \\ &= \langle in\uparrow | \, I_{k\uparrow} \, | jm\uparrow\rangle \langle jm\downarrow | \, in\downarrow\rangle + \langle jm\downarrow | \, I_{k\downarrow} \, | in\downarrow\rangle \langle in\uparrow | \, jm\uparrow\rangle\end{aligned} \tag{5.0.4}$$

and, again, without initial orbital overlap of the two electrons, the expression vanishes. Clearly, orbital overlap is in conflict with the notion of entanglement being nonlocal or, more specifically, with the aim of Cooper pair splitting.

The scattering matrix formalism and Wick's theorem do not work in the Tomonaga–Luttinger model, at least not for the electronlike quasiparticles the spin of which I investigate here. In physical terms, if interactions can turn product states into entangled states, why should they not be able to map entanglement back onto a single-particle property like the current in the time evolution of an interacting system? The surprising result is that the current in the interacting system is, in fact, sensitive to entanglement and, intriguingly, that this can be clearly attributed to one specific non-Fermi-liquid phenomenon: spin–charge separation.

5.1 Tomonaga–Luttinger liquid and bosonization

Before setting up the model of an interacting beam splitter, I need to clarify some conventions regarding the bosonization formalism, which solves the Tomonaga–Luttinger model. Sadly, there is no universally accepted way to do so even though virtually every article on the technique

complains about it. The degree of confusion ranges from only calling the same thing different names or calling different things the same name, over choosing different normalizations and signs, to silently swapping two similar quantities altogether. Having complained, like everyone else, I will now present my own set of conventions; sincerely believing that it is superior for the specific problem I discuss — probably like everyone else.

Apart from Tomonaga [224] and Luttinger [225], after whom the model is named, many contributed to developing the theory of one-dimensional interacting fermions. Among others, Bloch [239, 240] already treated collective bosonic excitations of fermions, Mattis and Lieb actually solved the model [241] and Haldane [223] put the relation between the fermions and the bosons on a solid footing. The Tomonaga–Luttinger model in a modern formulation reads

$$H_{\mathrm{TLL}} = \sum_{j\nu ks} \hbar v_F (k - k_F) \Big[c^\dagger_{j\nu s}(k) c_{j\nu s}(k) - \langle c^\dagger_{j\nu s}(k) c_{j\nu s}(k) \rangle_0 \Big] + \int dx \sum_{j\nu\nu' ss'} g_{j\nu\nu'} \psi^\dagger_{j\nu s}(x) \psi_{j\nu s}(x) \psi^\dagger_{j\nu' s'}(x) \psi_{j\nu' s'}(x), \tag{5.1.1}$$

where $c^\dagger_{j\nu s}(k)$ creates a left-moving electron ($\nu = L \equiv -1$) or a right-moving electron ($\nu = R \equiv +1$) with momentum νk and spin s, and $\psi^\dagger_{j\nu s}(x) = \frac{1}{\sqrt{L}} \sum_k e^{-i\nu k x} c^\dagger_{j\nu s}(k)$ is the corresponding field operator in real space. I already introduced the index j to distinguish independent copies of the model because I will later construct the beam splitter as a crossing of two conductors. Eq. (5.1.1) is, more or less, a universal one-dimensional Hamiltonian with a density–density interaction term. There are, however, a few subtleties. The spectrum is linearized around the Fermi points $\pm k_F$, which is why we need to distinguish left-moving electrons from right-moving electrons. This is similar to the valleys in graphene I discussed in Chap. 2 but, here, the two branches are thought of as two pieces of a single, typically parabolic, dispersion relation. They are not separated by the entire Brillouin zone but only by $2k_F$, so there will be scattering between left movers and right movers. Since the linearized spectrum is unbounded from below, the Fermi sea has an infinite but irrelevant energy contribution which is subtracted in

Eq. (5.1.1). The Fermi sea involves unphysical states like $c_{jRs}(-|k|)$ which are labeled as right movers but have a negative momentum or vice versa. These states are assumed to be sufficiently far away in energy that they do not affect physical quantities, which also implies that the physical electron field operator is $\psi_{js}(x) \approx \psi_{jRs}(x) + \psi_{jLs}(x)$. The linear approximation is usually a very good one considering that the Fermi temperature in metals is on the order of $T_F = 10^4$ K. If higher-order corrections need to be taken into account, they enter as interactions between the bosons which will diagonalize Eq. (5.1.1) and can be treated perturbatively [222], which is still much better than the original problem in terms of electrons, which is not even accessible by perturbation theory. The interaction term is local. The rationale is that, even in a one-dimensional conductor, the long-range interactions will be screened by nearby gates and other conductors and that there is no divergence in the short-range limit because at very small length scales, i.e., at high energies, the transversal spatial dimensions become important [242]. So for the low-energy excitations with wavelengths much larger than the screening radius, the screened interaction can be replaced by a purely local one. Of course, this ad-hoc fashion of adding an interaction term to the already-linearized model does not necessarily yield the correct low-energy approximation of the original model with a parabolic band and the interaction term but renormalization-group studies confirm that, in this case, it does [243].

Amazingly, the Tomonaga–Luttinger Hamiltonian H_{TLL} can be rewritten as a quadratic Hamiltonian,

$$H_0 = \sum_{j\alpha} \int dx \frac{\hbar v_\alpha}{2} \Big[g_\alpha \Big(\frac{\partial \phi_{j\alpha}}{\partial x} \Big)^2 + \frac{1}{g_\alpha} \Big(\frac{\partial \theta_{j\alpha}}{\partial x} \Big)^2 \Big], \tag{5.1.2}$$

with the dual phase fields ϕ and θ, which are called *dual* because they obey the commutation relation $[\theta_{j\alpha}(x,t), \phi_{j'\alpha'}(x',t)] = (i/2)\mathrm{sgn}(x - x')\delta_{jj'}\delta_{\alpha\alpha'}$. They are, essentially, linear combinations of bosonic density operators [242]. The spatially localized electron is a coherent state of these bosons [244–248],

$$\psi_{j\nu s}(x,t) = (2\pi a)^{-1/2} F_{j\nu s} e^{i\nu k_F x + 2\pi i \Phi_{j\nu s}(x,t)}, \tag{5.1.3}$$

where

$$\Phi_{j\nu s} = \Big[\phi_{j\rho} + s\phi_{j\sigma} + \nu(\theta_{j\rho} + s\theta_{j\sigma}) \Big], \tag{5.1.4}$$

together with a unitary, anticommuting Klein factor $F_{j\nu s}$. The Klein factor changes the number of ν-moving spin-s electrons in system j by one, which the bosonic density part of the operator is obviously unable to do. The index α, in which the model is now diagonal, distinguishes the charge degrees of freedom ($\alpha = \rho$) and the spin degrees of freedom ($\alpha = \sigma$). The two parameters g_α and $v_\alpha = v_F/g_\alpha$ capture the effect of the Coulomb interaction $g_{j\nu\nu'}$. In the spin sector, $g_\sigma = 1$, which corresponds to no interactions, because the Coulomb interaction of the model, Eq. (5.1.1), is spin independent and so the complete model is spin-rotation invariant. In the charge sector, $0 < g_\rho < 1$ for repulsive interactions. For the purpose of describing the interacting beam splitter, we do not need to consider attractive interactions, where $g_\rho > 1$. We will see that, just as its name suggests, v_α is the effective velocity of the charge and spin excitations. Since $v_\sigma = v_F$ but $v_\rho > v_F$, spin–charge separation occurs. Finally, the factor a in the bosonization identity, Eq. (5.1.3), is a cutoff parameter which corresponds to the inverse bandwidth of the one-dimensional system. The transformation from Eq. (5.1.1) to Eq. (5.1.2) is exact in the spinless or spin-polarized case. In the spinful case, an additional approximation is required: the interaction term in Eq. (5.1.1) includes a process in which, say, a right-moving spin-up electron scatters with a left-moving spin-down electron such that the final state is a left-moving spin-up electron and a right-moving spin-down electron. But this cannot be a density–density interaction and, as can hence be expected, apart from the quadratic contribution, Eq. (5.1.2), the transformation produces an additional term. It reads $H_{\mathrm{SG}} = \sum_j \int dx (2/2\pi^2 a^2) \cos(2\sqrt{2\pi}\theta_{j\sigma})$, where the subscript SG indicates that the equation of motion for the spin waves is the sine–Gordon equation when H_{SG} is included. Again, renormalization-group theory comes to the rescue: in spin-rotation-invariant systems, the sine–Gordon term is irrelevant, i.e., in the low-energy limit, it can be dropped when renormalizing the interaction parameters g_α [222]. Since the actual value of g_α is only of quantitative consequence for the beam splitter, I will directly use the quadratic Hamiltonian, Eq. (5.1.2).

The details of how to get from Eq. (5.1.1) to Eq. (5.1.2) are rather intricate and well explained in a number of reviews [242, 249]. What we require in order to discuss the beam splitter are the Keldysh contour-ordered electron–electron correlation functions of the theory and I will

now outline a way to derive them only knowing the transformed Hamiltonian H_0, the commutation relations of ϕ and θ, and the bosonization identity, Eq. (5.1.3). In the remainder of this section, I will drop all redundant indices. First, we obtain the equations of motion for the phase fields from Heisenberg's equation using the commutation relations,

$$\partial_t \phi = \frac{1}{i\hbar}[\phi, H_0] = -\frac{v}{g}\frac{\partial \theta}{\partial x} \tag{5.1.5}$$

$$\partial_t \theta = \frac{1}{i\hbar}[\theta, H_0] = -vg\frac{\partial \phi}{\partial x}, \tag{5.1.6}$$

which can be combined into the wave equation $\partial_t^2 \phi = v^2 \partial_x^2 \phi$. Here it becomes evident that v_α from the Hamiltonian is, indeed, the propagation velocity of the elementary excitations. The wave equation is easily solved in Fourier space,

$$\phi = \frac{1}{\sqrt{L}} \sum_{\substack{\omega>0 \\ \xi=\pm 1}} \frac{1}{\sqrt{2\omega g/v}} \Big(e^{i\omega(\xi x/v - t)} a_{\omega\xi} + e^{-i\omega(\xi x/v - t)} a_{\omega\xi}^\dagger \Big), \tag{5.1.7}$$

and, by virtue of Eq. (5.1.6),

$$\theta = \frac{1}{\sqrt{L}} \sum_{\substack{\omega>0 \\ \xi=\pm 1}} \xi \sqrt{\frac{vg}{2\omega}} \Big(e^{i\omega(\xi x/v - t)} a_{\omega\xi} + e^{-i\omega(\xi x/v - t)} a_{\omega\xi}^\dagger \Big), \tag{5.1.8}$$

where I chose the coefficients for convenience. The commutation relation of the phase fields implies that the conjugate momentum to ϕ is $\Pi_\phi = -\hbar \frac{\partial \theta}{\partial x}$. When we impose the canonical quantization condition, $[\phi(x,t), \Pi_\phi(x',t)] = i\hbar\delta(x-x')$, we find that the operators $a_{\omega\xi}$ have to fulfill bosonic commutation relations, so we have recovered the bosons underlying the bosonization procedure. If we plug the solutions for ϕ and θ, Eqs. (5.1.7) and (5.1.8), into the normal-ordered Hamiltonian H_0, Eq. (5.1.2), it becomes

$$H_0 = \sum_{\substack{j\alpha\xi \\ \omega>0}} \hbar\omega a_{j\alpha\omega\xi}^\dagger a_{j\alpha\omega\xi}, \tag{5.1.9}$$

from which we know that the bosons $a_{j\alpha\omega\xi}$ follow the Bose–Einstein

distribution in the ground state. So, now, we can calculate the correlators of the phase fields on the Keldysh contour,

$$C^{\alpha}_{\phi\phi}(x,t;x',t') = \langle \mathrm{T}_{\mathcal{C}}\phi_\alpha(x,t)\phi_\alpha(x',t')\rangle \tag{5.1.10}$$

$$= \frac{1}{4\pi}\frac{1}{g_\alpha}\sum_\xi \int\limits_{(-\infty,\infty)\setminus[-2\pi/L,2\pi/L]} dp \frac{1}{p}\frac{e^{-i\mathrm{sgn}_{\mathcal{C}}(t-t')p[\xi(x-x')-v_\alpha(t-t')]-a|p|}}{e^{\beta\hbar v p}-1} \tag{5.1.11}$$

$$\approx -\frac{1}{g_\alpha}\frac{1}{4\pi}\sum_\xi \log\Big(\frac{2\beta\hbar v_\alpha}{L} i \times \sinh\Big\{\frac{\pi}{\beta\hbar v_\alpha}\Big[-\xi(x-x')+v_\alpha(t-t')-ia\Big]\Big\}\Big) \tag{5.1.12}$$

$$\approx -\frac{1}{g_\alpha}\frac{1}{4\pi}\Big[\log\Big(\frac{2\pi}{L}f_+\Big)+\log\Big(\frac{2\pi}{L}f_-\Big)\Big], \tag{5.1.13}$$

where

$$f_{\alpha\pm} := -i\mathrm{sgn}_{\mathcal{C}}(t-t')\big[\pm(x-x')-v_\alpha(t-t')\big]+a. \tag{5.1.14}$$

The contour-ordering operator $\mathrm{T}_{\mathcal{C}}$ rearranges all operators it acts on according to increasing contour time from the right to the left and includes the necessary fermionic signs. Similarly, the contour sign function is $\mathrm{sgn}_{\mathcal{C}}(t-t')=1$, when t is later on the Keldysh contour than t', and -1 otherwise. Note that I introduced a band cutoff $\hbar v_F/a$ in Eq. (5.1.11), which regularizes the singular pointlike field operator involving infinitely-high energies. To solve the integral, I used a clever approximation presented in Ref. 249 such that we can conveniently take the zero-temperature limit, $\beta\to\infty$, afterwards. In the same fashion, we obtain

$$C^{\alpha}_{\theta\theta}(x,t;x't') = \langle \mathrm{T}_{\mathcal{C}}\theta_\alpha(x,t)\theta_\alpha(x',t')\rangle$$

$$\approx -g_\alpha\frac{1}{4\pi}\Big[\log\Big(\frac{2\pi}{L}f_{\alpha+}\Big)+\log\Big(\frac{2\pi}{L}f_{\alpha-}\Big)\Big], \tag{5.1.15}$$

$$C^{\alpha}_{\phi\theta}(x,t;x't') = \langle \mathrm{T}_{\mathcal{C}}\phi_\alpha(x,t)\theta_\alpha(x',t')\rangle = \langle \mathrm{T}_{\mathcal{C}}\theta_\alpha(x,t)\phi_\alpha(x',t')\rangle$$

$$\approx -\frac{1}{4\pi}\Big[\log\Big(\frac{2\pi}{L}f_{\alpha+}\Big)-\log\Big(\frac{2\pi}{L}f_{\alpha-}\Big)\Big] \tag{5.1.16}$$

and this is all we need in order to calculate an arbitrary contour-ordered n-point fermion correlation function: with the bosonization identity, Eq. (5.1.3), it becomes the expectation value of an exponential of the phase fields, which is, by the Debye–Waller identity, $\langle e^{\sum x_i}\rangle = e^{\frac{1}{2}\langle(\sum x_i)^2\rangle}$, just an exponential of the very correlators of the phase fields I derived.

As a simple but instructive application, consider the time evolution of a single right-moving spin-up electron injected into a Tomonaga–Luttinger liquid at the point x_0 and at the time t_0, i.e., consider a system with the initial state $|\varphi\rangle = \psi^\dagger_{1R\uparrow}(x_0,t_0)\,|\rangle$, where $|\rangle$ is the interacting Fermi sea. In the notation I chose, the charge-current density and the spin-current density are $I_{1\rho}(x,t) = -\partial_t \sum_{\nu s} \Phi_{1\nu s}(x,t)$ and $I_{1\sigma}(x,t) = -\partial_t \sum_{\nu s} s\Phi_{1\nu s}(x,t)$ (cf. Ref. 242). In order to calculate the expectation value of a product of both exponentials of the phase fields, which enter via the definition of the initial state, and of the phase fields themselves, which enter via the current operator, we follow the seminal paper on tunneling between Tomonaga–Luttinger liquids by Kane and Fisher [250] and construct a generating functional

$$Z^\varphi = \langle\varphi|\mathrm{T}_\mathcal{C} e^{\int dx \int_\mathcal{C} dt \sum_{i\nu s} j_{i\nu s}(x,t)\Phi_{i\nu s}(x,t)}|\varphi\rangle\,, \tag{5.1.17}$$

where the expectation value is taken with respect to the initial state $|\varphi\rangle$ with one additional electron, i.e.,

$$Z^\varphi \propto \langle|\mathrm{T}_\mathcal{C} e^{2\pi i\left[\Phi_{1R\uparrow}(x_0,t_0^-)-\Phi_{1R\uparrow}(x_0,t_0^+)\right]+\int dx\int_\mathcal{C} dt\sum_{i\nu s} j_{i\nu s}(x,t)\Phi_{i\nu s}(x,t)}|\rangle\,. \tag{5.1.18}$$

Now, the expectation value of $\Phi_{1\nu s}(x,t)$ is obtained as a functional derivative of Z^φ with respect to the source field $j_{1\nu s}(x,t)$ but only *after* already having applied the Debye–Waller identity. In the framework of full counting statistics, the generating functional is usually called *cumulant-generating function* and the source field is called the *counting field* but, basically, they are the same objects. What results, is

$$\begin{aligned}\langle\varphi\,|\,I_\rho(x,t)\,|\,\varphi\rangle &= \frac{1+g}{2}\delta_a\Big[x-x_0-v_\rho(t-t_0)\Big]\\ &\quad -\frac{1-g}{2}\delta_a\Big[x-x_0+v_\rho(t-t_0)\Big] \qquad (5.1.19)\\ \langle\varphi\,|\,I_\sigma(x,t)\,|\,\varphi\rangle &= \delta_a\Big[x-x_i-v_\sigma(t-t_0)\Big], \qquad (5.1.20)\end{aligned}$$

where $\delta_a(x) = a/\pi(a^2 + x^2)$ is the Lorentz function. I used $g_\sigma = 1$ and will, from now on, abbreviate $g_\rho \equiv g$. According to Eqs. (5.1.19) and (5.1.20), the electron decays into a collective charge and a collective spin excitation after injection, which propagate with different velocities $v_{\rho,\sigma}$ and which have a spread a determined by the bandwidth. The wave packets keep their Lorentzian shape while propagating since the linear spectrum is not dispersive. Charge fractionalization is present, too: only the fraction $(1 + g)/2$ of the charge propagates to the right after injecting a right-moving free electron. It was believed that charge fractionalization would affect the quantization of conductance but this is in disagreement with the Landauer–Bütticker theory of conduction, in which the conductance quantization originates from the statistical properties of the noninteracting leads. The experimental facts were hardly convincing either [251] and a number of authors reported almost simultaneously that charge fractionalization cannot be observed if the Tomonaga–Luttinger is realistically assumed to have a finite length [252–254]. Multiple reflections occur at the interfaces to the noninteracting reservoirs such that, asymptotically, one complete electron is transmitted. This Fabry–Perot behavior is lost in the limit of an infinitely-long interacting system. Later on, fractional charges were conjectured to enter the zero-frequency current–current correlator, i.e., the shot noise [255], but this, too, turned out not to be true in finite systems [256]. This is unfortunate because it would have provided an easy way to measure the interaction parameter g other than power laws. What might work is looking at the finite-frequency noise. The Fabry–Perot behavior at finite frequencies was studied in detail assuming perfect interfaces between the conductor and the leads [257, 258] and with weak impurities at the interfaces [259]. Coming back to our case, the correct expressions with the influence of noninteracting leads are obtained by setting $g \to 1$ in the prefactors of Eq. (5.1.19). For the purpose of entanglement detection, this leads only to minor quantitative changes, in particular, because there is no fractionalization in the crucial spin sector anyway. So I will not make the distinction between finite and infinite leads in the following.

5.2 Beam splitter built from one-dimensional nanowires

Going from two independent Tomonaga–Luttinger liquids to an interacting beam splitter is now a simple matter. I will discuss the slightly more general case of nanowires first. With quantum-Hall edge states, which are chiral, a number of expressions simplify because there are only, say, right-moving electrons. I will discuss what changes in Chap. 5.3.

As illustrated in Fig. 5.1, I assume that there is a tunnel contact between two Tomonaga–Luttinger liquids $j = 1, 2$ at $x = 0$ described by the Hamiltonian

$$H_T = T \sum_{\substack{\nu,\nu' \in \{R,L\} \\ s \in \{\uparrow,\downarrow\}}} \Big(\psi^\dagger_{1\nu' s}(0) \psi_{2\nu s}(0) + \psi^\dagger_{2\nu' s}(0) \psi_{1\nu s}(0) \Big). \tag{5.2.1}$$

Komnik and Egger showed that this is, indeed, the correct low-energy Hamiltonian to describe tunneling between two Tomonaga–Luttinger liquids as long as the interactions are moderate, $1/2 < g < 1$, in the spinless case [260] and with an even smaller lower bound in the spinful case [233]. At stronger interactions, $0 < g < 1/2$, electrostatic repulsion between the wires at the tunnel point becomes a relevant perturbation in the sense of the renormalization group. In this scenario, backscattering is dominant and so the device behaves rather different from a typical beam splitter. But as long as we conservatively limit the discussion to $1/2 < g < 1$, we can use H_T to describe electrons tunneling between the two wires and we can treat H_T in perturbation theory.

Due to a voltage bias V between the entangler and the beam splitter or due to time-dependent pumping, entangled pairs are injected to the left of the junction, one electron at $x_1 < 0$ in wire 1 and one electron at $x_2 < 0$ in wire 2. The injection happens far away from the tunnel contact, $|x_{1,2}| \gg a$, and with a rate $\Gamma_{2e} \ll v_F/a$ sufficiently low for subsequent pairs to be uncorrelated. This situation is captured by the

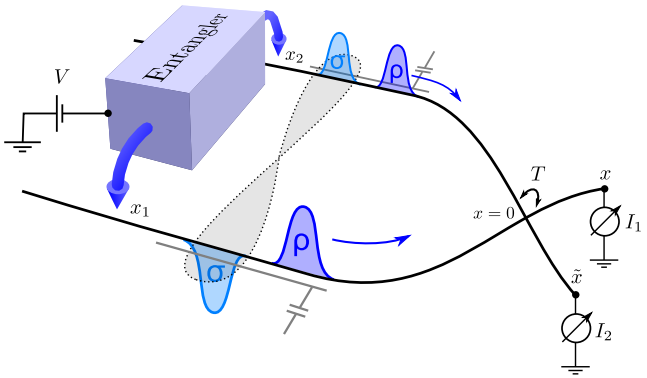

Figure 5.1: Tunnel junction with amplitude T at $x = 0$ between two interacting one-dimensional wires. Via an entangler biased with a voltage V, two spin-entangled electrons are injected simultaneously at x_1 in wire 1 and at x_2 in wire 2 with an amplitude I, and subsequently decay into collective spin and charge excitations. The current expectation values $I_{1,2}$ measured at $x, \tilde{x}$ at the far opposite side of the junction and their cross-correlations are influenced by the entanglement of the original electrons. Figure and caption reproduced from the original publication, Ref. 118.

initial state

$$|\varphi\rangle = \frac{\pi a}{\sqrt{2}}\Big(\psi^\dagger_{2\downarrow}(x_2)\psi^\dagger_{1\uparrow}(x_1) + e^{i\varphi}\psi^\dagger_{2\uparrow}(x_2)\psi^\dagger_{1\downarrow}(x_1)\Big)\,|\rangle$$
$$:= 2^{-1/2}\sum_{\nu_1,\nu_2}\Big(|\nu_1\uparrow,\nu_2\downarrow\rangle + e^{i\varphi}\,|\nu_1\downarrow,\nu_2\uparrow\rangle\Big), \tag{5.2.2}$$

where the phase φ interpolates between a pure triplet state ($\varphi = 0$) and a pure singlet state ($\varphi = \pi$). We are interested in the current in, say, wire 1 behind the tunnel junction, i.e., at $x \gg a$. It is sufficient and experimentally convenient to consider only the averaged dc current,

$$I_1 = e\Gamma_{2e}\int_{t_0}^{\infty} dt\,\langle\varphi|\,I_{\rho 1}(x,t)\,|\varphi\rangle\,. \tag{5.2.3}$$

I will additionally consider the symmetrized zero-frequency cross-correlations between the two wires,

$$S_{12} = \frac{e^2\Gamma_{2e}}{2}\int_{t_0}^{\infty} dt d\tilde{t}\,\langle\varphi|\,\Big\{\delta I_1(x,t),\delta I_2(\tilde{x},\tilde{t})\Big\}\,|\varphi\rangle\,, \tag{5.2.4}$$

with $\delta I_j = I_j - \langle\varphi|\,I_j\,|\varphi\rangle$, which are the central object of interest in the noninteracting case because they exhibit the bunching and antibunching behavior. Both I_1 and S_{12} do not depend on the measurement points x and $\tilde{x}$ because, no matter where in the wire the current is measured, after some time, all the charge has passed. It does make a difference whether the current is measured in front of the tunnel junction or behind the tunnel junction but I will only discuss the more natural latter case.

Like in the single-wire case, Eqs. (5.2.3) and (5.2.4) are most conveniently evaluated by introducing a contour-ordered generating functional, which, like any expectation value, decomposes into a direct and an exchange contribution,

$$Z^{\varphi}_{x_1,x_2} = \langle\varphi|\,\mathrm{T}_{\mathcal{C}} e^{\int dx\int_{\mathcal{C}} dt\sum_{i\nu s} j_{i\nu s}(x,t)\Phi_{i\nu s}(x,t)}\,|\varphi\rangle$$
$$= Z^{\mathrm{dir}}_{x_1,x_2} + \cos(\varphi)\,Z^{\mathrm{exc}}_{x_1,x_2}, \tag{5.2.5}$$

such that the current becomes

$$I_1 = -\Gamma_{2e}\int dt\sum_{\nu s}\nu\partial_t\frac{\delta Z^{\varphi}_{x_1,x_2}}{\delta j_{1\nu s}(x,t^+)}\Big|_{j=0}, \tag{5.2.6}$$

and the current noise

$$S_{12} = \Gamma_{2e}\mathrm{Re}\int dtd\tilde{t}\sum_{\nu\tilde{\nu}s\tilde{s}}\nu\tilde{\nu}\partial_t\partial_{\tilde{t}} \times\Big(\frac{\delta^2 Z^{\varphi}_{x_1,x_2}}{\delta j_{1\nu s}(x,t^-)\delta j_{2\tilde{\nu}\tilde{s}}(\tilde{x},\tilde{t}^+)} - \frac{\delta Z^{\varphi}_{x_1,x_2}}{\delta j_{1\nu s}(x,t^-)}\frac{\delta Z^{\varphi}_{x_1,x_2}}{\delta j_{2\tilde{\nu}\tilde{s}}(\tilde{x},\tilde{t}^+)}\Big)\Big|_{j=0}. \tag{5.2.7}$$

Note that the exchange parts of the current and of the current noise acquire an oscillating prefactor $\cos(\varphi)$. Following standard perturbation theory, we now rewrite the generating functional in the interaction picture with respect to H_0,

$$\begin{aligned} Z^{\mathrm{dir/exc}}_{x_1,x_2} =& \frac{1}{4}\langle \mathrm{T}_{\mathcal{C}} F_{1R\uparrow}F_{2R\downarrow}F^{\dagger}_{2R\downarrow/\uparrow}F^{\dagger}_{1R\uparrow/\downarrow}\exp\Big\{-i\int_{\mathcal{C}}dt\ H_T \\ &+\int dx\int_{\mathcal{C}}dt\sum_{i\nu s}j_{i\nu s}(x,t)\Phi_{i\nu s}(x,t) \\ &+2\pi i[\Phi_{1R\uparrow}(x_1,t_0^-)-\Phi_{1R\uparrow/\downarrow}(x_1,t_0^+)] \\ &+2\pi i[\Phi_{2R\downarrow}(x_2,t_0^-)-\Phi_{2R\downarrow/\uparrow}(x_2,t_0^+)]\Big\}\rangle_0 \end{aligned} \tag{5.2.8}$$

where $\langle\cdot\rangle_0$ denotes the expectation value of two decoupled Tomonaga–Luttinger liquids, i.e., the expectation value with respect to the ground state of H_0. The generating functional is now expanded to second order in H_T, and the functional derivatives are performed. Using the assumptions $x, \tilde{x} \gg a$, the t integral and the $\tilde{t}$ integral from Eqs. (5.2.3) and (5.2.4) are solved. I drop $2k_F$ processes, in which injected left-moving electrons, which do not move towards the beam splitter but away from it, are supposed to tunnel. Strictly speaking, because of charge fractionalization, some of the charge of an injected left mover does move towards the beam splitter, producing a small correction. This correction turns out to be negligible [118] so I suppress it in favor of transparency. Importantly, the correction is insensitive for entanglement.

In zeroth order, i.e., without tunneling, we obtain $I_1^{(0)} = -e\Gamma_{2e}/2$, the current of charges $-e$ injected with the rate Γ_{2e} and moving right towards the current probe or left away from it with equal probability. There are no correlations between the two (decoupled) wires,

$S_{12}^{(0)} = 0$. The second-order direct contributions, i.e., the entanglement-insensitive contributions are

$$I_1^{(2)\mathrm{dir}} = -e\Gamma_{2e}\sum_{\nu_1\nu_2\nu\nu' s}\frac{1+\nu g}{2}\Big[|U^{(1)s}_{2\nu'\to 1\nu}\,|\nu_1\uparrow,\nu_2\downarrow\rangle\,|^2 - |U^{(1)s}_{1\nu\to 2\nu'}\,|\nu_1\uparrow,\nu_2\downarrow\rangle\,|^2\Big] \tag{5.2.9}$$

$$S_{12}^{(2)\mathrm{dir}} = -e^2\Gamma_{2e}\sum_{\nu_1\nu_2\nu\nu' s}\frac{1+\nu g}{2}\frac{1+\nu' g}{2}\mathrm{Re}\Big[|U^{(1)s}_{2\nu'\to 1\nu}\,|\nu_1\uparrow,\nu_2\downarrow\rangle\,|^2 + |U^{(1)s}_{1\nu\to 2\nu'}\,|\nu_1\uparrow,\nu_2\downarrow\rangle\,|^2\Big], \tag{5.2.10}$$

where $U^{(1)s}_{j\nu\to k\nu'} = -i\hbar^{-1}\int_{t_0}^{\infty} dt'\; H_T(t')|^s_{j\nu\to k\nu'}$ is the first-order expansion of the time evolution operator which transforms the initial state into a final state in the distant future, including only the parts of the tunnel Hamiltonian H_T which describe tunneling of ν-moving spin-s electrons from wire j into wire k becoming ν' movers. So, we can distinguish final states $U^{(1)}_{2\to 1}\,|\cdot\rangle$ in which an electron tunneled from wire 2 into wire 1 from final states $U^{(1)}_{1\to 2}\,|\cdot\rangle$ in which an electron tunneled from wire 1 into wire 2. Quite intuitively, we see from Eq. (5.2.9) that, correspondingly, the current in wire 1 is either increased or decreased. The weight of each process is given by the quantum-mechanical probability of the final states. Note that $U^{(1)}$ is not unitary since it includes only part of the tunnel Hamiltonian H_T, and that therefore $U^{(1)}$ affects the magnitude of the state vector it acts on. The fractions $(1+\nu g)/2$ reflect charge fractionalization as discussed before. The current noise, Eq. (5.2.10), has a similar structure. Both directions of tunneling produce negative cross-correlations since whenever the number of charges is increased in one lead, it is decreased in the other.

To gain further insight, the integrand contained in $U^{(1)}$ in Eqs. (5.2.9)

and (5.2.10), e.g.,

$$\begin{aligned}
&\langle \nu_1\uparrow, \nu_2\downarrow|\, \mathrm{T}_{\mathcal{C}} H_T(t')|^s_{1\nu\to 2\nu'} H_T(t'')|^s_{2\nu'\to 1\nu}\, |\nu_1\uparrow, \nu_2\downarrow\rangle = \\
&\frac{a^{(g^{-1}+g-2)/2}}{4(2\pi)^2}\Big[f_\rho^{-\frac{g^{-1}+g}{2}} f_\sigma^{-1}\Big](0,t';0,t'') \\
&\times \Xi_{\nu_1\nu s}(x_1,t_0^-;0,t')\Xi_{\nu_1\nu s}(x_1,t_0^+;0,t'')\Xi^{-1}_{\nu_1\nu s}(x_1,t_0^-;0,t'') \\
&\times \Xi^{-1}_{\nu_1\nu s}(x_1,t_0^+;0,t')\Xi^{-1}_{\nu_2\nu'\,-s}(x_2,t_0^-;0,t')\Xi_{\nu_2\nu'\,-s}(x_2,t_0^-;0,t'') \\
&\times \Xi_{\nu_2\nu'\,-s}(x_2,t_0^+;0,t')\Xi^{-1}_{\nu_2\nu'\,-s}(x_2,t_0^+;0,t'')
\end{aligned} \tag{5.2.11}$$

with the abbreviation

$$\Xi_{\nu\nu' s} = f_{\rho+}^{\frac{g^{-1}+\nu+\nu'+\nu\nu' g}{8}} f_{\rho-}^{\frac{g^{-1}-\nu-\nu'+\nu\nu' g}{8}} f_{\sigma\nu}^{\frac{1+\nu\nu'}{4s}}, \tag{5.2.12}$$

is evaluated numerically [Figs. 5.2(a) and 5.2(c)]. We see that, first, the tunnel current becomes weaker with stronger interactions, i.e., smaller g, second, that it always reduces the total current measured in wire 1, and, third, that it is mostly independent of the injection points $x_{1,2}$. The first observation is expected since the single-particle tunnel density of states in Tomonaga–Luttinger liquids decreases with increasing interaction [222]. The second observation requires a little more thought: when the electron from wire 1 tunnels into wire 2, the current in wire 1 is decreased. But an electron tunneling from wire 2 into wire 1 only increases the current if it becomes a right mover while left movers never reach the current probe, which is located at the right of the tunnel point. So, on average, the current is reduced because of backscattering at the beam splitter. The third observation appears even paradoxical. At a first glance, it seems natural that the current does not depend on the injection points. This is certainly true in a Fermi-liquid system: the electron is injected at some point and travels to the tunnel junction. There, it tunnels with a certain amplitude, which is independent of the other particles (there is no Pauli dip for opposite spin particles), and eventually contributes to the average current. The distance from the injection point to the tunnel point only determines when, but not if, the electron contributes to the current in wire 1. But in the presence of interactions, spin–charge separation sets in. If the electron is injected very far away from the junction, the faster charge excitation has long since passed the tunnel junction when the slower spin excitation arrives.

Now, the tunnel Hamiltonian, Eq. (5.2.1), explicitly transports entire electrons. Since no entire electron arrives at the tunnel point at any time, it appears that the tunnel current should be strongly suppressed with increasing distances between the injection point and the tunnel point, i.e., with increasing spin–charge separation. In fact, the Green's function

$$\langle \Psi_{j\nu s}(x,t)\Psi^\dagger_{j\nu s}(0,0)\rangle = \frac{a^{2\gamma-1}}{2\pi} f_{\rho\nu}^{-\gamma} f_{\rho,-\nu}^{-\gamma+\frac{1}{2}} f_{\sigma\nu}^{-\frac{1}{2}}, \tag{5.2.13}$$

where $\gamma = (g^{-1}+g+2)/8$, does decay algebraically with the distance x, and even exponentially at finite temperature. But the reasoning is still wrong: on average, charge and spin excitations can tunnel independently from one another. Formally, we are not allowed to do a Wick decomposition because the Tomonaga–Luttinger Hamiltonian is not quadratic in the physical electrons Ψ. Hence, an argument based on two-point Green's functions is flawed. In more physical terms, when a charge excitation arrives at the tunnel point, either a spin-up or a spin-down electron may tunnel. On average only charge is transported. Conversely, when a spin-up excitation arrives at the tunnel point, either a spin-up electron tunnels out of the wire or a spin-down electron tunnels into the wire. On average only spin is transported. We could, e.g., rewrite the tunnel Hamiltonian as

$$\begin{aligned} H_T = \frac{T}{4}\Big[&\underbrace{\Big(\Psi^\dagger_{2\uparrow} - \Psi^\dagger_{2\downarrow}\Big)\Big(\Psi_{1\uparrow} - \Psi_{1\downarrow}\Big) + \Big(\Psi^\dagger_{2\uparrow} + \Psi^\dagger_{2\downarrow}\Big)\Big(\Psi_{1\uparrow} + \Psi_{1\downarrow}\Big)}_{\text{average charge transport}} \\ &+ \underbrace{\Big(\Psi^\dagger_{2\uparrow} + \Psi_{2\downarrow}\Big)\Big(\Psi_{1\uparrow} - \Psi^\dagger_{1\downarrow}\Big)}_{\text{average spin-up transport}} + \underbrace{\Big(\Psi^\dagger_{2\downarrow} + \Psi_{2\uparrow}\Big)\Big(\Psi_{1\downarrow} - \Psi^\dagger_{1\uparrow}\Big)}_{\text{average spin-down transport}}\Big]. \end{aligned} \tag{5.2.14}$$

The current I_1 we investigate is only sensitive to charge excitations. But because tunneling, H_T, mixes the charge and spin excitations, in which H_0 is diagonal, interesting things happen when a charge excitation arrives simultaneously with another excitation at the tunnel point. Two charge excitations can only meet in a symmetric situation, $x_1 = x_2$. If they affect each other, they affect each other equally such that both

tunneling into wire 1 and tunneling out of wire 1 change roughly by the same amount and we cannot expect a substantial effect in the current measured behind the beam splitter. The charge excitation of one electron can, however, interfere with the spin-excitation of the other if $x_1/v_\rho = x_2/v_\sigma$ or if $x_1/v_\sigma = x_2/v_\rho$. This process is clearly visible as two peaks in Figs. 5.2(a) and 5.2(c). The sign of the peaks tells us that the probability for the charge excitation to tunnel is reduced if there already is a spin excitation in the other wire.

The peaks in the current and in the current noise are direct consequences of spin-charge separation. Shortly before these results were published, similar phenomena have been predicted to exist in chiral edge channels [261] and recently they have been observed experimentally [262]. But, of course, what is most interesting in the context of entanglement detection, are the exchange contributions

$$I_1^{(2)\mathrm{exc}} = e\Gamma_{2e}\frac{1+g}{2}\Big[\langle R\uparrow, R\downarrow| U^{(1)\uparrow\dagger}_{1R\to 2R} U^{(1)\downarrow}_{1R\to 2R} |R\downarrow, R\uparrow\rangle - \langle R\uparrow, R\downarrow| U^{(1)\downarrow\dagger}_{2R\to 1R} U^{(1)\uparrow}_{2R\to 1R} |R\downarrow, R\uparrow\rangle\Big], \tag{5.2.15}$$

$$S_{12}^{(2)\mathrm{exc}} = -e^2\Gamma_{2e}\Big(\frac{1+g}{2}\Big)^2 \mathrm{Re}\Big[\langle R\uparrow, R\downarrow| U^{(1)\uparrow\dagger}_{1R\to 2R} U^{(1)\downarrow}_{1R\to 2R} |R\downarrow, R\uparrow\rangle + \langle R\uparrow, R\downarrow| U^{(1)\downarrow\dagger}_{2R\to 1R} U^{(1)\uparrow}_{2R\to 1R} |R\downarrow, R\uparrow\rangle\Big]. \tag{5.2.16}$$

Their structure and interpretation closely follows the direct contributions, Eqs. (5.2.9) and (5.2.10). Here, the strength of a tunnel process is not given by the standard quantum-mechanical probability but by the overlap of the corresponding final state $U^{(1)s}|{\downarrow\uparrow}\rangle$ with its *spin-flipped* counterpart $\langle{\uparrow\downarrow}| U^{(1)-s\dagger}$. In other words, the exchange process is strong when the final state is mostly invariant under spin flip, which is somewhat reminiscent of a theoretical entanglement measure, the

concurrence [74]. Solving the integrand numerically, where, e.g.,

$$\begin{aligned}\langle R\uparrow, R\downarrow|\mathrm{T}_{\mathcal{C}} H_T(t')|^{\downarrow}_{1R\to 2R} H_T(t'')|^{\uparrow}_{2R\to 1R}\,|R\downarrow, R\uparrow\rangle = \\ -\frac{a^{(g^{-1}+g+2)/2}}{4(2\pi)^2}\Big[f_\rho^{-\frac{g^{-1}+g}{2}} f_\sigma\Big](0,t';0,t'') \\ \times \Xi_{RR\downarrow}(x_1,t_0^-;0,t')\Xi_{RR\downarrow}(x_1,t_0^+;0,t'')\Xi_{RR\downarrow}(x_2,t_0^-;0,t'') \\ \times \Xi_{RR\downarrow}(x_2,t_0^+;0,t')\Xi^{-1}_{RR\uparrow}(x_1,t_0^-;0,t'')\Xi^{-1}_{RR\uparrow}(x_1,t_0^+;0,t') \\ \times \Xi^{-1}_{RR\uparrow}(x_2,t_0^-;0,t')\Xi^{-1}_{RR\uparrow}(x_2,t_0^+;0,t''),\end{aligned} \tag{5.2.17}$$

demonstrates that there is a small but finite exchange contribution to the current [Fig. 5.2(b)] as soon as interactions are switched on, $g < 1$. In the interacting system, entanglement is therefore detectable by a dc current measurement alone. Moreover, if we artificially remove spin–charge separation from the model by setting $v_\rho \equiv v_\sigma$ but leave the interaction parameter $g < 1$ untouched everywhere else, the signal vanishes. To understand, why spin–charge separation is crucial for this detection mechanism, we need to understand under which circumstances the final state after scattering at the beam splitter is mostly invariant under spin flip. More precisely, we have to understand under which circumstances the final state after a tunneling event from wire 1 into wire 2 has a different spin-flipped overlap than the final state after a tunneling event from wire 2 into wire 1. Only then will the current be affected by the entanglement, as can be seen clearly from Eq. (5.2.15).

Assume that the charge excitation created by the injection of a spin-down electron in wire 1 reaches the tunnel contact and causes a spin-down electron to tunnel from wire 1 into wire 2. As illustrated in Fig. 5.3(a), this means that an additional charge excitation and an additional spin-down excitation are created in wire 2 and that a spin-down hole is left behind in wire 1. So, now, there are two opposite-spin excitations in each wire: in wire 1, there is the spin-down excitation injected by the entangler and the spin-up excitation left behind by the tunnel event, and in wire 2, there is the spin-up excitation injected by the entangler and the spin-down excitation created by the tunnel event. The final state is mostly invariant under spin flip if the opposite-spin excitations in each wire cancel. Because all spin excitations move with the same velocity, it is inessential at which time the spin-flipped overlap

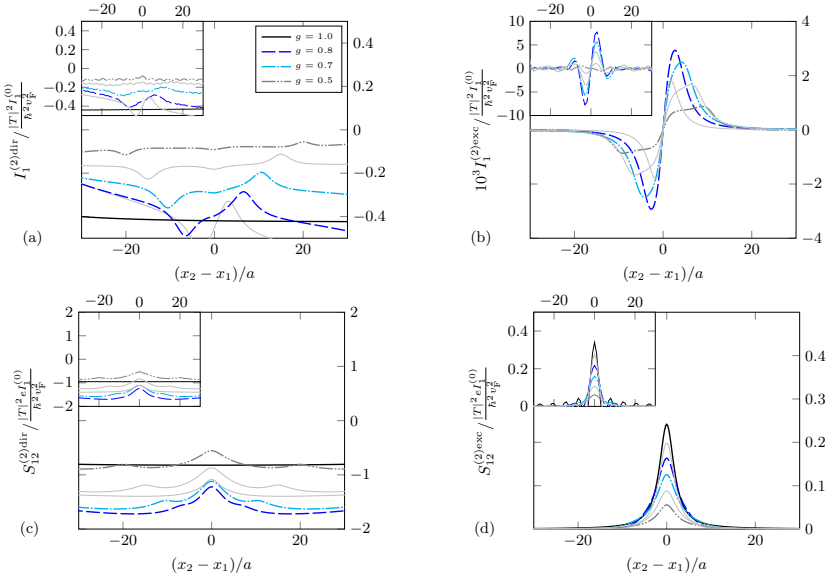

Figure 5.2: (a) direct and (b) exchange current in wire 1, (c) direct and (d) exchange zero-frequency current cross-correlations between wire 1 and wire 2 for different interaction parameters g and injection distances. $(x_1 + x_2)/2$ is fixed at $-30a$ [(a), (c)] or $-15a$ [(b), (d)]. Gray lines represent equidistant intermediate g values. Insets: a large voltage bias modeled as an injection Hamiltonian with a Peierls phase reproduces the initial state approximation for large voltages $2eV \to \hbar v_F a^{-1}$ up to residual oscillations. Figure reproduced and caption adapted from the original publication, Ref. 118.

is evaluated as long as it happens after the tunnel event.

The spin hole in wire 1 is created where the charge excitation used to be because it was the charge excitation, which triggered the tunnel event in the first place. So, if at the time of tunneling spin–charge separation is already too large, the two opposite spin excitations cannot compensate each other and the process is weak. It follows that the distance between the injection point and the tunnel junction must not be too large. Note that this is different from the direct current, which, as I explained, is unaffected by the distance between the injection point and the tunnel

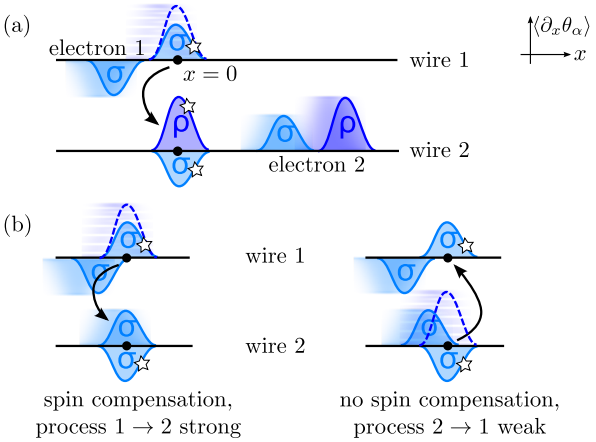

Figure 5.3: Exchange process. (a) $x_1 \ll x_2$. When the charge excitation of electron 1 (dashed line) reaches the tunnel junction at $x = 0$, the charge imbalance can trigger a tunnel event. This creates a new charge and a new spin excitation in wire 2 and leaves behind a spin hole in wire 1 (all marked by stars). Spin and charge excitations are drawn with different height for better visibility. (b) For suitable injection points $x_1/v_\rho = x_2/v_\sigma$ the new spin excitations compensate the one already present in each wire, leading to a strong exchange process. The competing process cannot have spin compensation at the same time and is weak. This asymmetry caused by spin–charge separation gives rise to a finite exchange current. Figure and caption reproduced from the original publication, Ref. 118.

point.

In wire 2, the new spin-down excitation created by the tunnel event needs to coincide with the spin-up excitation created when the entangler injected an electron into wire 2. So, the process is strong if $x_1/v_\rho = x_2/v_\sigma$. By exactly the same reasoning, the competing process, in which a spin-up electron tunnels from wire 1 into wire 2 is strong if $x_2/v_\rho = x_1/v_\sigma$. In the presence of spin–charge separation, $v_\rho = g v_\sigma \neq v_\sigma$, these two conditions cannot be fulfilled simultaneously (except in in the trivial case, $x_1 = x_2$) so there is no complete cancellation and a finite exchange current results, which becomes largest whenever the condition

$$\frac{x_2 - x_1}{x_2 + x_1} = \pm \frac{g-1}{g+1} \tag{5.2.18}$$

is met (Fig. 5.4). In this interpretation, I did not consider tunnel events caused by spin-excitations because they do not produce charge current on average but only charge noise. They can, however, cause interferences as in the direct current. To put the analysis on a more quantitative footing, we expect the final state after tunneling from wire 1 into wire 2 to be

$$|1 \to 2\rangle := \sum_t \psi^\dagger_{2\downarrow}(0,t)\psi_{1\downarrow}(0,t)\psi^\dagger_{1\downarrow}(x_1,t_0)\psi^\dagger_{2\uparrow}(x_2,t_0)\,|\rangle\,, \tag{5.2.19}$$

where $t \in \{x_1/v_\rho, x_1/v_\sigma, x_2/v_\sigma\}$ is summed over all possible tunnel times. The strength of this process is $P_{1\to 2} := \langle \widetilde{1 \to 2} | 1 \to 2\rangle$, where we obtain the spin-flipped final state $|\widetilde{1 \to 2}\rangle$ by flipping all the spin indices in Eq. (5.2.19). Likewise, we can construct $P_{2\to 1}$ and estimate the exchange current as

$$I_1^{(2)\mathrm{exc}} \approx e\Gamma_{2e}\left|\frac{T}{\hbar v_F}\right|^2 \frac{1+g}{2}\Big(P_{2\to 1} - P_{1\to 2}\Big). \tag{5.2.20}$$

This expression does, in fact, reproduce all of the features of the exact calculation (Fig. 5.4, left inset) and it enables us to extract the asymptotic behavior $I^{(2)\mathrm{exc}} \propto |x_1 + x_2|^{-3}$ by expanding Eq. (5.2.20).

The exchange noise is much easier to interpret. Because tunneling both from wire 1 into wire 2 and from wire 2 into wire 1 contribute equally to the noise, there are no subtle cancellations and the exchange noise

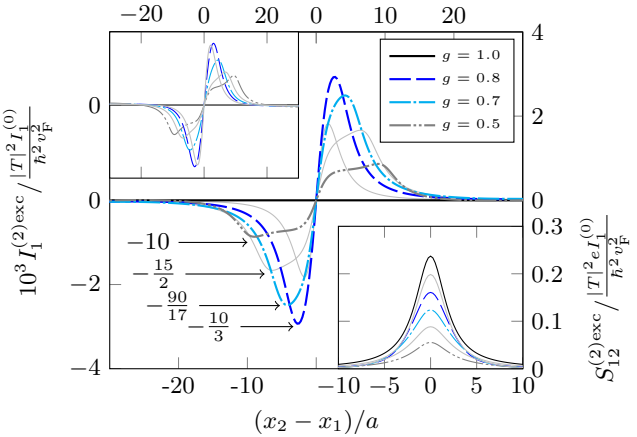

Figure 5.4: Exchange contributions to the tunnel current in wire 1 and the zero-frequency current cross-correlations between wire 1 and wire 2 (right inset) for different interaction parameters g and injection distances. $(x_1+x_2)/2 = -15a$ is fixed. The exchange contribution to the tunnel current is nonzero if $x_1 \approx x_2$ because spin–charge separation induces an asymmetry between the two directions of tunneling. The arrow tips indicate the expected positions of the maxima, cf. Eq. (5.2.18). Gray lines represent equidistant intermediate g values. The exchange part of the current noise is finite only if the spins meet at the junction. Left inset: analytic approximation, Eq. (5.2.20). Figure and caption reproduced from the original publication, Ref. 118.

is strongest when the spin excitations meet at the tunnel contact, i.e., when the injection points are the same distance from the beam splitter, $d = x_2 - x_1 = 0$. All of the relevant tunnel events are then caused by the spin excitations. Without interactions, $g = 1$, their overlap directly reflects the Lorentzian shape of the wave packets and solving Eq. (5.2.16) analytically we obtain

$$S_{12}^{(2)\mathrm{exc}} = e^2 \frac{\Gamma_{2e}}{2} \left| \frac{T}{\hbar v_F} \right|^2 \frac{1}{4 + (d/a)^2}, \tag{5.2.21}$$

which agrees with the earlier noninteracting results in the energy domain [41, 95, 263] and the time domain [264]. With interactions, the maximum at $d = 0$ decreases with a power law,

$$S_{12}^{(2)\mathrm{exc}} \propto \left(\frac{1+g}{2}\right)^2 \left(\frac{2}{g} + 1\right)^{-\frac{g^{-1}+g}{2}}. \tag{5.2.22}$$

Because electron–electron repulsion reduces the probability to tunnel, the electrons prefer to stay in the wire into which they have been injected from the entangler and the exchange noise is reduced.

5.2.1 Case of a voltage bias

The initial state, Eq. (5.2.2), mimics the time-resolved on-demand injection of entangled pairs as could be realized, e.g., with quantum dot charge pumps [265]. If the entangler is driven by a constant bias voltage V instead, we can find a more accurate description by including the injection process itself into the model,

$$\begin{aligned} H_I(t) = I e^{i\frac{2eV}{\hbar}t} \sum_{\nu_1\nu_2} \Big[& \psi_{1\nu_1\uparrow}(x_1,t)\psi_{2\nu_2\downarrow}(x_2,t) \\ & + e^{i\varphi}\psi_{1\nu_1\downarrow}(x_1,t)\psi_{2\nu_2\uparrow}(x_2,t) + \mathrm{H.c.}\Big] \end{aligned} \tag{5.2.23}$$

where the voltage enters as Peierls phase [266]. Because an entangler should always emit at sufficiently low rates to avoid correlations between subsequent pairs, we need to consider only the leading order contribution in H_I and expand the generating functional

$$Z \approx Z^{(2I)} + Z^{(2I,2T)}, \tag{5.2.24}$$

where the superscripts denote the expansion orders in tunneling, T, and injection, I. All of the terms which are of zeroth order in the injection do not carry a charge current or charge noise because they are equilibrium expectation values. In leading order, the current is a power law of the voltage bias,

$$I_1^{(2I)} = -\frac{ev_F}{a}\Big|\frac{I}{\hbar v_F}\Big|^2 \frac{\pi 2^{4\gamma}}{\Gamma(4\gamma)}\mathrm{sgn}(V)\Big|\frac{ea}{\hbar v_F}V\Big|^{4\gamma-1}, \tag{5.2.25}$$

which is a typical result for a Tomonaga–Luttinger liquid [255, 256]. Even without tunneling, there is shot noise from the injection process,

$$S_{12}^{(2I)} = \frac{e}{2}|I_1^{(2I)}|. \tag{5.2.26}$$

Auto-correlations have been reported to contain an anomalous charge in infinitely long wires [255] but here we see that this artifact does not occur in the case of cross-correlations.

A large injection voltage, $eV \to \hbar v_F/a$, means that electrons are injected over a broad range of momenta, i.e., spatially as localized as the bandwidth allows. Indeed, in this limit, the results from the initial state calculation are recovered (Fig. 5.2, insets). At low voltages, on the other hand, the voltage replaces the bandwidth as a high energy cutoff and sets the length scale of the theory: the overlap integral $\mathcal{I}$ which determines the exchange current is of the form

$$\mathcal{I}(\{x\}, V, a) = \frac{1}{a^{\alpha+2}}\int\Big(\prod_{m=1\ldots3} d\tau_m\Big)e^{2iV\tau_1}\prod_n\Big(i(x_n \pm v_n\tau_n) + a\Big)^{\alpha_n}, \tag{5.2.27}$$

where $\alpha = \sum_n \alpha_n$. With η a flow parameter, we obtain the scaling law

$$\begin{aligned}\mathcal{I}(\{x\}, \eta V, a) &= \frac{\eta^{-1}}{(\eta a)^{\alpha+2}}\int\Big(\prod_{m=1\ldots3} d\tilde{\tau}_m\Big)e^{2iV\tilde{\tau}_1}\prod_n\Big(i(\eta x_n \pm v_n\tilde{\tau}_n) + \eta a\Big)^{\alpha_n} \\ &\approx \frac{\eta^{-1}}{(\eta a)^{\alpha+2}}\int\Big(\prod_{m=1\ldots3} d\tilde{\tau}_m\Big)e^{2iV\tilde{\tau}_1}\prod_n\Big(i(\eta x_n \pm v_n\tilde{\tau}_n) + a\Big)^{\alpha_n} \\ &= \eta^{-3-\alpha}\mathcal{I}(\{\eta x\}, V, a),\end{aligned} \tag{5.2.28}$$

where I neglected the scaling of the bandwidth a because the behavior at low voltages is independent of the high energy cutoff, which can be confirmed numerically [118]. Specifically, the exchange currents at two voltages V, V' are related by

$$I^{\mathrm{exc}}_{1\,x_1,x_2}(V) \approx \left(\frac{V}{V'}\right)^{g^{-1}+g-1} I^{\mathrm{exc}}_{1\,\frac{V}{V'}x_1,\frac{V}{V'}x_2}(V'). \tag{5.2.29}$$

Put differently, the $x_{1,2}$ dependence of the exchange current can be accessed not only by changing the geometry, a task which is probably challenging in a nanowire device, but also by changing the injection voltage.

To be concrete, assume a voltage of $V \sim 0.1$ mV, i.e., well below the typical superconducting gap energy $\Delta \sim 1$ meV (niobium), and choose two asymmetric injection points at $x_1 = \hbar v_F/eV \sim 500$ nm and $x_2 = 3\hbar v_F/eV \sim 1500$ nm (assuming a Fermi velocity of $v_F \sim 10^5$ m/s). In this way, injection happens close to the beam splitter, which increases the signal strength, but still far enough to regard injection and tunneling at the beam splitter as two distinct events. With a total transmission $|I|^2|T|^2 \sim 10^{-2}\hbar^4 v_F^4$ through the device and employing the scaling relation, Eq. (5.2.29), we obtain the exchange current $I^{\mathrm{exc}}_{1\,x_1,x_2}(V) \approx e^2\hbar^{-1}V I^{\mathrm{exc,init}}_{1\,x_1=a,x_2=3a}/(ev_F/a) \sim 1$ pA from the initial state result $I^{\mathrm{exc,init}}_1$. I set $g^{-1}+g-1 \approx 1$ to remove the explicit cutoff dependence. At a typical nanowire interaction parameter $g = 0.8$, this is a good approximation. A current of a few picoampere is well accessible. The actual challenge is to extract it from the background given by the direct contributions, which are two to three orders of magnitude larger. This is where the phase parameter φ introduced in the initial state, Eq. (5.2.2), and in the injection Hamiltonian, Eq. (5.2.23), becomes important. It is conceivable to influence it via the Rashba spin-orbit interaction [94, 96, 267–269] if a symmetry-breaking transversal electric field E is applied to the nanowires as illustrated by the gray gates in Fig. 5.1. The Rashba interaction shifts the Fermi vector of spin-up and of spin-down electrons to $k_F \pm k_R$, respectively, where $k_R = 2\pi/\lambda_R \propto E$ can be tuned in situ [270, 271]. When the electrons travel the distances $|x_1|$ and $|x_2|$ from the entangler towards the beam splitter, they hence pick up a spin-dependent phase $e^{\pm ik_R x_{1,2}}$ and by the time they reach the junction, they have acquired $\varphi = 4\pi(x_1 - x_2)/\lambda_R \propto E$. More

rigorously, k_F is substituted by $k_F \pm k_R$ in the bosonization identity, Eq. (5.1.3), with the same result. Either way, the exchange contribution oscillates with $\cos(\varphi)$ and can be isolated from the constant direct background via lock-in amplification. Apart from the electric field, all parameters can remain fixed in this measurement. In indium arsenide, Rashba lengths λ_R as short as 150 nm have been realized [272], so the exchange current can undergo several oscillations within one sweep of the electric field.

5.3 Beam splitter built from quantum-Hall edge states

An integer-quantum-Hall device may be the most promising platform to realize the interacting beam splitter. Since the edge states are chiral, very large mean free paths and coherence lengths up to several 10 μm can be achieved. Chirality also removes charge fractionalization and backscattering, which are unnecessary side effects in the beam splitter. Unlike nanowire crossings, the geometry can be fabricated deterministically with high precision and even changed in the running experiment by gating, so the injection distances x_1 and x_2 are directly accessible. The large magnetic field required to achieve ballistic transport probably conflicts with the superconducting order a Cooper pair splitter relies on but recently a new method to inject correlated pairs of electrons into quantum-Hall edge states on demand has been demonstrated [265], which might emit spin singlets. Ubbelohde et al. fabricated a dynamical quantum-dot charge pump in a two-dimensional gallium-arsenide electron gas. The quantum dot was defined by two gates. By lowering and rising the potential of the entrance gate they could, on demand, first load the quantum dot with electrons and then lift them above the exit gate to inject them into a quantum-Hall edge state. Pairwise emission was demonstrated by the partition noise at a tunnel barrier. The beam splitter itself can be realized as a constriction in a Corbino geometry (Fig. 5.5). To conclude the discussion of the interacting beam splitter, I will outline how to repeat the calculation of the current and of the current noise for quantum-Hall edge states and point out the

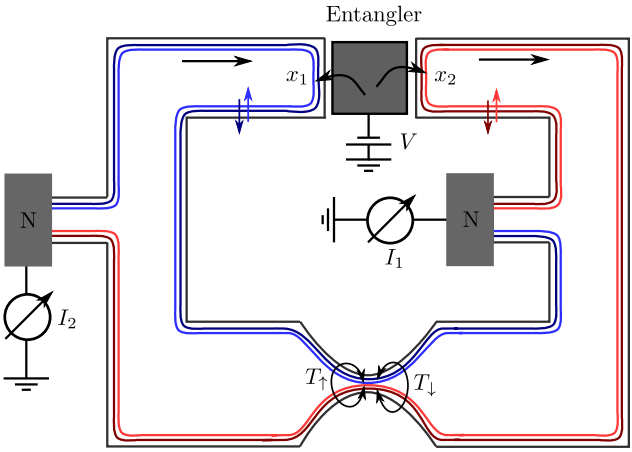

Figure 5.5: Beam splitter realized in a quantum-Hall sample of Corbino geometry. Two copropagating channels with opposite spin form a spinful chiral Tomonaga–Luttinger liquid at each edge. At a finite Zeeman splitting, they are spatially separated and the tunnel amplitudes at the constriction become spin dependent. Figure and caption reproduced from the original publication, Ref. 118.

major differences to the case of nanowires.

The quantum-Hall sample has to be operated at the filling factor 2 with two copropagating modes of opposite spin, i.e., the Zeeman splitting needs to be much smaller than the Landau splitting. Because of the difference in the Zeeman energy the two channels have different Fermi wave vectors and are slightly separated in real space. Under these conditions, which have already been demonstrated experimentally [235], two spinful Tomonaga–Luttinger liquid form, one at each edge, which has already been observed, too [236]. At each edge, the interactions within the two channels and between the two channels can be described exactly by bosonization if the spectrum is linearized. This

yields the Hamiltonian

$$H_0 = \sum_{i\alpha} \int dx \hbar v_\alpha \Big(\frac{\partial \phi_{i\alpha}}{\partial x}\Big)^2, \tag{5.3.1}$$

with only one phase field $\phi_{i\alpha}$ per edge $i = 1, 2$ and charge or spin degree of freedom $\alpha = \rho, \sigma$ because of chirality. The bosonization identity is $\psi_{js}(x) = (2\pi a)^{-1/2} F_{js} \exp\big[ik_s x + 2\pi i \Phi_{js}(x)\big]$, where $\Phi_{js} = \sqrt{\pi/2}(\phi_{j\rho} + s\phi_{j\sigma})$ with k_s the spin-dependent Fermi vector. The tunnel Hamiltonian

$$H_T = \sum_s \Big(T_s \psi^\dagger_{1s}(0)\psi_{2s}(0) + T_s^* \psi^\dagger_{2s}(0)\psi_{1s}(0) \Big) \tag{5.3.2}$$

is spin dependent because the spin-up channel and the spin-down channel have different distances at the constriction (cf. Fig. 5.5). The tunnel amplitude T_s is complex because of the magnetic field required for the quantum Hall effect. The initial state remains the same,

$$\begin{aligned} |\varphi\rangle &= \sqrt{2}\pi a \Big(\psi^\dagger_{2\downarrow}(x_2)\psi^\dagger_{1\uparrow}(x_1) + e^{i\varphi}\psi^\dagger_{2\uparrow}(x_2)\psi^\dagger_{1\downarrow}(x_1) \Big) |\rangle \\ &:= 2^{-1/2}(|\uparrow,\downarrow\rangle + e^{i\varphi} |\downarrow,\uparrow\rangle), \end{aligned} \tag{5.3.3}$$

but in the absence of spin-rotation invariance, we need to redefine the direct and the exchange contribution,

$$\langle \mathcal{O} \rangle_{\text{dir}} := \frac{1}{2} \Big(\langle \uparrow,\downarrow | \, \mathcal{O} \, | \uparrow,\downarrow \rangle + \langle \downarrow,\uparrow | \, \mathcal{O} \, | \downarrow,\uparrow \rangle \Big), \tag{5.3.4}$$

$$\langle \mathcal{O} \rangle_{\text{exc}} := \frac{1}{2} \Big(e^{i\varphi} \langle \uparrow,\downarrow | \, \mathcal{O} \, | \downarrow,\uparrow \rangle + e^{-i\varphi} \langle \downarrow,\uparrow | \, \mathcal{O} \, | \uparrow,\downarrow \rangle \Big). \tag{5.3.5}$$

Without further approximations we can find the second order contri-

butions

$$I_1^{(2)\mathrm{dir}} = -e\Gamma_{2e}\frac{|T_\uparrow|^2+|T_\downarrow|^2}{\hbar^2 v_F^2}\sum_s\Big[||U_{2\to1}^{(1)s}\,|\uparrow,\downarrow\rangle\,||^2 - ||U_{1\to2}^{(1)s}\,|\uparrow,\downarrow\rangle\,||^2\Big], \tag{5.3.6}$$

$$I_1^{(2)\mathrm{exc}} = e\Gamma_{2e}\frac{\mathrm{Re}(T_\uparrow^* T_\downarrow e^{i(k_\uparrow-k_\downarrow)(x_1-x_2)+i\varphi})}{\hbar^2 v_F^2} \times\Big[\langle\uparrow,\downarrow|\,U_{1\to2}^{(1)\uparrow\dagger}U_{1\to2}^{(1)\downarrow}\,|\downarrow,\uparrow\rangle - \langle\uparrow,\downarrow|\,U_{2\to1}^{(1)\downarrow\dagger}U_{2\to1}^{(1)\uparrow}\,|\downarrow,\uparrow\rangle\Big], \tag{5.3.7}$$

$$S_{12}^{(2)\mathrm{dir}} = -e^2\Gamma_{2e}\frac{|T_\uparrow|^2+|T_\downarrow|^2}{\hbar^2 v_F^2}\sum_s\Big[||U_{2\to1}^{(1)s}\,|\uparrow,\downarrow\rangle\,||^2 + ||U_{1\to2}^{(1)s}\,|\uparrow,\downarrow\rangle\,||^2\Big], \tag{5.3.8}$$

$$S_1^{(2)\mathrm{exc}} = -e\Gamma_{2e}\frac{\mathrm{Re}(T_\uparrow^* T_\downarrow e^{i(k_\uparrow-k_\downarrow)(x_1-x_2)+i\varphi})}{\hbar^2 v_F^2} \times\Big[\langle\uparrow,\downarrow|\,U_{1\to2}^{(1)\uparrow\dagger}U_{1\to2}^{(1)\downarrow}\,|\downarrow,\uparrow\rangle + \langle\uparrow,\downarrow|\,U_{2\to1}^{(1)\downarrow\dagger}U_{2\to1}^{(1)\uparrow}\,|\downarrow,\uparrow\rangle\Big], \tag{5.3.9}$$

where $U_{j\to k}^{(1)s} = -i\int_{t_0}^{\infty}dt'\;H_T(t')|_{j\to k}^{s}$,

$$\begin{aligned}\langle\uparrow,\downarrow|\mathrm{T}_{\mathcal{C}}H_T(t')|_{1\to2}^{s}H_T(t'')|_{2\to1}^{s}\,|\uparrow,\downarrow\rangle &= \frac{1}{4(2\pi)^2}\Big[f_\rho^{-1}f_\sigma^{-1}\Big](0,t';0,t'')\\ &\times\Xi_\uparrow(x_1,t_0^-;0,t'')\Xi_\uparrow(x_1,t_0^+;0,t')\Xi_\uparrow^{-1}(x_1,t_0^-;0,t')\\ &\times\Xi_\uparrow^{-1}(x_1,t_0^+;0,t'')\Xi_\downarrow(x_2,t_0^-;0,t')\Xi_\downarrow(x_2,t_0^+;0,t'')\\ &\times\Xi_\downarrow^{-1}(x_2,t_0^-;0,t'')\Xi_\downarrow^{-1}(x_2,t_0^+;0,t')\end{aligned} \tag{5.3.10}$$

and

$$\begin{aligned}\langle\uparrow,\downarrow|\mathrm{T}_{\mathcal{C}}H_T(t')|_{1\to2}^{\downarrow}H_T(t'')|_{2\to1}^{\uparrow}\,|\downarrow,\uparrow\rangle &= -\frac{a^2}{4(2\pi)^2}\Big[f_\rho^{-1}f_\sigma\Big](0,t';0,t'')\\ &\times\Xi_\uparrow(x_1,t_0^-;0,t'')\Xi_\uparrow(x_1,t_0^+;0,t')\Xi_\uparrow(x_2,t_0^-;0,t'')\\ &\times\Xi_\uparrow(x_2,t_0^+;0,t'')\Xi_\downarrow^{-1}(x_1,t_0^-;0,t')\Xi_\downarrow^{-1}(x_1,t_0^+;0,t'')\\ &\times\Xi_\downarrow^{-1}(x_2,t_0^-;0,t'')\Xi_\downarrow^{-1}(x_2,t_0^+;0,t')\end{aligned} \tag{5.3.11}$$

with

$$\Xi_s = f_\rho^{-\frac{1}{2}} f_\sigma^{-\frac{s}{2}}. \tag{5.3.12}$$

Compared to the case of nanowires, the exchange contributions are modified only quantitatively because the chiral system has different fractional exponents and because there is no charge fractionalization. There is no constant background in the direct current since only forward scattering is possible and there are as many scattering events which increase the current in edge 1 as there are scattering events which decrease the current in edge 1. The satellite peaks caused by spin–charge separation are still present. Finally, the Zeeman splitting gives the exchange contributions an oscillating prefactor, and provides us with a handle to detect them, just as the Rashba interaction did in the case of nanowires.

6 Conclusion

I described a new way to split Cooper pairs and three new entanglement detection schemes.

The bilayer-graphene Cooper pair splitter offers a way to extract entangled pairs of electrons from a superconductor without energy filtering and without Coulomb interaction. It relies on the fact that the electrons of a Cooper pair have opposite momentum and that their direction of motion is topologically protected in a guided one-dimensional mode. This mode can be defined electrostatically and far away from the sample edges, which eliminates the main sources of scattering. It is conceivable that electronically-tuned channels provide a platform to integrate both the Cooper pair splitter and a beam-splitter entanglement test in a single device, in particular, because the spin relaxation and decoherence rates in graphene are low thanks to small spin-orbit interaction and sparse nuclear spins.

A first indication that Cooper pairs remain spin entangled when split is provided by the critical current through the double-quantum-dot Josephson junction. Although the critical current is arguably a macroscopic quantity, it contains signatures for nonlocal Cooper pair transport, i.e., there are cross-correlations between the quantum dots, which are absent in the normal-state transport. A few-level model of the quantum dots reproduces these features consistently with a recent experiment. Furthermore, the model predicts a new singlet–triplet phase transition for the quantum-dot spins, which manifests in the critical current, too. It may serve as an additional indicator of nonlocal transport since local currents are oblivious to nonlocal features of the ground state. Nonlocal Josephson current is equivalent to spin-entangled split

Cooper pairs because the entire transport process is necessarily coherent.

The superconducting p–n junction emits two entangled photons when an entangled Cooper pair is transferred across it. It allows to use the tools of quantum optics for detecting electronic entanglement. Although the device is certainly challenging to fabricate, it can be made robust against parasitic processes and imperfections and is easy to operate, driven by just a constant dc voltage. Once emitted, the photons are easily separated over a macroscopic distance and investigated with a Bell test without risking decoherence. But even at macroscopic distances, the entanglement, if present, goes back directly to nonlocal microscopic Cooper pairs.

Finally, the Tomonaga–Luttinger liquid beam splitter provides an unconventional entanglement-detection strategy based on the non-Fermi-liquid effect of spin–charge separation. It can be realized both as a nanowire device and via quantum-Hall edge states and it promises entanglement detection with neither correlation measurements nor magnetic elements. In combination with earlier proposals, it is conceivable to build an entangler and detector setup completely based on Tomonaga–Luttinger liquids.

All of the proposals have rather different foundations and requirements. On the one hand, this led to a number of new discoveries, e.g., that nonlocal pairs of electrons can be produced by local Andreev reflection, that there can be a localized triplet ground state in a singlet-driven Josephson junction, and that spin–charge separation is connected to entanglement detection. On the other hand, of course, the more different schemes there are to create and to detect nonlocal Cooper pairs, the higher are the chances that one of them will eventually be realized and enable us to successfully demonstrate mobile entangled spin qubits. This will be the capstone of Cooper pair splitting and may be just the beginning of its application as a building block of advanced quantum devices.

Bibliography

[1] W. Heisenberg, Z. Phys. **33**, 879 (1925).

[2] E. Schrödinger, Ann. Phys. (Berlin) **384**, 361 (1926).

[3] P. A. M. Dirac, *Quantum Mechanics*, Ph.D. thesis, St. John's College, Cambridge (1926).

[4] A. Einstein, Annalen der Physik **14**, 164 (1905).

[5] A. Einstein, B. Podolsky, and N. Rosen, Phys. Rev. **47**, 777 (1935).

[6] J. J. Sakurai, *Modern Quantum Mechanics* (Prentice Hall, 1993).

[7] W. Heisenberg, *Physics and Philosophy* (Harper, 1958).

[8] M. Schlosshauer, Rev. Mod. Phys. **76**, 1267 (2005).

[9] J. Bardeen, L. N. Cooper, and J. R. Schrieffer, Phys. Rev. **106**, 162 (1957).

[10] C. W. J. Beenakker, Proc. Int. School Phys. E. Fermi **162**, 307 (2006).

[11] C. W. J. Beenakker, C. Emary, M. Kindermann, and J. L. van Velsen, Phys. Rev. Lett. **91**, 147901 (2003).

[12] S. Bose and D. Home, Phys. Rev. Lett. **88**, 050401 (2002).

[13] A. V. Lebedev, G. Blatter, C. W. J. Beenakker, and G. B. Lesovik, Phys. Rev. B **69**, 235312 (2004).

[14] J. S. Bell, Physics **1**, 195 (1964).

[15] S. J. Freedman and J. F. Clauser, Phys. Rev. Lett. **28**, 938 (1972).

[16] A. Aspect, J. Dalibard, and G. Roger, Phys. Rev. Lett. **49**, 1804 (1982).

[17] W. Tittel, J. Brendel, H. Zbinden, and N. Gisin, Phys. Rev. Lett. **81**, 3563 (1998).

[18] G. Weihs, T. Jennewein, C. Simon, H. Weinfurter, and A. Zeilinger, Phys. Rev. Lett. **81**, 5039 (1998).

[19] M. Giustina, A. Mech, S. Ramelow, B. Wittmann, J. Kofler, J. Beyer, A. Lita, B. Calkins, T. Gerrits, S. W. Nam, R. Ursin, and A. Zeilinger, Nature (London) **497**, 227 (2013).

[20] B. Hensen, H. Bernien, A. E. Dreau, A. Reiserer, N. Kalb, M. S. Blok, J. Ruitenberg, R. F. L. Vermeulen, R. N. Schouten, C. Abellan, W. Amaya, V. Pruneri, M. W. Mitchell, M. Markham, D. J. Twitchen, D. Elkouss, S. Wehner, T. H. Taminiau, and R. Hanson, Nature (London) **526**, 682 (2015).

[21] L. K. Shalm, E. Meyer-Scott, B. G. Christensen, P. Bierhorst, M. A. Wayne, M. J. Stevens, T. Gerrits, S. Glancy, D. R. Hamel, M. S. Allman, K. J. Coakley, S. D. Dyer, C. Hodge, A. E. Lita, V. B. Verma, C. Lambrocco, E. Tortorici, A. L. Migdall, Y. Zhang, D. R. Kumor, W. H. Farr, F. Marsili, M. D. Shaw, J. A. Stern, C. Abellán, W. Amaya, V. Pruneri, T. Jennewein, M. W. Mitchell, P. G. Kwiat, J. C. Bienfang, R. P. Mirin, E. Knill, and S. W. Nam, Phys. Rev. Lett. **115**, 250402 (2015).

[22] M. Giustina, M. A. M. Versteegh, S. Wengerowsky, J. Handsteiner, A. Hochrainer, K. Phelan, F. Steinlechner, J. Kofler, J.-A. Larsson, C. Abellán, W. Amaya, V. Pruneri, M. W. Mitchell, J. Beyer, T. Gerrits, A. E. Lita, L. K. Shalm, S. W. Nam, T. Scheidl, R. Ursin, B. Wittmann, and A. Zeilinger, Phys. Rev. Lett. **115**, 250401 (2015).

[23] B. M. Terhal, Theor. Comp. Sci. **287**, 313 (2002).

[24] M. A. Nielsen and I. L. Chuang, *Quantum Computation and Quantum Information* (Cambridge University Press, Cambridge, England, 2000).

[25] C. H. Bennett, G. Brassard, C. Crépeau, R. Jozsa, A. Peres, and W. K. Wootters, Phys. Rev. Lett. **70**, 1895 (1993).

[26] C. H. Bennett and S. J. Wiesner, Phys. Rev. Lett. **69**, 2881 (1992).

[27] A. K. Ekert, Phys. Rev. Lett. **67**, 661 (1991).

[28] D. Bouwmeester, J.-W. Pan, K. Mattle, M. Eibl, H. Weinfurter, and A. Zeilinger, Nature (London) **390**, 575 (1997).

[29] D. Boschi, S. Branca, F. De Martini, L. Hardy, and S. Popescu, Phys. Rev. Lett. **80**, 1121 (1998).

[30] K. Mattle, H. Weinfurter, P. G. Kwiat, and A. Zeilinger, Phys. Rev. Lett. **76**, 4656 (1996).

[31] N. Gisin, G. Ribordy, W. Tittel, and H. Zbinden, Rev. Mod. Phys. **74**, 145 (2002).

[32] P. Shor, in *35th Annual Symposium on Foundations of Computer Science, 1994 Proceedings* (1994) pp. 124–134.

[33] R. Feynman, Int. J. Theor. Phys. **21**, 467 (1982).

[34] S. Lloyd, Science **273**, 1073 (1996).

[35] I. Bloch, J. Dalibard, and W. Zwerger, Rev. Mod. Phys. **80**, 885 (2008).

[36] D. Wecker, B. Bauer, B. K. Clark, M. B. Hastings, and M. Troyer, Phys. Rev. A **90**, 022305 (2014).

[37] J. M. Kikkawa and D. D. Awschalom, Phys. Rev. Lett. **80**, 4313 (1998).

[38] D. Loss and D. P. DiVincenzo, Phys. Rev. A **57**, 120 (1998).

[39] G. Burkard, D. Loss, and D. P. DiVincenzo, Phys. Rev. B **59**, 2070 (1999).

[40] J. Clarke and F. K. Wilhelm, Nature (London) **453**, 1031 (2008).

[41] G. Burkard, D. Loss, and E. V. Sukhorukov, Phys. Rev. B **61**, R16303 (2000).

[42] F. W. J. Hekking, L. I. Glazman, K. A. Matveev, and R. I. Shekhter, Phys. Rev. Lett. **70**, 4138 (1993).

[43] G. Lesovik, T. Martin, and G. Blatter, Eur. Phys. J. B **24**, 287 (2001).

[44] P. Recher, E. V. Sukhorukov, and D. Loss, Phys. Rev. B **63**, 165314 (2001).

[45] I. A. Sadovskyy, G. B. Lesovik, and V. M. Vinokur, New J. Phys. **17**, 103016 (2015).

[46] P. Recher and D. Loss, Phys. Rev. B **65**, 165327 (2002).

[47] D. Feinberg, Eur. Phys. J. B **36**, 419 (2003).

[48] J. Cayssol, Phys. Rev. Lett. **100**, 147001 (2008).

[49] J. Linder, M. Zareyan, and A. Sudbø, Phys. Rev. B **80**, 014513 (2009).

[50] W. Chen, R. Shen, L. Sheng, B. G. Wang, and D. Y. Xing, Phys. Rev. B **84**, 115420 (2011).

[51] J. Wang, L. Hao, and K. S. Chan, Phys. Rev. B **91**, 085415 (2015).

[52] C. Bena, S. Vishveshwara, L. Balents, and M. P. A. Fisher, Phys. Rev. Lett. **89**, 037901 (2002).

[53] P. Recher and D. Loss, Phys. Rev. Lett. **91**, 267003 (2003).

[54] K. Sato, D. Loss, and Y. Tserkovnyak, Phys. Rev. Lett. **105**, 226401 (2010).

[55] J. Nilsson, A. R. Akhmerov, and C. W. J. Beenakker, Phys. Rev. Lett. **101**, 120403 (2008).

[56] R. W. Reinthaler, P. Recher, and E. M. Hankiewicz, Phys. Rev. Lett. **110**, 226802 (2013).

[57] L. Hofstetter, S. Csonka, A. Baumgartner, G. Fülöp, S. d'Hollosy, J. Nygård, and C. Schönenberger, Phys. Rev. Lett. **107**, 136801 (2011).

[58] L. Hofstetter, S. Csonka, J. Nygård, and C. Schönenberger, Nature (London) **461**, 960 (2009).

[59] C. Kurtsiefer, M. Oberparleiter, and H. Weinfurter, Phys. Rev. A **64**, 023802 (2001).

[60] P. Samuelsson and M. Büttiker, Phys. Rev. B **66**, 201306 (2002).

[61] L. G. Herrmann, F. Portier, P. Roche, A. Levy Yeyati, T. Kontos, and C. Strunk, Phys. Rev. Lett. **104**, 026801 (2010).

[62] J. Wei and V. Chandrasekhar, Nat. Phys. **6**, 494 (2010).

[63] Z. B. Tan, D. Cox, T. Nieminen, P. Lähteenmäki, D. Golubev, G. B. Lesovik, and P. J. Hakonen, Phys. Rev. Lett. **114**, 096602 (2015).

[64] J. Schindele, A. Baumgartner, and C. Schönenberger, Phys. Rev. Lett. **109**, 157002 (2012).

[65] G. Fülöp, S. d'Hollosy, A. Baumgartner, P. Makk, V. A. Guzenko, M. H. Madsen, J. Nygård, C. Schönenberger, and S. Csonka, Phys. Rev. B **90**, 235412 (2014).

[66] A. Das, Y. Ronen, M. Heiblum, D. Mahalu, A. V. Kretinin, and H. Shtrikman, Nat. Commun. **3**, 1165 (2012).

[67] G. Fülöp, F. Domínguez, S. d'Hollosy, A. Baumgartner, P. Makk, M. H. Madsen, V. A. Guzenko, J. Nygård, C. Schönenberger, A. Levy Yeyati, and S. Csonka, Phys. Rev. Lett. **115**, 227003 (2015).

[68] W. D. Oliver, F. Yamaguchi, and Y. Yamamoto, Phys. Rev. Lett. **88**, 037901 (2002).

[69] D. S. Saraga and D. Loss, Phys. Rev. Lett. **90**, 166803 (2003).

[70] A. T. Costa and S. Bose, Phys. Rev. Lett. **87**, 277901 (2001).

[71] P. Sodano, A. Bayat, and S. Bose, Phys. Rev. B **81**, 100412 (2010).

[72] Y. Aharonov, P. G. Bergmann, and J. L. Lebowitz, Phys. Rev. **134**, B1410 (1964).

[73] A. Ström, H. Johannesson, and P. Recher, Phys. Rev. B **91**, 245406 (2015).

[74] W. K. Wootters, Phys. Rev. Lett. **80**, 2245 (1998).

[75] J. F. Clauser, M. A. Horne, A. Shimony, and R. A. Holt, Phys. Rev. Lett. **23**, 880 (1969).

[76] B. Cirel'son, Lett. Math. Phys. **4**, 93 (1980).

[77] P. Recher, E. V. Sukhorukov, and D. Loss, Phys. Rev. Lett. **85**, 1962 (2000).

[78] R. Hanson, L. M. K. Vandersypen, L. H. W. van Beveren, J. M. Elzerman, I. T. Vink, and L. P. Kouwenhoven, Phys. Rev. B **70**, 241304 (2004).

[79] P. Recher, D. S. Saraga, and D. Loss, in *Fundamental Problems of Mesocopic Physics: Interactions and Decoherence*, NATO Science Series II, Vol. 154, edited by I. V. Lerner, B. L. Altshuler, and Y. Gefen (Kluwer Academic Publishers, Dordrecht, 2004) pp. 179–202.

[80] W. Chen, R. Shen, L. Sheng, B. G. Wang, and D. Y. Xing, Phys. Rev. Lett. **109**, 036802 (2012).

[81] K. Sato and Y. Tserkovnyak, Phys. Rev. B **90**, 045419 (2014).

[82] W. Izumida, K. Sato, and R. Saito, J. Phys. Soc. Jpn. **78**, 074707 (2009).

[83] J.-S. Jeong and H.-W. Lee, Phys. Rev. B **80**, 075409 (2009).

[84] B. Braunecker, P. Burset, and A. Levy Yeyati, Phys. Rev. Lett. **111**, 136806 (2013).

[85] F. Mazza, B. Braunecker, P. Recher, and A. Levy Yeyati, Phys. Rev. B **88**, 195403 (2013).

[86] N. M. Chtchelkatchev, G. Blatter, G. B. Lesovik, and T. Martin, Phys. Rev. B **66**, 161320 (2002).

[87] P. Samuelsson, E. V. Sukhorukov, and M. Büttiker, Phys. Rev. Lett. **91**, 157002 (2003).

[88] E. Prada, F. Taddei, and R. Fazio, Phys. Rev. B **72**, 125333 (2005).

[89] A. Bednorz and W. Belzig, Phys. Rev. B **83**, 125304 (2011).

[90] X. Maître, W. D. Oliver, and Y. Yamamoto, Physica E **6**, 301 (2000).

[91] S. Kawabata, J. Phys. Soc. Jpn. **70**, 1210 (2001).

[92] R. S. Deacon, A. Oiwa, J. Sailer, S. Baba, Y. Kanai, K. Shibata, K. Hirakawa, and S. Tarucha, Nat. Commun. **6**, 7446 (2015).

[93] S. Datta, *Electronic Transport in Mesoscopic Systems*, Cambridge Studies in Semiconductor Physics and Microelectronic Engineering (Cambridge University Press, Cambridge, England, 1997).

[94] G. Burkard and D. Loss, Phys. Rev. Lett. **91**, 087903 (2003).

[95] P. Samuelsson, E. V. Sukhorukov, and M. Büttiker, Phys. Rev. B **70**, 115330 (2004).

[96] J. C. Egues, G. Burkard, D. S. Saraga, J. Schliemann, and D. Loss, Phys. Rev. B **72**, 235326 (2005).

[97] V. Giovannetti, D. Frustaglia, F. Taddei, and R. Fazio, Phys. Rev. B **74**, 115315 (2006).

[98] P. San-Jose and E. Prada, Phys. Rev. B **74**, 045305 (2006).

[99] F. Taddei and R. Fazio, Phys. Rev. B **65**, 075317 (2002).

[100] I. Neder, N. Ofek, Y. Chung, M. Heiblum, D. Mahalu, and V. Umansky, Nature (London) **448**, 333 (2007).

[101] E. Bocquillon, V. Freulon, J.-M. Berroir, P. Degiovanni, B. Plaçais, A. Cavanna, Y. Jin, and G. Fève, Science **339**, 1054 (2013).

[102] E. Bocquillon, V. Freulon, F. D. Parmentier, J.-M. Berroir, B. Plaçais, C. Wahl, J. Rech, T. Jonckheere, T. Martin, C. Grenier, D. Ferraro, P. Degiovanni, and G. Fève, Ann. Phys. (Berlin) **526**, 1 (2014).

[103] R. Hanbury Brown and R. Q. Twiss, Nature (London) **177**, 27 (1956).

[104] C. K. Hong, Z. Y. Ou, and L. Mandel, Phys. Rev. Lett. **59**, 2044 (1987).

[105] Z. Scherübl, A. Pályi, and S. Csonka, Phys. Rev. B **89**, 205439 (2014).

[106] P. Lodahl, S. Mahmoodian, and S. Stobbe, Rev. Mod. Phys. **87**, 347 (2015).

[107] A. Cottet, T. Kontos, and A. Levy Yeyati, Phys. Rev. Lett. **108**, 166803 (2012).

[108] A. Cottet, Phys. Rev. B **90**, 125139 (2014).

[109] A. Cottet, Phys. Rev. B **86**, 075107 (2012).

[110] S. E. Nigg, R. P. Tiwari, S. Walter, and T. L. Schmidt, Phys. Rev. B **91**, 094516 (2015).

[111] M. R. Delbecq, V. Schmitt, F. D. Parmentier, N. Roch, J. J. Viennot, G. Fève, B. Huard, C. Mora, A. Cottet, and T. Kontos, Phys. Rev. Lett. **107**, 256804 (2011).

[112] J. J. Viennot, M. R. Delbecq, M. C. Dartiailh, A. Cottet, and T. Kontos, Phys. Rev. B **89**, 165404 (2014).

[113] A. Wallraff, D. I. Schuster, A. Blais, L. Frunzio, R.-S. Huang, J. Majer, S. Kumar, S. M. Girvin, and R. J. Schoelkopf, Nature (London) **431**, 162 (2004).

[114] H. Sasakura, S. Kuramitsu, Y. Hayashi, K. Tanaka, T. Akazaki, E. Hanamura, R. Inoue, H. Takayanagi, Y. Asano, C. Hermannstädter, H. Kumano, and I. Suemune, Phys. Rev. Lett. **107**, 157403 (2011).

[115] A. Schroer, P. G. Silvestrov, and P. Recher, Phys. Rev. B **92**, 241404 (2015).

[116] B. Probst, F. Domínguez, A. Schroer, A. Levy Yeyati, and P. Recher, Phys. Rev. B **94**, 155445 (2016).

[117] A. Schroer and P. Recher, Phys. Rev. B **92**, 054514 (2015).

[118] A. Schroer, B. Braunecker, A. Levy Yeyati, and P. Recher, Phys. Rev. Lett. **113**, 266401 (2014).

[119] E. Prada and F. Sols, New J. Phys. **7**, 231 (2005).

[120] A. H. Castro Neto, F. Guinea, N. M. R. Peres, K. S. Novoselov, and A. K. Geim, Rev. Mod. Phys. **81**, 109 (2009).

[121] C. W. J. Beenakker, Phys. Rev. Lett. **97**, 067007 (2006).

[122] C. W. J. Beenakker, Rev. Mod. Phys. **80**, 1337 (2008).

[123] C. Benjamin and J. K. Pachos, Phys. Rev. B **78**, 235403 (2008).

[124] S. Gómez, P. Burset, W. J. Herrera, and A. Levy Yeyati, Phys. Rev. B **85**, 115411 (2012).

[125] V. V. Cheianov, V. Fal'ko, and B. L. Altshuler, Science **315**, 1252 (2007).

[126] V. G. Veselago, Sov. Phys. Usp. **10**, 509 (1968).

[127] S. Das Sarma, S. Adam, E. H. Hwang, and E. Rossi, Rev. Mod. Phys. **83**, 407 (2011).

[128] E. McCann and V. I. Fal'ko, Phys. Rev. Lett. **96**, 086805 (2006).

[129] E. McCann and M. Koshino, Rep. Prog. Phys. **76**, 056503 (2013).

[130] R. van Gelderen and C. M. Smith, Phys. Rev. B **81**, 125435 (2010).

[131] F. Guinea, New J. Phys. **12**, 083063 (2010).

[132] S. Konschuh, M. Gmitra, D. Kochan, and J. Fabian, Phys. Rev. B **85**, 115423 (2012).

[133] I. Martin, Y. M. Blanter, and A. F. Morpurgo, Phys. Rev. Lett. **100**, 036804 (2008).

[134] M. Z. Hasan and C. L. Kane, Rev. Mod. Phys. **82**, 3045 (2010).

[135] J. Li, I. Martin, M. Büttiker, and A. F. Morpurgo, Physica Scr. **2012**, 014021 (2012).

[136] L. Ju, Z. Shi, N. Nair, Y. Lv, C. Jin, J. Velasco Jr, C. Ojeda-Aristizabal, H. A. Bechtel, M. C. Martin, A. Zettl, J. Analytis, and F. Wang, Nature (London) **520**, 650 (2015).

[137] A. Vaezi, Y. Liang, D. H. Ngai, L. Yang, and E.-A. Kim, Phys. Rev. X **3**, 021018 (2013).

[138] F. Zhang, A. H. MacDonald, and E. J. Mele, Proc. Nat. Acad. Sci. USA **110**, 10546 (2013).

[139] H. Meissner, Phys. Rev. **117**, 672 (1960).

[140] A. Levy Yeyati, F. S. Bergeret, A. Martin-Rodero, and T. M. Klapwijk, Nat. Phys. **3**, 455 (2007).

[141] E. Prada and F. Sols, Eur. Phys. J. B **40**, 379 (2004).

[142] P. Samuelsson, E. V. Sukhorukov, and M. Büttiker, New J. Phys. **7**, 176 (2005).

[143] A. S. Núñez, E. Suárez Morell, and P. Vargas, Appl. Phys. Lett. **98**, 262107 (2011).

[144] R. Winkler, *Spin-Orbit Coupling Effects in Two-Dimensional Electron and Hole Systems* (Springer, Berlin, 2003).

[145] B. Josephson, Phys. Lett. **1**, 251 (1962).

[146] P. W. Anderson and J. M. Rowell, Phys. Rev. Lett. **10**, 230 (1963).

[147] O. Kulik, JETP **22**, 841 (1966).

[148] H. Shiba and T. Soda, Prog. Theor. Phys. **41**, 25 (1969).

[149] B. I. Spivak and S. A. Kivelson, Phys. Rev. B **43**, 3740 (1991).

[150] A. V. Rozhkov and D. P. Arovas, Phys. Rev. Lett. **82**, 2788 (1999).

[151] E. Vecino, A. Martín-Rodero, and A. Levy Yeyati, Phys. Rev. B **68**, 035105 (2003).

[152] A. A. Clerk and V. Ambegaokar, Phys. Rev. B **61**, 9109 (2000).

[153] I. Affleck, J.-S. Caux, and A. M. Zagoskin, Phys. Rev. B **62**, 1433 (2000).

[154] M.-S. Choi, M. Lee, K. Kang, and W. Belzig, Phys. Rev. B **70**, 020502 (2004).

[155] F. Siano and R. Egger, Phys. Rev. Lett. **93**, 047002 (2004).

[156] M. Governale, M. G. Pala, and J. König, Phys. Rev. B **77**, 134513 (2008).

[157] J. A. van Dam, Y. V. Nazarov, E. P. A. M. Bakkers, S. De Franceschi, and L. P. Kouwenhoven, Nature (London) **442**, 667 (2006).

[158] J.-P. Cleuziou, W. Wernsdorfer, V. Bouchiat, T. Ondarcuhu, and M. Monthioux, Nat. Nano **1**, 53 (2006).

[159] J. J. A. Baselmans, T. T. Heikkilä, B. J. van Wees, and T. M. Klapwijk, Phys. Rev. Lett. **89**, 207002 (2002).

[160] F. S. Bergeret, A. Levy Yeyati, and A. Martín-Rodero, Phys. Rev. B **74**, 132505 (2006).

[161] F. S. Bergeret, A. Levy Yeyati, and A. Martín-Rodero, Phys. Rev. B **76**, 174510 (2007).

[162] M.-S. Choi, C. Bruder, and D. Loss, Phys. Rev. B **62**, 13569 (2000).

[163] Z. Wang and X. Hu, Phys. Rev. Lett. **106**, 037002 (2011).

[164] R. Jacquet, J. Rech, T. Jonckheere, A. Zazunov, and T. Martin, Phys. Rev. B **92**, 235429 (2015).

[165] H. Pan and T.-H. Lin, Phys. Rev. B **74**, 235312 (2006).

[166] R. López, M.-S. Choi, and R. Aguado, Phys. Rev. B **75**, 045132 (2007).

[167] M. Lee, T. Jonckheere, and T. Martin, Phys. Rev. B **81**, 155114 (2010).

[168] F. Hassler, G. Catelani, and H. Bluhm, Phys. Rev. B **92**, 235401 (2015).

[169] H. Bruus and K. Flensberg, *Many-Body Quantum Theory in Condensed Matter Physics* (Oxford University Press, Oxford, England, 2004).

[170] R. Fiederling, M. Keim, G. Reuscher, W. Ossau, G. Schmidt, A. Waag, and L. W. Molenkamp, Nature (London) **402**, 787 (1999).

[171] Y. Ohno, D. K. Young, B. Beschoten, F. Matsukura, H. Ohno, and D. D. Awschalom, Nature (London) **402**, 790 (1999).

[172] O. Gywat, G. Burkard, and D. Loss, Phys. Rev. B **65**, 205329 (2002).

[173] V. Cerletti, O. Gywat, and D. Loss, Phys. Rev. B **72**, 115316 (2005).

[174] M. Titov, B. Trauzettel, B. Michaelis, and C. W. J. Beenakker, New J. Phys. **7**, 186 (2005).

[175] Y. Hayashi, K. Tanaka, T. Akazaki, M. Jo, H. Kumano, and I. Suemune, Appl. Phys. Exp. **1**, 011701 (2008).

[176] E. Hanamura, Phys. Status Solidi B **234**, 166 (2002).

[177] Y. Asano, I. Suemune, H. Takayanagi, and E. Hanamura, Phys. Rev. Lett. **103**, 187001 (2009).

[178] I. Suemune, H. Sasakura, Y. Hayashi, K. Tanaka, T. Akazaki, Y. Asano, R. Inoue, H. Takayanagi, E. Hanamura, J.-H. Huh, C. Hermannstädter, S. Odashima, and H. Kumano, Jpn. J. Appl. Phys. **51**, 010114 (2012).

[179] Y.-J. Doh, J. A. van Dam, A. L. Roest, E. P. A. M. Bakkers, L. P. Kouwenhoven, and S. De Franceschi, Science **309**, 272 (2005).

[180] R. P. Feynman, R. B. Leighton, and M. Sands, *The Feynman Lectures on Physics, Vol. III: Quantum Mechanics* (Addison-Wesley Longman, Amsterdam, 1970).

[181] O. Benson, C. Santori, M. Pelton, and Y. Yamamoto, Phys. Rev. Lett. **84**, 2513 (2000).

[182] R. J. Young, R. M. Stevenson, P. Atkinson, K. Cooper, D. A. Ritchie, and A. J. Shields, New J. Phys. **8**, 29 (2006).

[183] R. Hafenbrak, S. M. Ulrich, P. Michler, L. Wang, A. Rastelli, and O. G. Schmidt, New J. Phys. **9**, 315 (2007).

[184] C. L. Salter, R. M. Stevenson, I. Farrer, C. A. Nicoll, D. A. Ritchie, and A. J. Shields, Nature (London) **465**, 594 (2010).

[185] A. Mohan, M. Felici, P. Gallo, B. Dwir, A. Rudra, J. Faist, and E. Kapon, Nat. Phot. **4**, 302 (2010).

[186] R. M. Stevenson, R. J. Young, P. Atkinson, K. Cooper, D. A. Ritchie, and A. J. Shields, Nature (London) **439**, 179 (2006).

[187] K. Kowalik, O. Krebs, A. Lemaître, B. Eble, A. Kudelski, P. Voisin, S. Seidl, and J. A. Gaj, Appl. Phys. Lett. **91**, 183104 (2007).

[188] B. D. Gerardot, S. Seidl, P. A. Dalgarno, R. J. Warburton, D. Granados, J. M. Garcia, K. Kowalik, O. Krebs, K. Karrai, A. Badolato, and P. M. Petroff, Appl. Phys. Lett. **90**, 041101 (2007).

[189] M. M. Vogel, S. M. Ulrich, R. Hafenbrak, P. Michler, L. Wang, A. Rastelli, and O. G. Schmidt, Appl. Phys. Lett. **91**, 051904 (2007).

[190] M. E. Reimer, M. Korkusiński, D. Dalacu, J. Lefebvre, J. Lapointe, P. J. Poole, G. C. Aers, W. R. McKinnon, P. Hawrylak, and R. L. Williams, Phys. Rev. B **78**, 195301 (2008).

[191] M. Korkusinski, M. E. Reimer, R. L. Williams, and P. Hawrylak, Phys. Rev. B **79**, 035309 (2009).

[192] M. E. Reimer, M. P. van Kouwen, A. W. Hidma, M. H. M. van Weert, E. P. A. M. Bakkers, L. P. Kouwenhoven, and V. Zwiller, Nano Lett. **11**, 645 (2011).

[193] F. Ding, R. Singh, J. D. Plumhof, T. Zander, V. Křápek, Y. H. Chen, M. Benyoucef, V. Zwiller, K. Dörr, G. Bester, A. Rastelli, and O. G. Schmidt, Phys. Rev. Lett. **104**, 067405 (2010).

[194] N. Akopian, N. H. Lindner, E. Poem, Y. Berlatzky, J. Avron, D. Gershoni, B. D. Gerardot, and P. M. Petroff, Phys. Rev. Lett. **96**, 130501 (2006).

[195] G. Rochat, C. Ciuti, V. Savona, C. Piermarocchi, A. Quattropani, and P. Schwendimann, Phys. Rev. B **61**, 13856 (2000).

[196] P. Recher, Y. V. Nazarov, and L. P. Kouwenhoven, Phys. Rev. Lett. **104**, 156802 (2010).

[197] F. Hassler, Y. V. Nazarov, and L. P. Kouwenhoven, Nanotechnology **21**, 274004 (2010).

[198] P. Baireuther, P. P. Orth, I. Vekhter, and J. Schmalian, Phys. Rev. Lett. **112**, 077003 (2014).

[199] F. Godschalk, F. Hassler, and Y. V. Nazarov, Phys. Rev. Lett. **107**, 073901 (2011).

[200] F. Godschalk and Y. V. Nazarov, Phys. Rev. B **87**, 094511 (2013).

[201] F. Godschalk and Y. V. Nazarov, Phys. Rev. B **89**, 104502 (2014).

[202] E. M. Purcell, in *Proceedings of the American Physical Society*, B. 10 (1946).

[203] J. C. Budich and B. Trauzettel, Nanotechnology **21**, 274001 (2010).

[204] G. Falci, D. Feinberg, and F. W. J. Hekking, Europhys. Lett. **54**, 255 (2001).

[205] J. R. Schrieffer and P. A. Wolff, Phys. Rev. **149**, 491 (1966).

[206] A. C. Hewson, *The Kondo Problem to Heavy Fermions* (Cambridge University Press, Cambridge, England, 1993).

[207] K. Hennessy, A. Badolato, M. Winger, D. Gerace, M. Atature, S. Gulde, S. Falt, E. L. Hu, and A. Imamoglu, Nature (London) **445**, 896 (2007).

[208] K. Srinivasan and O. Painter, Nature (London) **450**, 862 (2007).

[209] V. Loo, L. Lanco, A. Lemaître, I. Sagnes, O. Krebs, P. Voisin, and P. Senellart, Appl. Phys. Lett. **97**, 241110 (2010).

[210] R. Ohta, Y. Ota, M. Nomura, N. Kumagai, S. Ishida, S. Iwamoto, and Y. Arakawa, Appl. Phys. Lett. **98**, 173104 (2011).

[211] N. Majlis, *The Quantum Theory of Magnetism* (World Scientific Publishing, Singapore, 2000).

[212] W. Vogel, D.-G. Welsch, and S. Wallentowitz, *Quantum Optics An Introduction* (WILEY-VCH Verlag, Berlin, 2001).

[213] D. F. Walls and G. J. Milburn, *Quantum Optics* (Springer, Berlin, 1994).

[214] V. Caprara Vivoli, P. Sekatski, J.-D. Bancal, C. C. W. Lim, B. G. Christensen, A. Martin, R. T. Thew, H. Zbinden, N. Gisin, and N. Sangouard, Phys. Rev. A **91**, 012107 (2015).

[215] P. Sekatski, B. Sanguinetti, E. Pomarico, N. Gisin, and C. Simon, Phys. Rev. A **82**, 053814 (2010).

[216] C. W. Gardiner and P. Zoller, *Quantum Noise* (Springer, Berlin, 2000).

[217] R. Hanson, L. P. Kouwenhoven, J. R. Petta, S. Tarucha, and L. M. K. Vandersypen, Rev. Mod. Phys. **79**, 1217 (2007).

[218] L. D. Landau, Sov. Phys. JETP **3**, 920 (1957).

[219] L. D. Landau, Sov. Phys. JETP **5**, 101 (1957).

[220] L. D. Landau, Sov. Phys. JETP **8**, 70 (1958).

[221] E. Wigner, Phys. Rev. **46**, 1002 (1934).

[222] T. Giamarchi, *Quantum Physics in One Dimension* (Oxford University Press, Oxford, England, 2003).

[223] F. D. M. Haldane, Journal of Physics C: Solid State Physics **14**, 2585 (1981).

[224] S.-i. Tomonaga, Prog. Theor. Phys. **5**, 544 (1950).

[225] J. M. Luttinger, J. Math. Phys. **4**, 1154 (1963).

[226] K.-V. Pham, M. Gabay, and P. Lederer, Phys. Rev. B **61**, 16397 (2000).

[227] O. M. Auslaender, H. Steinberg, A. Yacoby, Y. Tserkovnyak, B. I. Halperin, K. W. Baldwin, L. N. Pfeiffer, and K. W. West, Science **308**, 88 (2005).

[228] R. Claessen, M. Sing, U. Schwingenschlögl, P. Blaha, M. Dressel, and C. S. Jacobsen, Phys. Rev. Lett. **88**, 096402 (2002).

[229] B. J. Kim, H. Koh, E. Rotenberg, S.-J. Oh, H. Eisaki, N. Motoyama, S. Uchida, T. Tohyama, S. Maekawa, Z.-X. Shen, and C. Kim, Nat. Phys. **2**, 397 (2006).

[230] M. S. Fuhrer, J. Nygård, L. Shih, M. Forero, Y.-G. Yoon, M. S. C. Mazzoni, H. J. Choi, J. Ihm, S. G. Louie, A. Zettl, and P. L. McEuen, Science **288**, 494 (2000).

[231] J. Kim, K. Kang, J.-O. Lee, K.-H. Yoo, J.-R. Kim, J. W. Park, H. M. So, and J.-J. Kim, J. Phys. Soc. Jpn. **70**, 1464 (2001).

[232] J. W. Park, J. Kim, and K.-H. Yoo, J. Appl. Phys. **93**, 4191 (2003).

[233] B. Gao, A. Komnik, R. Egger, D. C. Glattli, and A. Bachtold, Phys. Rev. Lett. **92**, 216804 (2004).

[234] Y. Ji, Y. Chung, D. Sprinzak, M. Heiblum, D. Mahalu, and H. Shtrikman, Nature (London) **422**, 415 (2003).

[235] B. Karmakar, D. Venturelli, L. Chirolli, F. Taddei, V. Giovannetti, R. Fazio, S. Roddaro, G. Biasiol, L. Sorba, V. Pellegrini, and F. Beltram, Phys. Rev. Lett. **107**, 236804 (2011).

[236] E. Bocquillon, V. Freulon, J.-M. Berroir, P. Degiovanni, B. Plaçais, A. Cavanna, Y. Jin, and G. Fève, Nat. Commun. **4**, 1839 (2013).

[237] P. Rickhaus, P. Makk, M.-H. Liu, K. Richter, and C. Schönenberger, Appl. Phys. Lett. **107**, 251901 (2015).

[238] Y. Blanter and M. Büttiker, Phys. Rep. **336**, 1 (2000).

[239] F. Bloch, Z. Phys. **81**, 363 (1933).

[240] F. Bloch, Helv. Phys. Acta **7**, 385 (1934).

[241] D. C. Mattis and E. H. Lieb, J. Math. Phys. **6**, 304 (1965).

[242] H. Grabert, in *Exotic States in Quantum Nanostructures* (Kluwer Academic Publishers, Dordrecht, 2002).

[243] J. Sólyom, Adv. Phys. **28**, 201 (1979).

[244] K. D. Schotte and U. Schotte, Phys. Rev. **182**, 479 (1969).

[245] D. C. Mattis, J. Math. Phys. **15**, 609 (1974).

[246] A. Luther and I. Peschel, Phys. Rev. B **9**, 2911 (1974).

[247] R. Heidenreich, B. Schroer, R. Seiler, and D. Uhlenbrock, Phys. Lett. A **54**, 119 (1975).

[248] F. D. M. Haldane, J. Phys. C **12**, 4791 (1979).

[249] J. von Delft and H. Schoeller, Ann. Phys. (Berlin) **7**, 225 (1998).

[250] C. L. Kane and M. P. A. Fisher, Phys. Rev. Lett. **72**, 724 (1994).

[251] S. Tarucha, T. Honda, and T. Saku, Solid State Commun. **94**, 413 (1995).

[252] I. Safi and H. J. Schulz, Phys. Rev. B **52**, R17040 (1995).

[253] D. L. Maslov and M. Stone, Phys. Rev. B **52**, R5539 (1995).

[254] V. V. Ponomarenko, Phys. Rev. B **52**, R8666 (1995).

[255] A. Crépieux, R. Guyon, P. Devillard, and T. Martin, Phys. Rev. B **67**, 205408 (2003).

[256] A. V. Lebedev, A. Crépieux, and T. Martin, Phys. Rev. B **71**, 075416 (2005).

[257] B. Trauzettel, I. Safi, F. Dolcini, and H. Grabert, Phys. Rev. Lett. **92**, 226405 (2004).

[258] F. Dolcini, B. Trauzettel, I. Safi, and H. Grabert, Phys. Rev. B **71**, 165309 (2005).

[259] P. Recher, N. Y. Kim, and Y. Yamamoto, Phys. Rev. B **74**, 235438 (2006).

[260] A. Komnik and R. Egger, Phys. Rev. Lett. **80**, 2881 (1998).

[261] C. Wahl, J. Rech, T. Jonckheere, and T. Martin, Phys. Rev. Lett. **112**, 046802 (2014).

[262] V. Freulon, A. Marguerite, J.-M. Berroir, B. Placais, A. Cavanna, Y. Jin, and G. Feve, Nat. Commun. **6**, 6854 (2015).

[263] X. Hu and S. Das Sarma, Phys. Rev. B **69**, 115312 (2004).

[264] S. Ol'khovskaya, J. Splettstoesser, M. Moskalets, and M. Büttiker, Phys. Rev. Lett. **101**, 166802 (2008).

[265] N. Ubbelohde, F. Hohls, V. Kashcheyevs, T. Wagner, L. Fricke, B. Kästner, K. Pierz, H. W. Schumacher, and R. J. Haug, Nat. Nano **10**, 46 (2015).

[266] G. D. Mahan, *Many-Particle Physics* (Kluwer Academic Publishers, Dordrecht, 1981).

[267] Y. A. Bychkov and E. I. Rashba, J. Phys. C **17**, 6039 (1984).

[268] J. C. Egues, G. Burkard, and D. Loss, Phys. Rev. Lett. **89**, 176401 (2002).

[269] J. Pawłowski, P. Szumniak, and S. Bednarek, Phys. Rev. B **93**, 045309 (2016).

[270] D. Liang and X. P. Gao, Nano Lett. **12**, 3263 (2012).

[271] Y. Kanai, R. S. Deacon, S. Takahashi, A. Oiwa, K. Yoshida, K. Shibata, K. Hirakawa, Y. Tokura, and S. Tarucha, Nat. Nano **6**, 511 (2011).

[272] P. Wójcik, J. Adamowski, B. J. Spisak, and M. Wołoszyn, J. Appl. Phys. **115**, 104310 (2014).